Physik Department

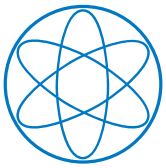

Enzyme mechanics studied by single molecule force spectroscopy

Dissertation

von

Benjamin Pelz

TECHNISCHE UNIVERSITÄT MÜNCHEN

TECHNISCHE UNIVERSITÄT MÜNCHEN
Lehrstuhl für Biophysik E22

Enzyme mechanics studied by single molecule force spectroscopy

Benjamin Pelz

Vollständiger Abdruck der von der Fakultät für Physik der Technischen Universität München zur Erlangung des akademischen Grades eines

Doktors der Naturwissenschaften

genehmigten Dissertation.

Vorsitzende(r): Univ.-Prof. Dr. Hendrik Dietz

Prüfer der Dissertation:

1. Univ.-Prof. Dr. Matthias Rief
2. Univ.-Prof. Dr. Martin Zacharias

Die Dissertation wurde am 05.11.2014 bei der Technischen Universität München eingereicht und durch die Fakultät für Physik am 09.12.2014 angenommen.

Abstract

Enzymes are macromolecules which catalyze chemical reactions by several orders of magnitude and thereby bring them to timescales needed for biological systems to work. Conformational changes and dynamics of the enzyme itself are often critical steps in their function as biocatalysts. Even though the chemical mechanisms of the catalyzed reaction is often well understood, how the conformational changes are influenced and how they play a role in the catalysis is not. For the enzyme adenylate kinase, it has been shown that it undergoes a large conformational change during catalysis and that these conformational dynamics are rate limiting for the catalytic activity.

To study the conformational dynamics of enzymes in detail, a high resolution dual beam optical trap was built. Between two micron sized glass beads single molecules can be tethered and manipulated using the optical trap. This so called dumbbell configuration allows the observation of conformational changes and can be used to collect kinetic and energetic information about the transitions. Several optimizations of the optical trap improved the time resolution to the ~10 µs timescale and allowed the observation of conformational changes down to 4 Å. It was possible to resolve the full opening and closing kinetics of adenylate kinase in presence of different inhibitors. From the data, it can be rationalized that the binding and closing of adenylate kinase in presence of the inhibitor follows a so called "induced fit" mechanism.

Furthermore, a single molecule competition assay allowed the determination of the affinity of the nucleotide substrates AMP, ADP and ATP to adenylate kinase. Additionally, the data provides insights about the conformational dynamics of adenylate kinase in presence of nucleotides. In combination with measurements of the stabilization of adenylate kinase in presence of ligands, it could be shown that the binding and closing process differs between inhibitors and nucleotides. For the inhibitors, a strong correlation between binding and closing could be observed, which was not the case for the nucleotides. These experiments also allowed the measurement of the binding affinities of the nucleotides to the open state of adenylate kinase, which is not possible with any other technique so far.

This work further gives insights into the adaption of proteins to extreme temperatures. The differences in folding and unfolding for a hyperthermophilic and mesophilic variant of adenylate kinase are shown.

Overall, the presented research demonstrates that the optical trap can be used as a tool to observe and manipulate conformational transitions between different native states of enzymes on the nanometer scale.

Zusammenfassung

Enzyme sind Makromoleküle die chemische Reaktionen katalysieren und sie damit auf eine Zeitskala bringen, die zur Funktion biologischer Systeme nötig ist. Dabei sind oft Konformationsänderungen der Enzyme selbst wichtige Schritte in der Katalyse. Die chemischen Mechanismen der katalysierten Reaktion sind gut verstanden, jedoch ist oft unklar welche Rolle Konformationsänderungen während der Katalyse spielen und wie diese beeinflusst werden. Für das Enzym Adenylatkinase wurde gezeigt, dass es während der Katalyse eine große Konformationsänderung durchläuft und diese ratenlimitierend für die katalytische Aktivität ist.

Um die Konformationsänderungen von Enzymen am einzelnen Molekül zu untersuchen, wurde im Rahmen dieser Arbeit eine hochauflösende optische Falle gebaut. Zwischen zwei, mit der optischen Falle gefangenen, Mikrometer großen Glaskugeln können einzelne Moleküle eingespannt und manipuliert werden. Hiermit lassen sich die Konformationsänderungen eines einzelnen Enzyms messen und daraus Informationen über deren Kinetik und die zugrundeliegende Energielandschaft gewinnen. Mehrere Verbesserungen der optischen Falle erhöhten die Zeitauflösung in den Bereich von ~10 µs und erlaubten die Beobachtung von Konformationsänderungen bis zu einer Größe von 4 Å. Somit war es möglich, die vollständige Öffnungs- und Schließkinetik von Adenylatkinase in Anwesenheit verschiedener Inhibitoren zu messen. Aus den Ergebnissen lässt sich ableiten, dass das Binden des Inhibitors und das Schließen von Adenylatkinase einem sogenannten „induced fit“-Mechanismus folgen.

Weiterhin konnte in einem Einzelmolekül-Kompetitionsexperiment die Affinität der Nukleotidsubstrate AMP, ADP und ATP an Adenylatkinase bestimmt werden. Ebenso kann mit diesen Daten ein Einblick in die Konformationsänderung von Adenylatkinase in Anwesenheit der Nukleotide gewonnen werden. So konnte gezeigt werden, dass sich das Binden und Schließen in Anwesenheit von Inhibitoren und Nukleotiden stark unterscheidet. In Anwesenheit der Inhibitoren konnte eine hohe Korrelation zwischen Bindung und Schließung beobachtet werden, was für die Nukleotide nicht der Fall ist. Die Experimente ermöglichten auch die Bestimmung der Affinität der Nukleotide an die offene Konformation von Adenylatkinase, welches bisher mit keiner anderen Technik möglich war.

Zusätzlich gibt diese Arbeit Einblicke in die Adaption von Proteinen an extreme Temperaturen. Dazu sind Unterschiede in der Faltung und Entfaltung einer hyperthermophilen und einer mesophilen Variante von Adenylatkinase untersucht worden.

Zusammengefasst zeigt die hier vorgestellte Arbeit, dass es möglich ist Konformationsänderungen im Nanometer Bereich zwischen verschiedenen nativen Zuständen von Enzymen zu beobachten und zu manipulieren.

Acknowledgment

A number of people helped me during the last few years to realize the work presented here. First of all I want to thank Matthias Rief, my thesis supervisor, for a lot of helpful and encouraging discussions, many ideas and a great lab atmosphere. His doors was always open to answer questions or help with tricky problems with the setup.

I want to especially thank Gabriel Zoldak with whom I started the first real experiments at the optical trap setup and continued to work on a several very interesting projects. He helped to get me started in the wet lab and as our biochemistry specialist had to endure many questions.

With Heinrich Grabmayr, Matthias "Schuppi" Schuppler, Martina Lindauer and Uli Merkel I had the pleasure to experience the joy and frustration of building an optical setup. They were always very helpful when one got stuck with seemingly unsolvable problems. The possibility to borrow optical components or technical equipment made the building much more easier. Rudi Lehrhuber built all the components I came up with and fixed them, if my design did not quite fit to the reality as I expected.

My office colleagues Uli Kleßinger, Anja Schlierf, Heinrich Grabmayr, Markus Harasim, Katharina Henneberg, Felix Keber and Philip Bleicher provided a great atmosphere in- and outside of lab and our stock of sweets got me out of the occasional afternoon slump.

A number of people always helped out with fruitful discussions, hands-on contributions or inspiring ideas: Alexander Mehlich, Anja Schlierf, Lorenz Rognoni, Leone Rossetti, Fabian Ziegler, Johannes Stigler, Markus Jahn, Marco Grison, Thomas Suren, Christian Wachauf and Fabian Kilchherr.

For the bureaucratic and technical help I want to thank Elke Fehsenfeld, Nicole Mittermüller, Gabi Chmel, Monica Rusp and Karin Vogt.

Everybody from the biophysics groups Rief, Bausch, Hugel, Woehlke and Dietz deserves a big thank you for making this more than just "getting" a PhD. Various activities from playing squash, kite surfing, skiing, group dinners to "special" seminars ensured that one did not get lost in the depth of a PhD thesis.

I have been blessed with many great friendships, some going back a long time. I want to thank them for always being there for me and keeping me balanced in all those years.

Finally, I want to thank my parents for their great support throughout my whole life.

Contents

List of Figures

List of Publications

Emanuel Pfitzner, Christian Wachauf, Fabian Kilchherr, Benjamin Pelz, William M. Shih, Matthias Rief, and Hendrik Dietz. Rigid DNA Beams for High-Resolution Single-Molecule Mechanics. *Angewandte Chemie*, 125(30):7920–7925, July 2013.

Lorenz Rognoni, Johannes Stigler, Benjamin Pelz, Jari Ylänne, and Matthias Rief. Dynamic force sensing of filamin revealed in single-molecule experiments. *Proceedings of the National Academy of Sciences of the United States of America*, 109(48):19679–84, November 2012.

Yann von Hansen, Alexander Mehlich, Benjamin Pelz, Matthias Rief, and Roland R Netz. Auto- and cross-power spectral analysis of dual trap optical tweezer experiments using Bayesian inference. *The Review of scientific instruments*, 83(9):095116, September 2012.

Gabriel Zoldák, Johannes Stigler, Benjamin Pelz, Hongbin Li, and Matthias Rief. Ultrafast folding kinetics and cooperativity of villin headpiece in single-molecule force spectroscopy. *Proceedings of the National Academy of Sciences of the United States of America*, 110(45):18156–61, November 2013.

1 Introduction

Proteins are one of the main building blocks of prokaryotic and eukaryotic cells. They do not only provide structural integrity for the cell, but are also involved in numerous other processes like DNA replication, molecular transport, signal transduction or catalysis of chemical reactions. Proteins consist of a long chain of amino acids, this primary sequence encodes for the three dimensional structure of the protein. The folding of proteins has been a big research topic and different techniques have provided insight in this complex and challenging process (Onuchic et al., 1997; Dill and MacCallum, 2012).

Although crystal structures of proteins convey the impression that the folded protein is a unique and rigid structure, they are able to sample a range of folded substates (Frauenfelder et al., 1991, 2003; McCammon et al., 1977). For some proteins this structural plasticity is essential for their function. Therefore, not only the folding of a protein itself is a very dynamic process but also the folded protein is able to undergo conformational transition between different states, which similar to the folding can happen through different pathways in an energy landscape.

Conformational changes of proteins have been reported for a wide variety of processes like signal transduction (De Bondt et al., 1993; Ogawa et al., 2002), enzymatic catalysis (Vonrhein et al., 1995; Hammes, 2002), chaperoning activity (Rüdiger et al., 1997; Hessling et al., 2009) or immune response (Stanfield et al., 1993). Different techniques have been used to shed light on these conformational transitions. Crystal structures have provided snapshots of different conformations in these cycles (Dreusicke et al., 1988; Müller and Schulz, 1992; Berry et al., 1994; Abele and Schulz, 1995) and transitions between different states have been measured by nuclear magnetic resonance (NMR) experiments Wolf-Watz et al. (2004); Henzler-Wildman et al. (2007b); Adén and Wolf-Watz (2007). Advances of computational methods allowed the simulation of various conformational changes (Cui et al., 2004; Klepeis et al., 2009; Yang et al., 2009; Matsunaga et al., 2012).

However, the molecular mechanisms of these conformational changes are still not clear. In many enzymes, domains undergo large-amplitude, low-frequency motions in response to ligand binding or the catalytic activity. Does the enzyme sample the full conformational spectrum observed in the crystal structures? How does ligand binding affect the conformation of the enzyme? At which stage is the ligand able to bind to the protein? How can a multi domain enzyme communicate between the different domains? These are just a few of the questions regarding conformational changes, which have been unanswered so far. This is in part caused by the fact that the ensemble techniques

used, can only sample an average conformation. Because the proteins do not move in a synchronized manner, many interesting features of conformational changes are hidden in the average of the ensemble in bulk experiments.

Recent advances in single molecule techniques allow us to observe conformational changes of single molecules over long time spans. One of the most widely used techniques to study protein dynamics on the single molecule level is Förster Resonance Energy Transfer (FRET). It has been used to study the conformational changes of different heat shock proteins, like HSP70 (Mapa et al., 2010) and HSP90 (Ratzke et al., 2010, 2012) or the opening and closing dynamics of adenylate kinase (Hanson et al., 2007; Henzler-Wildman et al., 2007b).

Another single molecule technique that has been successfully used is force spectroscopy. Especially optical tweezers have advanced significantly in recent years to study a wide array of different biological systems from protein folding (Cecconi et al., 2005; Stigler et al., 2011), to the folding of nucleic acids (Woodside et al., 2006b,a; Wen et al., 2007) or molecular motors. Even though optical tweezers have been used indirectly to observe conformational changes in enzymes like kinesin (Svoboda et al., 1993; Schnitzer and Block, 1997), polymerases (Shaevitz et al., 2003; Abbondanzieri et al., 2005a) or protease machineries (Aubin-Tam et al., 2011; Maillard et al., 2011), so far it has not been used to study the conformational change of an enzyme directly.

In this work I will present a custom-built high resolution optical tweezer setup, which is used to study the conformational change of adenylate kinase in presence of inhibitors and nucleotides.

Chapter 2 contains a general introduction and theoretical background of optical tweezers. Furthermore, the design and characterization of the optical tweezer setup, I have built in the frame of this work, is presented in this chapter. An overview about the models and the tools needed for analysis of the data, obtained from optical trap experiments, is described in chapter 3. In chapter 4, I will present single molecules studies of adenylate kinase using the optical tweezer setup, starting with folding and unfolding of adenylate kinase and followed by the observation of conformational changes, induced by different inhibitors and nucleotides. In the end, the difference between a thermophilic and mesophilic homolog of adenylate kinase is discussed.

2 Optical trapping concepts

2.1 Principle of optical trapping

Trapping of small particles by a highly focused laser beam, so called optical trapping, was demonstrated first by Ashkin in the 1980s (Ashkin et al., 1986). Shortly afterwards the optical trap was used to study biological systems by trapping yeast, bacteria and viruses (Ashkin and Dziedzic, 1987). Since then optical traps have been used to study a broad variety of biological systems from single molecules to cells. Notably, stepping of molecular motors like kinesin (Svoboda et al., 1993), myosin (Finer et al., 1994) and polymerases (Abbondanzieri et al., 2005b), protease machinery (Aubin-Tam et al., 2011; Maillard et al., 2011) or unfolding and folding of proteins (Stigler et al., 2011) and nucleic acids (Woodside et al., 2006a) have been studied with optical traps.

The working principle of an optical trap can be explained in a simple ray-optical picture. Due to the conservation of momentum, a light ray refracted or reflected by an object will transfer momentum on the object in the opposite direction. Using a laser and a high numerical aperture objective, it is possible to create a stable trap if the scattering force in direction of the light is overcome by the gradient force in direction of increasing light gradient. In most optical trap experiments, polystyrene or silica spheres are used but it is also possible to trap other shaped particles, like cylinders (Deufel et al., 2007).

Figure 2.1 shows the forces acting on a spherical particle. For a spherical particle the scattering force, caused by reflection or absorption, will cancel out in all directions but the direction of the light. The light rays passing the particle get refracted at the first and second surface, thereby transferring momentum on the bead. Near the focus of the laser this transfer of momentum results in a force acting against the direction of the light. If gradient force and scattering force cancel out, the particle is stably trapped. When the particle is deflected out of this position by an external force, a restoring force is exerted, bringing it back into the equilibrium position.

The ray optics approximation only holds true for particles which are much larger than the wavelength of the light. On the other hand if the sphere is much smaller than the wavelength trapping of the particle can be described in the Rayleigh regime. The particle is then treated like a dipole in an electric field. The scattering force can be explained by absorption and reradiation of light by the dipole and is proportional to the intensity of the light and scattering cross section of the particle. Interactions of the

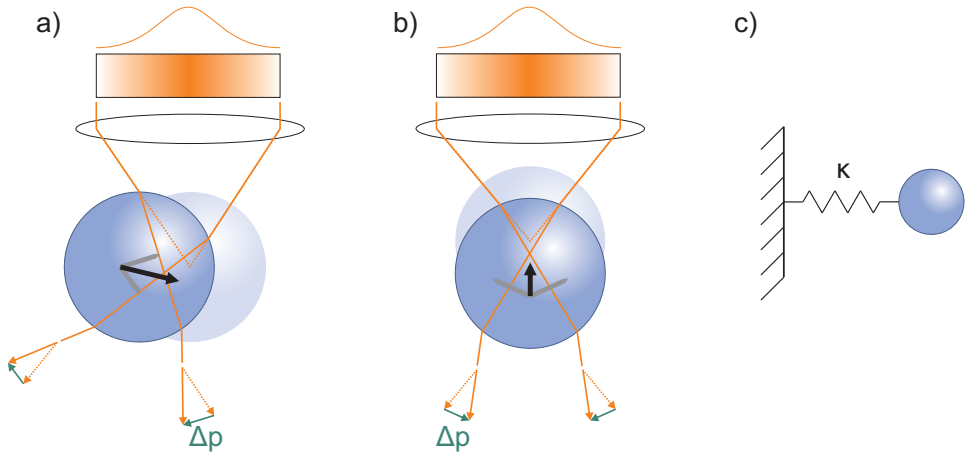

Figure 2.1 **Ray optics:** a) and b) show a cartoon of the forces acting on a bead which is displaced out of the trap center either in the horizontal a) or vertical direction b). The laser light of a Gaussian laser beam (orange) is focused by an objective lens and then diffracted by the bead. As an example, the optical path for two light beams is shown. The diffraction of the photons leads to a change in momentum Δp, shown as green arrows. The bead experiences the opposite momentum (grey arrows). The overall force on the bead is shown in black. For case a) it acts in direction of the focus, but is slightly pointed below the focus. For a vertical displacement the resulting force points toward the focus of the lens and consequently opposing to the to the direction of light. c) For small displacements out of the trap center the trap acts as an hookean spring with a spring constant κ.

induced dipole with the electrical field lead to the gradient force:

$$F_{\text{grad}} \sim \alpha \nabla I_0, \tag{2.1}$$

where α is the polarizability of the particle and I_0 the intensity of the incident light. Because the gradient force scales linearly with the laser intensity, also the trap stiffness κ will scale linearly with the laser power.

However, most experiments are done with particles which have a size around the wavelength of the incident laser light. In this case neither the Rayleigh regime nor the ray optics approximation hold true. Here the theoretical description is much more complicated and more advanced electromagnetic theories have to be used (Barton et al., 1989).

2.2 Bead dynamics and calibration

For small displacements of the bead the trap potential can be described as harmonic, therefore the optical trap acts as a Hookean spring on the trapped particle: $F = -\kappa x$, where F is the force on the particle, κ the trap stiffness and x the displacement out of the trap center. To measure forces it is therefore only necessary to measure the displacement x and calibrate the trap stiffness κ. This chapter describes some basic concepts of the bead dynamics in an optical trap potential and methods to calibrate the trap stiffness and position detection system.

The brownian motion of a bead in a harmonic trap potential can be described by the following Langevin equation (Berg-Sorensen and Flyvbjerg, 2004):

$$m\ddot{x}(t) + \gamma_0 \dot{x}(t) + \kappa x(t) = \sqrt{2k_B T \gamma_0}\eta(t) \tag{2.2}$$

Here $x(t)$ is the position of the Brownian particle, m its mass, κ the trap stiffness, and $\sqrt{2k_B T \gamma_0}\eta(t)$ a random thermal force with the properties:

$$\langle \eta(t) \rangle = 0; \ \langle \eta(t)\eta(t') \rangle = \delta(t - t') \tag{2.3}$$

The friction coefficient for a spherical particle is given by Stokes' law

$$\gamma_0 = 6\pi\rho\nu R, \tag{2.4}$$

where $\rho\nu$ is the shear viscosity of the medium, ρ the density of the medium, ν its kinematic viscosity and R the radius of the sphere. In water, the bead system is overdamped and therefore the inertial term in equation 2.2 can be neglected:

$$\dot{x}(t) + 2\pi f_c x(t) = \sqrt{2D}\eta(t) \tag{2.5}$$

with the corner frequency,

$$f_c \equiv \frac{\kappa}{2\pi\gamma_0} \tag{2.6}$$

and the Einstein relation between diffusion constant, Boltzmann energy and friction coefficient

$$D = \frac{k_B T}{\gamma_0}. \tag{2.7}$$

For calibration purposes it is useful to Fourier transform $x(t)$ to the frequency domain:

$$\hat{x}(f) = \int_{-\infty}^{\infty} \mathrm{d}t\, e^{i2\pi f t} x(t) = \frac{\hat{\eta}(f)\sqrt{2D}}{2\pi(f_c - if)}, \tag{2.8}$$

where $\hat{\eta}(f)$ is the Fourier transform of $\eta(f)$. The expectation value for the one-sided ($f \geqslant 0$) power spectral density (PSD) of the bead position is given by

$$P(f) = \frac{2\langle|\hat{x}(f)|^2\rangle}{t_{msr}} \xrightarrow[t_{msr}\to\infty]{} \frac{D}{\pi^2(f^2 + f_c^2)}. \tag{2.9}$$

This equation 2.9 describes a Lorentzian, originating from the Brownian motion of the bead in the parabolic trap potential.

2.2.1 Calibration of the optical trap

For the calibration of a bead in an optical trap, the position signal of the bead is recorded for a time t_{msr} at a frequency f_{sample}. The power spectral density of the measured data is then calculated. Equation 2.9 can be fit to the data, yielding the corner frequency f_c of the trapped particle. Together with equation 2.6 and the friction coefficient, the trap stiffness could be calculated. However, the friction coefficient γ_0 for a sphere is only given by $\gamma_0 = 6\pi\rho\nu R$ if the bead is far from any surface due to hydrodynamic effects. Additionally it has to be considered that the shear viscosity of the medium $\rho\nu$ depends on the temperature of the medium, which can substantially deviate from the room temperature due to heating of the sample chamber by the trapping laser (Peterman et al., 2003).

To overcome this problem Tolić-Nørrelykke et al. (2006) have developed a method which measures the drag coefficient experimentally. To achieve this, the sample chamber is driven in a sinusoidal motion with a translational stage. If the sample chamber is oscillated sinusoidally relative to the optical trap at a frequency f_{drive} and an amplitude A, the position of the stage as a function of time t is given by

$$x_{drive}(t) = A\sin(2\pi f_{drive} t). \tag{2.10}$$

With $v_{drive} \equiv \dot{x}_{drive}(t)$ the simplified Langevin equation 2.5 is changed to:

$$\dot{x}(t) - v_{drive} + 2\pi f_c x(t) = \sqrt{2D}\eta(t) \tag{2.11}$$

The Fourier transformation of this equation gives again the familiar Lorentzian with an additional delta-function peak at the driving frequency:

$$P(f) = P_{\mathrm{T}} + P_{\mathrm{response}} = \frac{D}{\pi^2(f^2 + f_{\mathrm{c}}^2)} + \frac{A^2}{2(1 + f_{\mathrm{c}}^2/f_{\mathrm{drive}}^2)}\delta(f - f_{\mathrm{drive}}). \tag{2.12}$$

Fig. 2.2 shows an exemplary power spectrum of a trapped bead, where the stage is moved in a sinusoidal fashion.

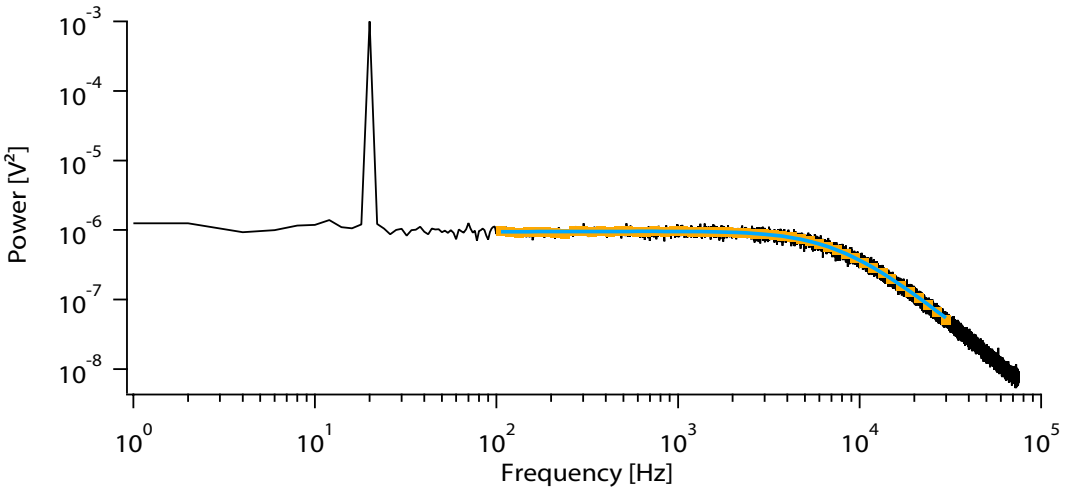

Figure 2.2 **Power spectral density:** Power spectral density of a trapped 1 µm silica bead with a corner frequency of $f_{\mathrm{c}} = 7654\,\mathrm{Hz}$. The sample chamber is moved sinusoidally at a frequency of 20 Hz. The displayed power spectral density is an average of 100 individual power spectra, each recorded at a frequency of $f_{\mathrm{sample}} = 150\,\mathrm{kHz}$ with a measurement time $t_{\mathrm{msr}} = 0.5\,\mathrm{s}$. The Lorentzian caused by thermal motion of the bead in the trapping potential can be seen, with an additional peak at driving frequency f_{drive} of the piezoelectric table. A fit to the blocked data (orange) is shown in blue.

Because the position of the bead is measured in volts, a calibration factor β has to be determined to know the positions in meters.

$$x(t) = \beta x^{\mathrm{volt}}(t) \tag{2.13}$$

This calibration factor can determined, using the measured PSD. With equation 2.13 the power spectral density in meter can be written as

$$P_{\mathrm{response}}(f) = \beta^2 P_{\mathrm{response}}^{\mathrm{volt}}(f). \tag{2.14}$$

$P_{\mathrm{response}}^{\mathrm{volt}}(f)$ is known experimentally. Since the driving amplitude A and frequency f_{drive} are known and f_{c} can be determined experimentally by fitting a Lorentzian to the power

spectrum, also P_{response} is known. Therefore the calibration factor β is given by

$$\beta = \sqrt{\frac{W_{\text{th}}}{W_{\text{ex}}}}, [\beta] = m/V, \tag{2.15}$$

with W_{ex} the experimentally determined power in the peak at the corresponding driving frequency in V^2 and W_{th} the theoretically calculated one in m^2. Following equation 2.12 the power W_{th} is determined by

$$W_{\text{th}} = \frac{A^2}{2(1 + f_c^2/f_{\text{drive}}^2)}. \tag{2.16}$$

With the previously described method, it is possible to determine the positional calibration factor β. To be able to analyze an experiment, one does not only need the positional calibration, but also a calibration of the force, respectively the trap stiffness κ. This can be achieved, by fitting equation 2.9 to the experimentally obtained PSD, determining f_c and D^{volt}. To improve the fitting procedure, noise reduction is done by blocking as described here (Tolić-Nørrelykke et al., 2006). Using equation 2.6 and 2.7 the trap stiffness is given by

$$\kappa = 2\pi f_c \frac{k_B T}{\beta^2 D^{\text{volt}}}. \tag{2.17}$$

With these values, the optical trap is sufficiently calibrated and the force on the bead κx and the displacement x out of the trap can be measured in their desired units.

For most experiments the accuracy of the previously described method is adequate and used throughout this thesis. If a more accurate calibration is needed, several factors have to be considered, e.g. the temporal response of the detector (see chapter 2.4.1), hydrodynamic effects, aliasing effects of the data acquisition board (Berg-Sorensen and Flyvbjerg, 2004; Berg-Sørensen et al., 2006).

2.3 Design of an optical trap setup

The setup, which was built as part of this thesis, is a dual beam optical trap. Various considerations, including temperature control and air fluctuations, have to be taken care of, to realize a low drift, high performance instrument. This chapter introduces the design of the trap. A schematic of the setup can be seen in Fig. 2.3. The trap consists of a laser which is split into its two polarization directions, resulting in two beams, of whom one can be steered by a piezo electric mirror. Both beams are focused by a water immersion objective in the specimen plane, creating two separate optical traps. With an identical objective the beams are collimated on the other side and split again according to their polarization directions. The backfocal plane of the collimating objective is imaged on two separate quadrant photo diodes allowing independent detection of both

traps. Additionally, bright field imaging is incorporated in the setup, allowing the observation of the specimen plane. Furthermore, epi and confocal fluorescence capabilities are integrated with two different excitation wavelengths. The fluorescence signal can be detected by an EMCCD camera as well as an avalanche photo diode.

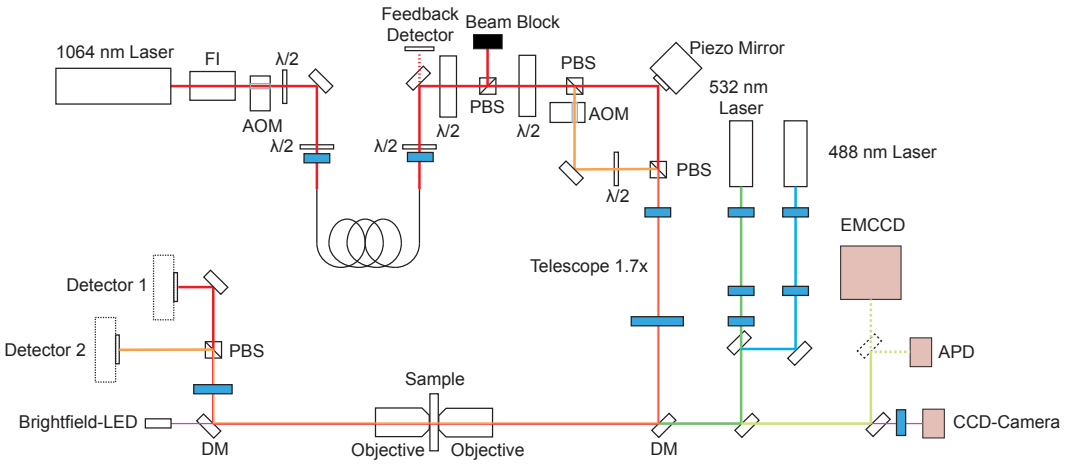

Figure 2.3 **Optical trap design:** Sketch of the optical trap design including the trapping and fluorescence parts. The trapping laser light is shown in red and orange, fluorescence excitation at 532 nm in green and 488 nm in blue. Light green represents the emitted fluorescence light. If not otherwise labeled black rectangles correspond to mirrors and blue rectangles to lenses. FI: Faraday isolator, AOM: Acousto optical modulator, PBS: Polarizing beam splitter cube, DM: Dichroic mirror, APD: Avalanche photodiode

2.3.1 Design considerations

Several design considerations have to be taken into account when planning an optical trap setup. One of the main issues is the telescope following the piezo electric mirror. It serves two purposes, the first one is expanding the beam to fill the back aperture of the objective. Recent investigations by Mahamdeh et al. (2011) have shown that underfilling the objective improve the use of the available laser power, but trapping the beads gets more difficult. The second purpose of the telescope is imaging the rotation plane of the piezo electric mirror onto the back focal plane of the objective. The second purpose of the telescope is crucial for uniform trap stiffness throughout the whole scan range of the piezo mirror. If the rotation plane is not imaged in the back focal plane of the objective, the beam is clipped by the back aperture when it is moved out of the center position, thereby decreasing the power going into the objective and affecting the trap stiffness. Imaging in the back focal plane has an additional function. The back focal plane of the trapping objective is conjugate to the back focal plane of the condensor objective. If the

back focal plane of the condensor objective is imaged onto the detector, the detector is in a conjugate plane to the back focal planes of the objectives as well as the piezo mirror rotation plane. In this configuration any scanning of the bead with the piezo mirror will not show up on the detector. The required distance and focal length relationship between piezo mirror, the telescope lenses, and the objective are well described by (Fällman and Axner, 1997). Because the piezo mirror has only a limited scan range, it is important to pay attention to the movement d of the laser in the specimen plane in relation to the tilt angle of the piezo mirror α

$$d = 2 f_{\mathrm{EFL}} \frac{f_1}{f_2} \alpha, \tag{2.18}$$

where f_1 and f_2 are the focal lengths of the two telescope lenses and f_{EFL} the effective focal length of the objective $f_{\mathrm{EFL}} = \frac{t}{M}$ with the tube length t and the magnification M. For our setup we chose a combination of lenses so that the movement of the laser in the specimen plane is at least 10 µm. The telescope does not only image the rotation plane of the piezo mirror on the back focal plane of the objective, but also expands the beam by $\frac{f_2}{f_1}$. Therefore additional restriction for the choice of focal lengths exist to ensure the desired filling ratio of the back aperture of the objective.

2.3.2 Trap layout and beam path

The optical trap uses a linearly polarized 4 W 1064 nm Nd:YVO_4 diode pumped solid state laser with a TEM_{00} mode for trapping (J20I-BL-106C, Spectra-Physics, USA). The laser head, containing the Nd:YVO_4 crystal, is mounted on the optical table. To prevent disturbances of the optical trap by the fan cooled pumping diodes, they are located in a room next door. The pumping light is transmitted to the laser head via a multimode optical fiber. The laser is operated at its maximum operating power. Tests at different power levels show no difference in output stability. The laser light passes a Faraday isolator (EOT-189.12011, Electro-Optics Technology Inc., USA) preventing back reflections entering the laser head, which will cause instabilities of the output beam.

To stabilize the laser further, a stabilization system including an acousto optical modulator (AOM) and a single mode optical fiber is incorporated. This system is described in more detail in the next chapter. Briefly, after passing an AOM, which can rapidly change the intensity of the laser, the laser is coupled into a single mode optical fiber. After the fiber, the laser light is collimated again and a small part of the laser light is sent to a detector, which can be used to feedback the AOM and thereby stabilize the laser output.

The stabilized and collimated laser beam passes a computer controlled motorized $\lambda/2$ plate, which in combination with a polarizing beam splitter cube (PBS) controls the overall laser power passing into the following optical parts. A second motorized

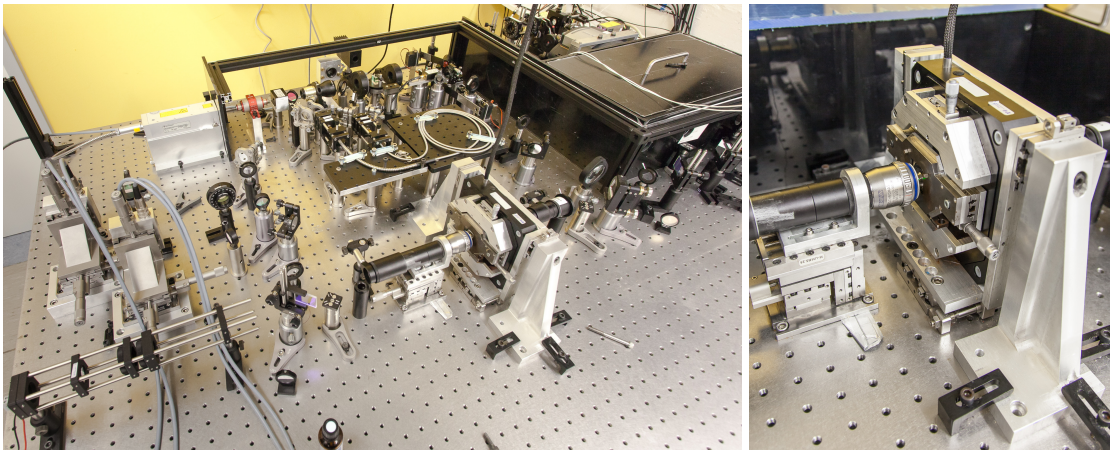

(a) (b)

Figure 2.4 **The optical trap setup:** a) The optical trap setup without enclosure, including the laser stabilization scheme. b) Closeup of the sample holder, including the piezo table and the manual linear stages to move the sample stage. Also visible is the back objective mounted on an xyz translational stage.

$\lambda/2$ plate sets the relative laser power in the two orthogonally polarized trapping beams separated by a second PBS. One of the beams is reflected by a mirror mounted on a two axis piezoelectric tip/tilt actuator (MTA2X HS, Mad City Labs, USA) allowing lateral displacement of the corresponding trap in the specimen plane. The second beam passes an AOM (M080-2G-LV10, Gooch & Housego, Great Britain) and gets frequency shifted by 80 MHz to reduce interference artifacts between the two beams (Mangeol and Bockelmann, 2008). The frequency shifted beam gets reflected by a mirror held in a manual mirror mount which allows aligning the beam in respect to the other beam. A $\lambda/2$ plate in this beam path compensates for the rotation of the polarization by the AOM. After recombination of the two beams by a third PBS, a telescope expands the beams to fill the 6.3 mm back aperture of the trapping objective (C-Apochromat 63x/1,20 W Korr M27, Zeiss, Germany). As mentioned in 2.3.1, the telescope has to image the rotation plane of the piezo mirror on the back focal plane of the objective as well. To achieve this, care has to be taken to position the objective at the right position corresponding to the telescope and piezo mirror. The objective focuses the beams to two diffraction limited spots in the sample chamber. A water immersion objective is used allowing trapping deep inside the sample chamber due to reduced spherical aberrations. For measurements, the distance of the beads from the coverslip is set to 20 µm to hydrodynamically decouple the trapped beads from the sample chamber. The sample chamber is mounted on a manually controlled two axis translation stage, which in turn is mounted on a three axis computer controlled piezoelectric table (P-517.3CL, Physik Instrumente, Germany). To simplify the alignment of the objective relative to the laser beam, the sample chamber

is perpendicular to the optical table. Therefore, the beam path can be kept on the same height throughout the whole setup. A second identical objective collimates the beams after the sample chamber. Both objectives are mounted on manual three axis translational stages (M-561D-XYZ, Newport, USA) allowing movement of the objectives in all directions 2.4. After the second objective, the beams are split by polarization and the back focal plane of the objective is imaged onto two quadrant photo diodes (QP154-Q-HVSD, First Sensor, Germany). This allows the detection of the position of the beads deflected out of the trap focus. Due to depolarization in the optical path and the intrinsic non-perfect separation and conservation of polarization upon transmission through and reflection by the PBSs, each of the detector signals also reflects the motion of the bead in the "wrong" trap to a certain degree; this effect, known as polarization crosstalk (Atakhorrami et al., 2008), has to be considered in the measurements as described in Gebhardt (2009).

For bright field illumination, a 780 nm LED is used in order to prevent interfere with the fluorescence or trapping. After the objective, the specimen plane is imaged onto a CMOS camera (DCC1545M, Thorlabs, USA).

Special care has been taken to mount all components with the highest stability. Standard optical components, like lenses and mirrors, are mounted on 1 inch posts. For other parts, like piezo mirror and Faraday isolator, custom built mounts were used. To reduce the effect of air fluctuations and temperature drifts the whole setup is enclosed with black IR-blocking 8 mm acrylic glass.

2.3.3 Laser stabilization

The 1064 nm laser used in this optical trap setup exhibited power and pointing instabilities on the tens of seconds timescale. To improve power and pointing properties of the laser, a stabilization scheme as shown by Carter et al. (2009) was implemented. The laser was coupled into a single mode polarization maintaining fiber via an aspheric lens. This translates pointing instabilities into intensity fluctuations at the output of the fiber. The output of the fiber is collimated and monitored with a beam sampler transmitting about 2 % onto a detector (DL100-7PCBA3, First Sensor, Germany). An AOM (FS080-2S2G-3-LV1, Gooch & Housego, Great Britain) is located before the laser enters the fiber and is able to stabilize the laser intensity with the detector in a feedback loop. When coupling the laser into the fiber, care has to be taken to align the polarization direction of the laser with one of the optical axis of the fiber. Otherwise the polarization maintaining properties of the fiber are not assured. To increase the polarization ratio of the output light a plate polarizer is added after the fiber. This stabilization scheme results in a intensity and pointing stabilized beam with an improved beam profile due to the use of a single mode optical fiber.

2.3.4 Electronics

The quadrant photo diodes (QPD) have a built-in preamplifier and output a signal for x- and y-deflection as well as a sum signal for the overall intensity reaching them. Custom built electronics are used for processing the analog position signals from the QPDs (Perpina et al., 2005). Residual offsets in the outputs are individually corrected to allow subsequent normalization with the sum signal and amplification for each channel. Because the x- and y-outputs of the QPDs are proportional to the incoming light intensity, the normalization serves two purposes. First it prevents mistaking intensity fluctuations for deflections in the x- or y-plane. Second it ensures that the same amplification settings can be used for different laser intensities. All custom built electronics were tested to perform even at high frequencies up to 500 kHz. Before recording, all signals are anti-alias filtered with an eighth order Butterworth filter with a 3dB-frequency set to half the acquisition frequency and further amplified (Model 3384 Filter, Kron-Hite, USA). For real-time steering and data aquisition, a custom written LABVIEW program runs on a field-programmable gate array (FPGA)-board (NI PCIe-7852R, National Instruments, USA).

2.3.5 Fluorescence microscope

A fluorescence microscope is integrated in the optical trap setup to observe fluorescently labeled beads as well as single molecule fluorescence. A 488 nm fiber coupled laser (BDL 488 SMC, Becker & Hickl, Germany) and a 532 nm solid state laser (RLTMGL-532-50, Roithner Lasertechnik, Austria) is expanded and collimated. The 532 nm laser is then focused onto the back focal plane of the objective. Both lasers are combined with a dichroic mirror. The collimated 488 nm laser creates a diffraction limited spot in the specimen plane. This makes it useful for observing single fluophores because the background illumination is limited. The 532 nm laser, on the other hand, illuminates a large area in the sample chamber, in a so called epi fluorescence illumination. The emitted fluorescence light is reflected by a dichroic mirror and imaged either on an EMCCD camera (DV887-DCS-BV, Andor Technology, USA) or an avalanche photo diode (ID100, IDQ, Switzerland) by removing or inserting a mirror on a kinematic base. To eliminate vibrations the EMCCD camera is water cooled with the water cooling device located in a different room.

2.4 Characterization

2.4.1 Temporal response of the detectors

Position detectors such as quadrant photodiodes or position sensitive devices (PSD) facilitate high bandwidth position detection compared to other techniques like video based

detection. These diode based detectors function by creating electron-hole pairs upon the absorption of photons. Due to the applied electrical field, the electron and hole in the depletion zone of the photodiode rapidly move to the cathode and anode respectively, thereby creating a photocurrent. For wavelengths below 800 nm, this simple picture reflects the reality fairly well. For wavelengths above 800 nm however, the optical absorption of silicon decreases (Green, 2008). Additional electron hole pairs are created outside the depletion zone. These pairs have to diffuse to the depletion zone first, before they can move to the anode and cathode. This diffusion process is much slower than the rapid movement in the depletion zone to the electrodes. This slow diffusion process causes an additional slow component to the otherwise fast electrical response. The slow component thereby limits the bandwidth of this kind of detector. For a trapped bead the diode's response can be described as the sum of two terms (Berg-Sørensen et al., 2006): A fraction $\alpha^{(\mathrm{diode})}$ that is instantaneous, corresponding to the electron-hole pairs created in the depletion zone, and a low-pass filtered one, corresponding to the electron hole pairs created outside the depletion zone.

$$\frac{P(f)}{P_0(f)} = \alpha^{(\mathrm{diode})2} + \frac{1-\alpha^{(\mathrm{diode})2}}{1+(f/f_{3\mathrm{dB}}^{(\mathrm{diode})})^2}, \tag{2.19}$$

where $P(f)$ is the recorded filtered power spectral density, $P_0(f)$ the ideal unfiltered power spectral density and $f_{3\mathrm{dB}}$ the 3dB frequency of the detector. If the Nyquist frequency is not significantly larger than $f_{3\mathrm{dB}}^{(\mathrm{diode})}$ and $\alpha^{(\mathrm{diode})2}$ is small, it is difficult to separate $f_{3\mathrm{dB}}^{(\mathrm{diode})}$ and $\alpha^{(\mathrm{diode})2}$ in the fit. If we introduce

$$f_{3\mathrm{dB}}^{(\mathrm{diode,eff})} \equiv (1-\alpha^{(\mathrm{diode})2})^{-\frac{1}{2}} f_{3\mathrm{dB}}^{(\mathrm{diode})} \tag{2.20}$$

equation 2.19 can be approximated by

$$\frac{P(f)}{P_0(f)} \approx \frac{1}{1+(f/f_{3\mathrm{dB}}^{(\mathrm{diode,eff})})}. \tag{2.21}$$

This equation can be fit more easily to the data, if the aforementioned conditions are met.

Fig. 2.5 shows the power spectral density of a trapped bead using two different detectors. The power spectral density recorded by the PSD starts to fall off at lower frequency than the one recorded with the QPD, indicating a smaller bandwidth of the PSD compared to the QPD. This is confirmed by fitting the data with a theory including filter effects of the diode as described in chapter 2.2.1. The 3dB frequency of the quadrant photodiode is about three times higher than the 3dB frequency of the position sensitive device. If the bandwidth of the detector is not significantly higher than the corner frequency of the trap, as it is in the case of the PSD, care has to be taken when fitting the

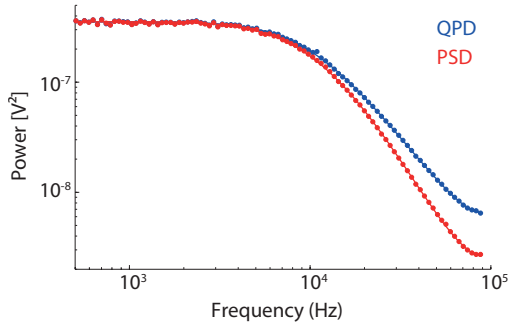

(a)

	QPD	PSD
$f_{3dB,Bead}$	(10169 ± 39) Hz	(9677 ± 52) Hz
$f_{3dB,Diode}$	(98866 ± 17620) Hz	(34199 ± 482) Hz
α_{Diode}	0.8	0.5

(b)

Figure 2.5 **Comparison of QPD and PSD:** a) Power spectral density of a trapped 1 µm silica bead recorded at 180 kHz for 10 seconds with a QPD (blue) and a position sensitive device (red). For this measurement the data was not anti-alias filtered before recording. Shown as dotted points is the blocked data of the original power spectral density. The solid lines are fits to the data. The fitting model includes the filter effects of the diode, see equation 2.19, aliasing effects and hydrodynamic coupling. The resulting fit coefficients are shown in b).

power spectrum of a trapped bead. In this case not considering the filtering effect of the diode may lead to an underestimation of the corner frequency of the trapped bead. For the shown example in Fig. 2.5, a fit without the filter effects results in an underestimation of the corner frequency of about 20 %. The reduced bandwidth of the PSD is not only critical for the calibration, but also the actual measurement will suffer from the smaller bandwidth. Therefore, we replaced the previously used PSD with the QPD in the optical trap setup.

2.4.2 Trap stiffness and sensitivity

As mentioned in chapter 2.1, the trap stiffness scales linearly with the power going into the trapping objective. For trapped 1 µm silica and polystyrene beads the trap stiffness over the power going into the objective is shown in Fig. 2.6a). Indeed, the relation between trap stiffness and intensity is linear. As expected, polystyrene beads, due to their higher index of refraction, show a higher trap stiffness per power going into the objective than the silica beads. As described earlier the difference in refractive index of the medium and the bead leads to refraction of the light which is bigger with a higher difference in refractive index. Thus it would be logical to choose polysterene over silica beads. However, Landry et al. (2009) showed that the presence of polystyrene beads in a laser trap lead to an increased amount of oxygen damage to the sample. The polystyrene surface together with the laser radiation catalyzes the production of oxygen radicals which can damage the protein of interest. They also showed that the

generation of oxygen radicals is reduced when silica beads are used. Since the trap stiffness achievable with silica beads is still high enough for most experiments, silica beads were solely used for this work.

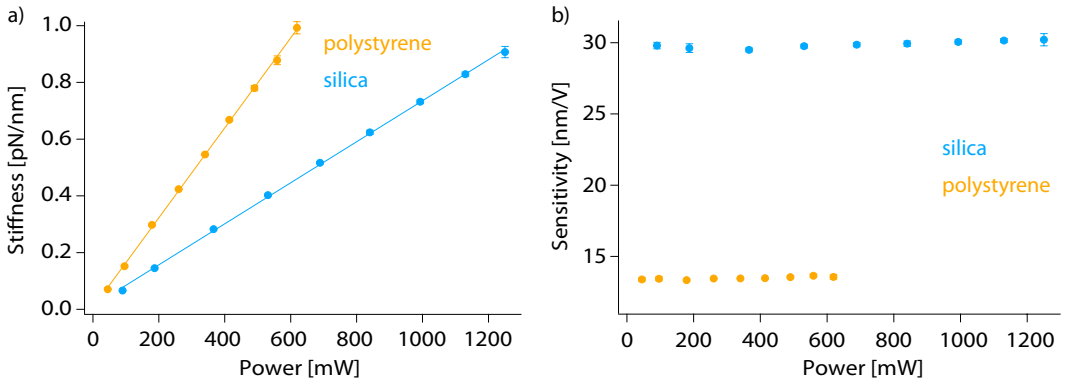

Figure 2.6 **Trap stiffness and sensitivity over power:** a) Trap stiffness for 1 µm polystyrene (orange) and silica (blue) beads versus the laser power going into the objective. As expected, the trap stiffness increases linearly with the intensity of the laser going into the objective. For a given laser power, the trap stiffness of polystyrene beads is about twice as high as for silica beads. b) Sensitivity of the trap versus the laser power going into the objective. For polystyrene beads and silica beads the sensitivity is constant over the whole power range, due to the normalization of the signals. The values plotted in a) and b) are averages of five individual measurements of the same bead pair for each power setting, error bars indicate the standard deviation.

Because the position signal of the beads is normalized by the sum signal of the QPD as described in 2.3.4, the sensitivity is constant independent of the laser power going into objective as shown in Fig. 2.6b). This confirms that the custom built normalization electronics work properly.

2.4.3 Linearity of the optical trap

The detector response of the deflection of a bead out of the trap focus is only linear for a limited displacement out of the trap center. Fig. 2.7 shows a scan with the piezo table of a bead stuck to the coverslip through the optical trap. It can be clearly seen that the linear region only extends about ±100 nm out of the center of the trap. For the experiment it has to be made sure that the trap stiffness is chosen not to exceed the linear region of the detection system under force.

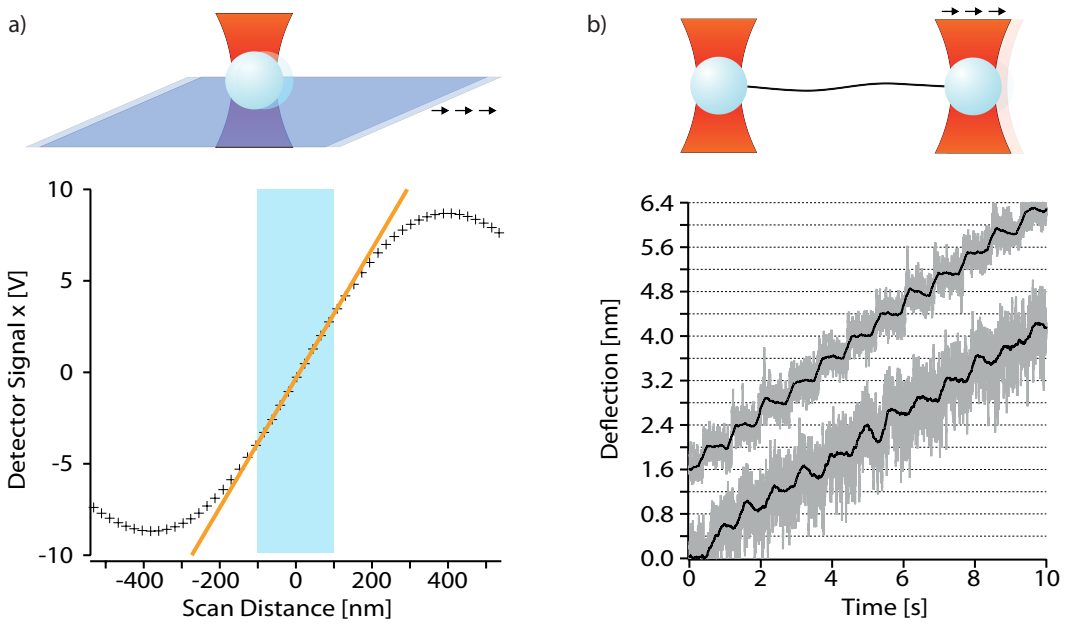

Figure 2.7 **Linearity and resolution of an optical trap:** a) A 1 µm silica bead stuck on the coverslip is moved in a step wise fashion through the laser beam with the piezo stage. The detector signal for each position is recorded and averaged. The orange line is a fit to the linear region (shaded blue) from about −100 nm to 100 nm. b) Demonstration of the resolution of the optical trap setup. Plotted is the difference signal of two 1 µm silica beads which are connected by a 370 nm dsDNA molecule. The bead to bead distance is increased with the piezo mirror in 4.8 Å steps. The upper trace corresponds to a force around 21 pN, the lower trace to around 8 pN. The data is box-car filtered from 30 kHz to 200 Hz (grey), respectively 4 Hz (black).

2.4.4 Resolution

The spatial resolution of the setup was tested by changing the bead to bead distance of two beads connected by a DNA molecule in small increments with the piezo mirror. As seen in Fig. 2.7 individual steps of 4.8 Å can be observed. The size of the steps with the piezo mirror is limited due to the 16 bit D/A converter of the FPGA board. The piezo mirror is controlled by −10 V to 10 V signal, therefore the smallest achievable step distance s_{min} is given by

$$s_{\mathrm{min}} = a_{\mathrm{calib}} \frac{20\,\mathrm{V}}{2^{16}}, \tag{2.22}$$

where a_{calib} is the calibration factor for the piezo mirror in nm/V. For this setup the smallest step distance is $s_{\mathrm{min}} = 2.4\,\text{Å}$.

Often it is assumed that the temporal resolution of the optical trap is given by the corner frequency $f_{3\mathrm{db}}$ of the bead or in a dual bead assay the roll-off frequency of the difference signal at zero force (in a typical experiment ca. 3.5 kHz). However, the time resolution to observe transitions is not given by the roll-off frequency, but the autocorrelation time of the relative bead motion $\tau = \frac{1}{2\pi f_{3\mathrm{db}}}$. Additionally, due to the increase in stiffness of the bead-DNA-bead system at higher forces the autocorrelation time decreases from 56 µs at 0 pN to 5 µs at 20 pN. The rather slow roll-off of the bead-DNA system acts as a single pole filter. If the sample rate is not significantly higher than the roll-off frequency $f_{3\mathrm{db}}$, kinetic information will be missed. Therefore, the acquisition frequency is set to 150 kHz, if a fast process is studied. A more detailed discussion with measurements of the ultrafast folding protein villin headpiece can be found here (Zoldák et al., 2013).

2.5 Measurement procedures

2.5.1 Dumbbell assay

To use optical traps for force spectroscopy measurements, the sample of interest has to be fixed on one side and pulled on the other by the optical trap. Many experiments have been done where the sample was fixed on one side on the surface or a bead which is held by glass pipette tip (Wen et al., 2008; Asbury et al., 2003; Ferrer et al., 2008). Forces up to ~100 pN can be reached in this configuration, because only one optical trap is used. However, linking the sample to a fixed surface leads to coupling of extrinsic noise into the measurement, e.g. vibrations of the optical table, drift of the sample chamber relative to the optical trap. Attempts have been made to counter these problems (Nugent-Glandorf and Perkins, 2004), but they rely on advanced feedback mechanisms. To overcome these issues, we work with our dual optical trap in a so called dumbbell configuration. The protein of interest is coupled to two beads with dsDNA handles. This approach decouples the measurement system from the sample chamber and the effect of

relative drifts of the sample chamber to the optical traps is greatly reduced. In this setup, both traps are formed by the same laser, therefore the influence of pointing instabilities of the laser or air fluctuations throughout the setup is reduced. If the force on the sample is not determined by the signal of the single bead itself, but the relative movement of the two beads the signal to noise ratio can be greatly increased (Moffitt et al., 2006).

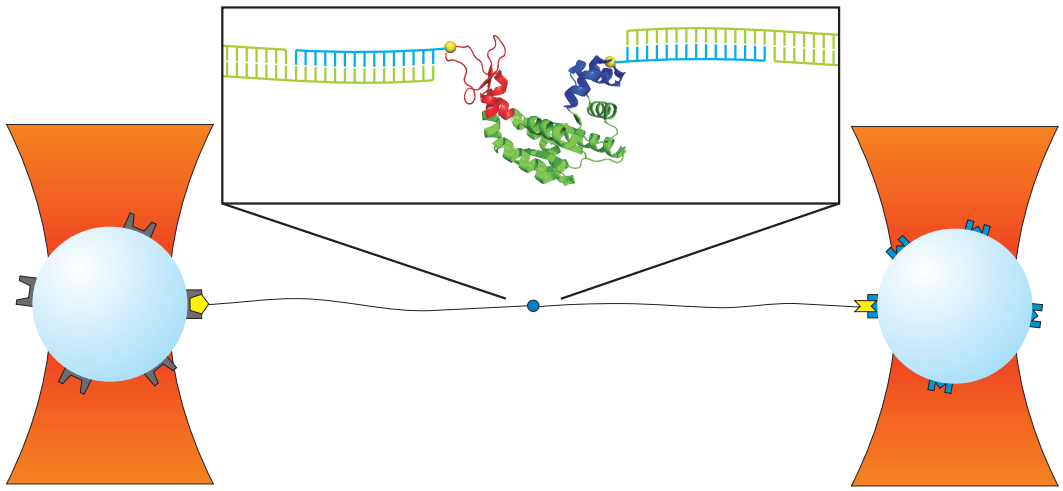

Figure 2.8 **Dumbbell configuration:** Sketch of the bead handle protein construct. The beads are functionalized with either anti-digoxigenin (dark grey) or streptavidin (blue). The DNA handles (black, respectively green in the insert) have digoxigenin (yellow) or biotin (orange) on one end and are connected via the maleimide cysteine linkage to the protein, in this case adenylate kinase, on the other end. In the insert the single stranded overhang of the dsDNA handles is shown, which binds to the maleimide modified oligo (blue).

For the dumbbell assay, we use two differently functionalized beads, one of them is coated with an antibody fragment of anti-digoxigenin and the other with streptavidin. For the functionalization carboxy-modified silica beads are used in a custom made protocol. The anti-digoxigenin respectively streptavidin is cross linked to the carboxy groups with NHS and EDC. One of the beads is additionally fluorescently labeled by rhodamine-BSA. Two different types of dsDNA are made using polymerase chain reaction (PCR). For both types, the 3'-5' primer contains an abasic site. If the DNA polymerase encounters the abasic site it falls off and leaves a 34 basepair (bp) single stranded overhang. The sense primer contains either three biotin or digoxigenin molecules. To link the protein of interest to the DNA handles, two cysteins have to be introduced at the positions where the force on the molecule should be exerted. Any other solvent exposed cysteins should be removed to reduce the possibility of unwanted pulling directions. Single stranded oligos of 34 bp with a maleimide at the 3'-end are covalently coupled to the cysteins by forming a stable carbon-sulfur bond. The oligos

coupled to the protein are complementary to the single strand overhang of the dsDNA handles. When the oligo coupled protein and the dsDNA handles are incubated, they hybridize and form the desired construct shown in Fig. 2.8.

2.5.2 Constant velocity experiments

Constant velocity experiments are generally performed to assess the overall force response of a protein of interest in the optical trap. Fig. 2.9 shows an exemplary trace of a constant velocity experiment. A streptavidin and an anti-dig coated bead are trapped and brought into close proximity. If a dumbbell of the protein handle construct with the bead forms, the beads are separated again with a constant velocity ranging between $10\,\mathrm{nm\,s^{-1}}$ and $1000\,\mathrm{nm\,s^{-1}}$. By retracting the mobile trap from the fixed trap, a force along the pulling direction is exerted on the construct. Upon approaching the contour length of the dsDNA handles the force rises until parts of the protein unfold. This is indicated by a contour length increase and a subsequent drop in force, caused by the bead relaxation in the trap potential. From the contour length increase, the number of unfolded amino acids can be calculated. Further stretching of the construct will lead to complete unfolding of the protein or detachment of the construct from the bead.

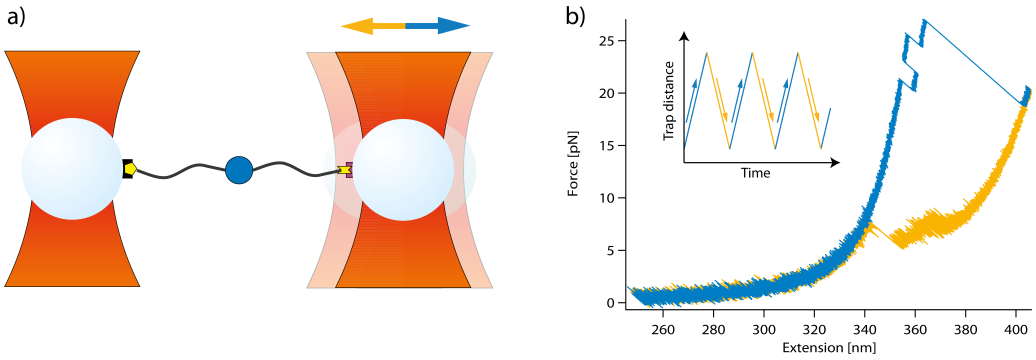

Figure 2.9 **Constant velocity experiment:** a) Sketch of a constant velocity experiment. Two beads (blue spheres) are held in a dual beam optical trap (orange cones). The protein of interest (small blue sphere) is linked to the two beads by dsDNA handles. The right trap is moved in a sawtooth like pattern with a constant velocity. b) By increasing and decreasing the trap to trap distance (inset) the construct will be stretched (blue) and relaxed (orange). This yields a typical force extension filtered to 1 kHz as shown in b).

If the beads are approached again, the force decreases and depending on the protein, it can refold against force. If this is not the case, waiting times at zero force enable the protein to refold without load. These stretch and relax cycles can be repeated up to several hundred times, yielding un- and refolding force distributions. If this is done at

several different pulling speeds, information about the energy landscape of the protein can be obtained (Hummer and Szabo, 2003; Dudko et al., 2008).

2.5.3 Constant distance experiments

As described in the previous chapter, constant velocity experiments give a good overview of the folding pattern of a protein but quantitative data about conformational fluctuations is more difficult to extract. For this purpose, constant distance experiments are performed. In this experimental procedure the two traps are held at a constant separation, thus applying a quasi constant force bias on the protein. Due to the length increase upon unfolding of the protein, the force bias in the folded state will be higher than the one in the unfolded state. Constant force experiments can circumvent this issue but they require a feedback mechanism to assure constant force conditions. The finite response time of the feedback loop limits the measurement bandwidth to typically < 1 kHz (Lang et al., 2002). We therefore performed all our experiments in constant distance conditions to allow the observation of fast conformational fluctuations. Fig. 2.10 shows the time trace of a typical constant distance experiment performed on a two state folding/unfolding process. The force trace shows two distinct levels, the one at high forces corresponding to the folded state, the one at low forces corresponding to the unfolded state. At forces where both states are populated, unfolding and folding transitions can be observerd, indicated by switching from the high force state to the low force state, or vice versa. At low biasing forces the protein is predominantly in the folded state. If the biasing force is increased, the equilibrium is shifted more towards the unfolded state, increasing the population of the unfolded state. Pair correlation analysis (Hoffmann and Woodside, 2011) or Hidden Markov Models (see chapter 3.2) can be used to extract quantitative data. The obtained dwell time distributions and population probabilities of the states can be used to calculate force-dependent kinetic rates as well as equilibrium free energies. Chapter 3 describes this in more detail and shows how kinetic and equilibrium information at zero force can be obtained.

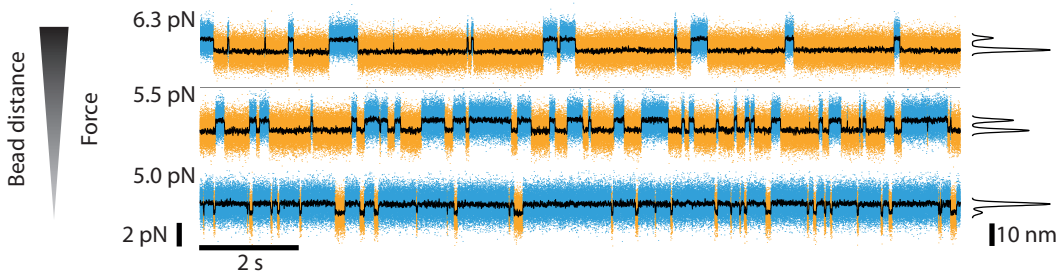

Figure 2.10 **Constant distance experiment:** Exemplary constant distance trace of the folding and unfolding transition of a protein at three different force biases, increasing force from bottom to top. The force respectively deflection signal is sampled at 20 kHz (dots) and filtered to 200 Hz (black line). The unfolded structure is depicted in orange and the folded in blue. By increasing the force the equilibrium is shifted from the folded to the unfolded state.

3 Analysis of single molecule experiments

The raw data obtained from optical trap experiments, either with the constant velocity or constant distance method contain all the relevant information. However, these results cannot be compared to other methods without further analysis. This chapter will give an introduction to the relevant models and techniques to extract force independent measures out of the optical trap data. First, polymer models are introduced, which describe the behavior of the DNA and protein under force. Then we will describe Hidden Markov Models, which help to assign different states in constant distance experiments. From this assignment transition rate constants and equilibrium free energies can be calculated. The obtained values are force dependent and two models are introduced which allow the extrapolation of these measures to force-free conditions. In the end the effect of ligand binding on transition rates and equilibrium free energies is described.

3.1 Polymer models

The force-extension behavior of polymers, seen in constant velocity experiments (see chapter 2.5.2), are mostly governed by entropic effects and can be described by different polymer models. The worm like chain (WLC) e.g. describes the force extension behavior of a protein well. Because exact solutions of the model are difficult to obtain, Bustamante et al. (1994) introduced the following interpolation formula:

$$F_{\mathrm{WLC}}(x) = \frac{k_{\mathrm{B}}T}{p}\left(\frac{1}{4\left(1-\frac{x}{L}\right)^2} - \frac{1}{4} + \frac{x}{L}\right) \tag{3.1}$$

with the persistence length p, the contour length L and the extension x. For DNA the extensibility of the molecule cannot be neglected anymore. To account for this, an elastic modulus K is introduced to extend the WLC model to an extensible worm like chain model (eWLC) (Wang et al., 1997):

$$F_{\mathrm{eWLC}}(x) = \frac{k_{\mathrm{B}}T}{p}\left(\frac{1}{4\left(1-\frac{x}{L}-\frac{F}{K}\right)^2} - \frac{1}{4} + \frac{x}{L} - \frac{F}{K}\right) \tag{3.2}$$

For constant velocity experiments the eWLC model is fit to the force extension data up to the force where the first unfolding occurs, to obtain the DNA-linker parameters. The combined force extension behavior of the DNA and the unfolded protein can then be described by the following serial combination of eWLC for the DNA and WLC model for the protein:

$$x_{\mathrm{Dumbbell}}(F) = x_{\mathrm{eWLC}}(F) + x_{\mathrm{WLC}}(F) \tag{3.3}$$

To obtain the contour length increase upon unfolding, the folded and unfolded parts of the force extension curve are fit to the previously described WLC models. The theoretically expected contour length increase between amino acid i and j is given by the number N_{ji} of unfolded amino acids each contributing $d_{\mathrm{aa}} = 3.65\,\text{Å}$ (Dietz and Rief, 2006):

$$d_{\mathrm{i,j}} = N_{\mathrm{ji}} d_{\mathrm{aa}} - \Delta L_{\mathrm{i,j}} \tag{3.4}$$

Here $\Delta L_{\mathrm{i,j}}$ is the distance between amino acid i and j in the folded structure before the unfolding event. $\Delta L_{\mathrm{i,j}}$ can be obtained from the crystal structure of the protein.

The persistence length of the unfolded peptide chain p_{prot} used to fit the WLC model to the data in force extension measurements previously ranged from 0.35 nm to 0.7 nm (Dietz and Rief, 2006; Gebhardt et al., 2010). However, if these persistence lengths are used to fit the unfolding transitions of the protein investigated in this thesis, systematic deviations from the data can be observed. To determine the appropriate persistence length, the force distance data of the unfolding transition itself can be used. Therefore, the distance between folded and unfolded state is calculated for each force.

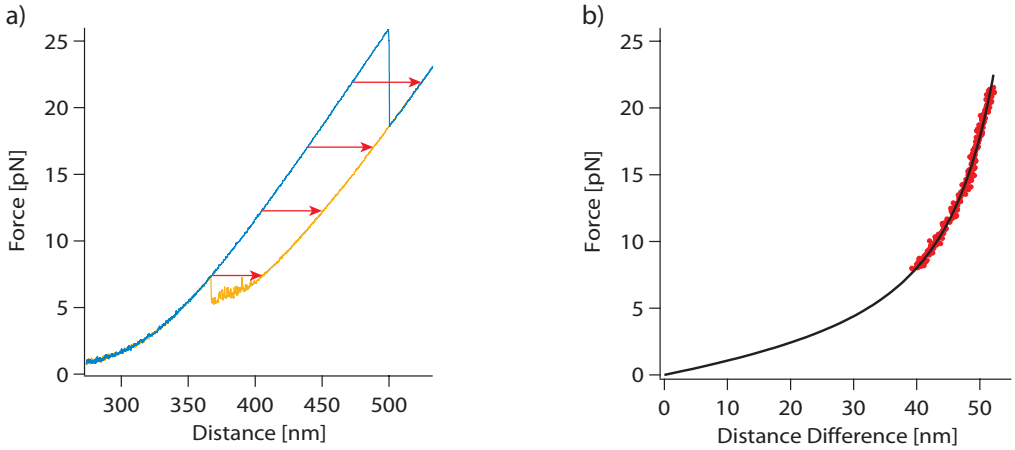

Figure 3.1 **Protein persistence length:** a) Force distance trace of an unfolding transition of adenylate kinase. The stretch curve is shown in blue and the relaxation curve in orange. Red lines are exemplary distances between folded and unfolded state. b) Distance between folded and unfolded state from a) for different forces. Black line is a fit of the WLC model to the data with a persistence length of 0.9 nm.

Fig. 3.1a) shows a exemplary force distance trace of an unfolding transition. The horizontal red lines indicate the distance between folded and unfolded state for four different forces. This distance is calculated over the whole force range, where the fully folded and unfolded state is present. A plot of these distances against the corresponding force as shown in Fig. 3.1b). A fit of equation 3.1 to the data yields the contour length increase upon unfolding, as well as the persistence length of the unfolded peptide chain. For adenylate kinase the data could best be fit with a persistence length of 0.9 nm. This is the persistence length used throughout the remainder of this thesis for the unfolded peptide chain. An advantage of this method is the independence of the DNA parameters. The fit does, therefore, not depend on choosing the right elastic modulus K for the DNA or the persistence length p_{DNA}. Additionally nonlinearities of the DNA or the optical trap are compensated in this method as well.

3.2 Hidden Markov Model analysis

As shown in chapter 2.5.3 the protein fluctuates between different conformations during constant distance experiments. Stigler and Rief (2012) have applied a Hidden Markov Model to assign each data point from a optical trap experiment to a specific state and account for missed events. The model is based on the assumption that the system undergoes a memory-less continuous-time Markov process, where the transition probability only depends on the current state and is constant over time.

The HMM analysis is used to assign each data point of the raw 30 kHz deflection trajectory to one of the system's conformations. At the beginning the raw difference signal is discretized in typically 50 bins. The initial level positions are either determined by calculating a histogram of the smoothed data or by eye. The emission values are initialized with Gaussian distributions around the previously determined initial level positions. Additionally the transition probability matrix has to be initialized. During the iteration process consisting of a so called forward-backward algorithm in combination with a Baum-Welch algorithm, each data point is classified to one of the states. During the iteration process the emission probabilities are optimized as well and are not constrained to Gaussian shapes anymore. The iteration process is repeated until the classification converges and only a small number of points are reclassified in each iteration (typically $< 0.5\,\%$). The dwell time distribution can be calculated from the assigned states and the quality of the assignment can be assessed by fitting a single exponential to the lifetime distributions. If necessary the transition matrix can be adjusted manually to optimize the dwell time distribution. The transition rate constants can be obtained by calculating a normalized integrated histogram of the dwell times and fitting a single exponential function to it. Due to the limited temporal resolution of the measurement system or the performance of the analysis, a number of transitions might be missed. To account for these missed events the integrated dwell time histogram is fit to the following function

with an off-rate from the state k, a temporal cutoff $T_{\min}$ and a maximal duration $T_{\max}$:

$$p(t) = \frac{exp(-k*t) - exp(-k*T_{\min})}{exp(-k*T_{\max}) - exp(-k*T_{\min})} \tag{3.5}$$

$T_{\max}$ is set to the trajectory's length, where as $T_{\min}$ depends on the applied force as mentioned earlier.

3.3 Equilibrium free energies

For easier calculation of the equilibrium free energy of the system, the bead-DNA-protein-DNA-bead system has been simplified to an equivalent bead-DNA-protein system. In the simplified system we have one the trap stiffness $k_{\text{eff}} = (\frac{1}{k_1} + \frac{1}{k_2})$ and the bead displacement is $x = x_1 + x_2$. For the calculation of the equilibrium free energy it has to be taken in account, that any change of the protein length in a constant distance measurement will lead to a change in force acting on the system. The energies of the beads, the DNA molecule, the folded protein and unfolded protein, all contribute to the free energy of the full dumbbell system. The free energy at a force F, when the protein is in state i, is given by

$$G_i(F_i) = G_i^0 + G_i^{\text{beads}}(F_i) + G_i^{\text{DNA}}(F_i) + G_i^{\text{protein}}(F_i) \tag{3.6}$$

with G_i^0 the free energy of the protein in state i,

$$G_i^{\text{beads}}(F_i) = \frac{1}{2} F_i x_i(F_i) \tag{3.7}$$

the energy stored in the displacement of the beads out of the trap centers,

$$G_i^{\text{DNA}}(F_i) = \int_0^{x_{\text{DNA}}(F_i)} F_{\text{eWLC}}(x_{\text{DNA}}) dx_{\text{DNA}} \tag{3.8}$$

the entropic energy from stretching the DNA linker and

$$G_i^{\text{protein}}(F_i) = \int_0^{x_{\text{protein}}(F_i)} F_{\text{WLC}}(x_{\text{protein}}) dx_{\text{protein}} \tag{3.9}$$

the entropic energy from stretching the protein in state i. As mentioned before, when the protein switches from state i to state j, the change in protein length leads to a force change from F_i to F_j. The corresponding free energy difference is

$$\Delta G_{ij}(F_i,F_j) = \Delta G_{ij}^0 + \Delta G_{ij}^{\text{beads}}(F_i,F_j) + \Delta G_{ij}^{\text{DNA}}(F_i,F_j) + \Delta G_{ij}^{\text{protein}}(F_i,F_j) \tag{3.10}$$

The Boltzmann equation relates the energy difference to the state probabilities P_i,P_j

$$\Delta G_{ij} = -k_B T ln \frac{P_j}{P_i}. \tag{3.11}$$

By using the Boltzmann relation the probability of finding the protein in state i at a certain force F is given by

$$P_i(F) = \frac{1}{1 + \sum_{j \neq i} exp\left(-\frac{\Delta G^0_{ij} + \Delta G^{\mathrm{DNA}}_{ij}(F_i,F_j) + \Delta G^{\mathrm{protein}}_{ij}(F_i,F_j)}{k_B T} \right)}. \tag{3.12}$$

This equation can be fit to the probability data, resulting in the ΔG^0_{ij} from equilibrium state occupancies.

3.4 Force dependence of transition rate constants

Constant distance measurements yield force-dependent transition rate constants. To understand conformational transitions of proteins under natural force-free conditions, models have to be used to extrapolate rate constants to zero force. In the following, two different models are described.

3.4.1 Bell model

The Bell model has been developed to describe the dissociation kinetics of ligand-receptor systems under force (Bell, 1978). In this model, the force defines a reaction coordinate, along which it influences an one-dimensional energy landscape. The external force F tilts the energy landscape by $-\Delta x F$ (see Fig. 3.2). The model neglects any nonlinear effects of the linkers and the unfolded protein chain. It also does not account for any potential force dependencies of Δx or k_0. For a conformational transition the zero-force rate constants are given by

$$k(F) = k_0 \, exp\left(\frac{F \Delta x}{k_B T} \right) \tag{3.13}$$

3.4.2 Berkemeier-Schlierf model

The Bell model can be used to describe the force dependence of rate constants in optical trap experiments, however better models exist. Gebhardt (2009) has adapted a model from Schlierf et al. (2007) for optical trap experiments which takes the nonlinear contributions of the DNA linker and unfolded protein into account. This model accounts for

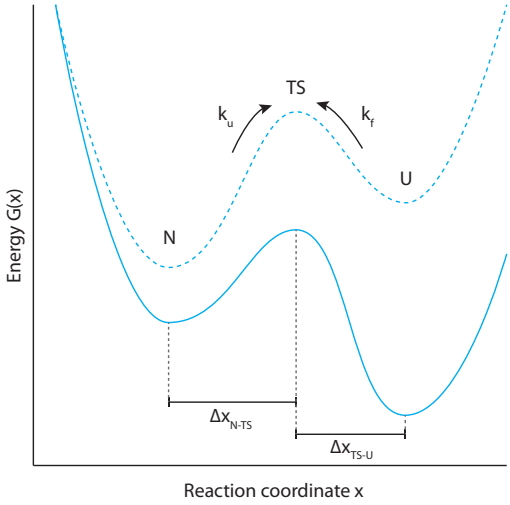

Figure 3.2 **Energy landscape under force:** The folding of a protein in a two state system can described in an energy landscape model (dashed blue line) with the native state (N), the transition state (TS) and the unfolded state (U). The distance from the folded and unfolded state to the transition state is given by $\Delta x_{\mathrm{N-TS}}$ and $\Delta x_{\mathrm{TS-U}}$, respectively. An external force acts as an additional linear potential and tilts the energy landscape (blue solid line), here the unfolded state (U) lies lower than the folded state (F). This leads to an increased unfolding rate k_{u} and a decreased folding rate k_{f}.

the additional energy, the deflection of the beads out of the trap and the stretching of the linker, which has to be brought up by the system to reach the transition state TS from the initial state i.

$$k_{ij}(F) = k_i^0 \, exp\left(-\frac{\Delta G^{\#}_{iTS}(F_i = F, F_{TS}}{k_{\mathrm{B}}T}\right), \tag{3.14}$$

where $\Delta G^{\#}_{iTS}$ is given by equation 3.10. This function can be fit to the data with the k_i^0, the rate constant at zero force and the transition state distance ΔL_{iTS}, measured in contour length, to which the system has to contract, before it passes the energy barrier.

3.5 Ligand binding

The protein adenylate kinase investigated in this thesis, is able to bind nucleotides. Depending on the ligation state, a protein will behave differently. This is not only true for conformational changes of the protein but also the folding and unfolding behavior is affected by ligand binding. An extensive discussion about the folding and unfolding in the presence of ligands is presented in (Stigler, 2012) and Junker (2009). This chapter will present some of the main ideas of ligand binding.

If only one binding site is present, the equilibrium between ligand free native conformation N and ligand bound native conformation can be described as $N + L \underset{k_{\mathrm{off}}}{\overset{k_{\mathrm{on}}}{\rightleftharpoons}} NL$ with the dissociation constant $K = \frac{k_{\mathrm{off}}}{k_{\mathrm{on}}}$. The protein can adopt four different configurations: N, native; NL, native ligand bound; U, unfolded; UL, unfolded ligand bound. The energy difference between ligand bound and ligand free conformation ΔG^{L} is defined by

the dissociation constant, e.g. for the native state N:

$$K_{\mathrm{N}} = \frac{[N][L]}{[NL]} = exp\left(\frac{\Delta G_{\mathrm{N}}^{\mathrm{NL}}}{k_{\mathrm{B}}T}\right) \tag{3.15}$$

The dissociation constant is defined in a similar way for the other states TS and U. The probability to find the protein in the native bound or unbound state is then given by

$$\begin{aligned} P(N) &= \frac{[N]}{[N]+[NL]} = \frac{1}{1+\frac{[L]}{K_{\mathrm{N}}}} \\ P(NL) &= \frac{[NL]}{[N]+[NL]} = \frac{\frac{[L]}{K_{\mathrm{N}}}}{1+\frac{[L]}{K_{\mathrm{N}}}} \end{aligned} \tag{3.16}$$

Similar probabilities can also be defined for the transitions state TS as well as the unfolded state U. Using the Arrhenius equation the effective folding rate in the presence of ligands can be calculated

$$\begin{aligned} k_{\mathrm{u}}(L) &= P(N)k_{\mathrm{u}}^{\mathrm{L}=0} + P(NL)k_{\mathrm{u}}^{\mathrm{L}} \\ &= k_{\mathrm{u}}^{\mathrm{L}=0}\frac{1+\frac{[L]}{K_{\mathrm{TS}}}}{1+\frac{[L]}{K_{\mathrm{N}}}}, \end{aligned} \tag{3.17}$$

where $k_{\mathrm{u}}^{\mathrm{L}=0}$ is the unfolding rate in absence of ligands. Similarly the overall folding rate

$$k_{\mathrm{f}}(L) = k_{\mathrm{f}}^{\mathrm{L}=0}\frac{1+\frac{[L]}{K_{\mathrm{TS}}}}{1+\frac{[L]}{K_{\mathrm{U}}}}, \tag{3.18}$$

where $k_{\mathrm{f}}^{\mathrm{L}=0}$ is the folding rate in absence of ligands. The free energy difference between folded and unfolded state in the presence of ligands is given by

$$-\frac{\Delta G_0}{k_{\mathrm{B}}T} = -ln\frac{k_{\mathrm{f}}(L)}{k_{\mathrm{u}}(L)} = -\frac{\Delta G_0^{\mathrm{L}=0}}{k_{\mathrm{B}}T} - ln\frac{1+\frac{[L]}{K_{\mathrm{N}}}}{1+\frac{[L]}{K_{\mathrm{U}}}} \tag{3.19}$$

At concentrations, where the unfolded state does not bind the ligand, equation 3.19 can be approximated by

$$-\frac{\Delta G_0}{k_{\mathrm{B}}T} \approx -\frac{\Delta G_0^{\mathrm{L}=0}}{k_{\mathrm{B}}T} - ln\left(1+\frac{[L]}{K_{\mathrm{N}}}\right) \tag{3.20}$$

At ligand concentrations below the dissociation constant K_{N} the native state is not stabilized by the ligand, the free energy difference is equal to the one in the apo state. At

higher concentrations the native state is stabilized by ln(10) for every ten-fold increase in ligand concentration.

If the protein has two binding sites for the same ligand, a similar approach for the folding and unfolding rate, as well as, the free energy difference can be made, as described in detail in Stigler (2012). The free energy difference between native and unfolded state for a protein with two binding sites for the ligand is given by

$$-\frac{\Delta G_0}{k_\mathrm{B}T} = -\frac{\Delta G_0^{\mathrm{L}=0}}{k_\mathrm{B}T} - ln\frac{1+\frac{[L]}{K_{\mathrm{N}1}}+\frac{[L]^2}{K_{\mathrm{N}1}K_{\mathrm{N}2}}}{1+\frac{[L]}{K_{\mathrm{U}1}}+\frac{[L]^2}{K_{\mathrm{U}1}K_{\mathrm{U}2}}}, \tag{3.21}$$

where $K_{\mathrm{N}1}$ and $K_{\mathrm{U}1}$ are the dissociation constants of the ligand to the first binding site of the native and unfolded state, respectively and $K_{\mathrm{N}2}$ and $K_{\mathrm{U}2}$ the dissociation constants of the ligand to the second binding site. Similarly to the one binding site case, 3.21 can be approximated for concentrations, where the unfolded state does not bind the ligand, by

$$-\frac{\Delta G_0}{k_\mathrm{B}T} \approx -\frac{\Delta G_0^{\mathrm{L}=0}}{k_\mathrm{B}T} - ln\left(1+\frac{[L]}{K_{\mathrm{N}1}}+\frac{[L]^2}{K_{\mathrm{N}1}K_{\mathrm{N}2}}\right) \tag{3.22}$$

For concentrations below the $K_{\mathrm{N}1}$ of the first binding site, the free energy difference is independent of ligand concentrations. For concentrations above $\sqrt{K_{\mathrm{N}1}K_{\mathrm{N}2}}$ the free energy increases with a factor of 2·ln(10) for every ten-fold increase in concentration. This is in contrast to the case, where only one binding site is present. Measuring the free energy in dependence of the ligand concentration, therefore, allows to determine if the native state gets stabilized by one or two ligands.

4 Adenylate Kinase

4.1 Introduction to the enzyme Adenylate Kinase

Adenylate kinase (ADK) is an enzyme which is responsible for the energy homeostasis in the cell. It catalyzes the reversible reaction of $Mg^{2+}ATP + AMP \rightleftharpoons Mg^{2+}ADP + ADP$. A wide variety of crystal structures of ADK from different organisms and in the presence of different substrates exists. The PDB database lists 60 different adenylate kinase structures. They show high sequence identity and structure homology (Vonrhein et al., 1995; Henzler-Wildman et al., 2007a). Overall adenylate kinase consists of three domains, the ATP lid, the AMP lid and the CORE domain. The CORE domain is composed of a five stranded beta sheet, surrounded by five α-helices, a so called Walker fold. The Walker fold is a super secondary structural motif, which is commonly found in nucleotide binding proteins and makes up part of the nucleotide binding sites (Walker et al., 1982). An important part of the ATP binding site is the Walker A motif, GXXXXGKT, which binds to the β-phosphate of ATP. The crystal structure for the thermophilic variant of adenylate kinase (thADK) from *Aquifex aeolicus* in the open and closed conformation is shown in Fig. 4.1.

Aquifex aeolicus is a rod shaped hyperthermophilic bacterium, with a growth maximum around 95°C (Deckert et al., 1998). It can be found near underwater volcanoes or hot springs and belongs to the group of chemolithoautotrophs, meaning it uses inorganic carbon for biosynthesis and an inorganic chemical energy source. Proteins of thermophilic organisms show several changes to adapt to the high temperature environment, but they don't seem to follow an overall pattern between the organisms or proteins (Jaenicke and Böhm, 1998; Petsko, 2001). Adenylate kinase of *A. aeolicus* e.g. has 5 additional prolines compared to mesophilic variant from *E. coli* (mesoADK) and shorter loops in its lid regions, leading to a decreased surface to volume ratio. In the case of adenylate kinase, the difference between thermophilic and mesophilic homologs is especially interesting. The thermophilic variant does not only have to withstand high temperature but it has to balance the increased stability with the flexibility needed to exert its catalytic function.

For crystallization of the closed structure in Fig. 4.1 AP_5A has been used. AP_5A consists of two adenine groups which are connected by five phosphates and is a strong inhibitor of ADK which was first shown by Lienhard and Secemski (1973). Despite the additional phosphate compared to the substrates, it is the inhibitor with the highest

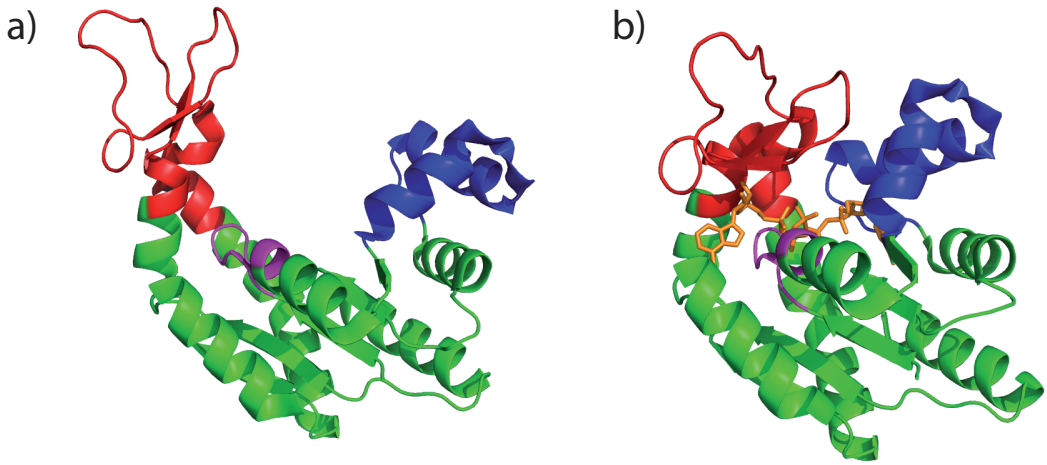

Figure 4.1 **Crystal structure of thADK:** Crystal structure of the open a) and closed b) structure of the thermophilic variant of adenylate kinase from *Aquifex aeolicus* (PDB Code 2RH5 and 2RGX). The ATP lid is colored in red (aa 120-160), CORE domain in green and AMP lid in blue (aa 30-59). The Walker A motif is colored in magenta. b) The closed structure is obtained by crystallizing thADK in presence of the inhibitor AP_5A (orange).

affinity and binds to adenylate kinase in the nanomolar range (Reinstein et al., 1990a). In addition to the closed structure crystallized in the presence of AP_5A, various other closed or partially closed structures of adenylate kinase in the presence of natural substrates AMP, ADP or substrate analogues like AMPPNP, $AMPPCF_2P$ have been solved (Berry et al., 1994, 2006; Schlauderer et al., 1996).

During catalysis ADK undergoes a large conformational change as it is seen in Fig. 4.1. Both ATP lid and AMP lid are involved in the conformational change and close on top of the CORE domain. The closed conformation is the catalytic active state in which the phosphotransfer occurs (Adén and Wolf-Watz, 2007). The large conformational change is essential for catalysis and serves two functions. First, it brings the two substrates close together, enabling the phosphotransfer between them. Second, it excludes water from the reaction volume, preventing non-productive ATP-hydrolysis. The phosphotransfer itself takes place in a nucleophilic attack of the α-phosporyl group of AMP on the γ-phosphate of ATP (Müller and Schulz, 1992).

NMR relaxation experiments by Wolf-Watz et al. (2004) have shown that in saturating substrate conditions, the lid-opening rate of ADK is similar to the catalytic rate, see Tab. 4.1. The lid-closing rate, on the other hand, is much faster. This implies that the lid-opening is the rate limiting step. This is consistent with early experiments showing that the rate limiting step involves the dissociation of the bound nucleotides (Rhoads and Lowenstein, 1968). Under saturating substrate concentrations the equilibrium between open and closed conformation lies far toward the closed side. Further experiments by

	mesoADK	thADK
k_{open}	$(286 \pm 85)\ s^{-1}$	$(44 \pm 20)\ s^{-1}$
k_{close}	$(1374 \pm 110)\ s^{-1}$	$(1571 \pm 100)\ s^{-1}$
k_{cat}	$(263 \pm 30)\ s^{-1}$	$(30 \pm 10)\ s^{-1}$

Table 4.1 **ADK rate constants:** Opening, closing and catalytic rates in saturating AMP, ADP, ATP and Mg^{2+} conditions for meso and thADK from NMR relaxation experiments (Wolf-Watz et al., 2004).

Henzler-Wildman et al. (2007b) have shown that adenylate kinase samples the closed state even in the absence of substrates. Here, however, the opening rate is much faster than the one observed in the presence of substrates. The opening and closing rates for thADK in the absence of substrates are $6500\,s^{-1}$ and $2000\,s^{-1}$, respectively. Even without nucleotides present, adenylate kinase is able to undergo the full conformational change but the equilibrium now lies toward the open side. This is in contrast to single molecule FRET measurements performed by Hanson et al. (2007) on mesoADK in the absence and presence of substrates. They observed an opening rate of $120\,s^{-1}$ and a closing rate of $220\,s^{-1}$ for substrate-free ADK. The rates are about an order of magnitude lower to the ones observed by Henzler-Wildman et al. (2007b) with the closed state slightly more favorable.

The conformational transition of ADK has also been investigated extensively using different computational methods (Kubitzki and de Groot, 2008; Beckstein et al., 2009; Arora and Brooks, 2007; Matsunaga et al., 2012; Snow et al., 2007; Potoyan et al., 2012; Song and Zhu, 2013). Arora and Brooks (2007) used advanced sampling methods to calculate the free energy difference as a function of the difference in root mean square deviations from the open and closed state in ligand free and ligand bound conditions. Their observations agree with the ones from NMR measurements that ADK undergoes conformational transitions between open and near closed state even in the absence of substrates. The free energy minimum, however, is near the open state and the closed conformation is energetically unfavorable, which has been confirmed by other simulations (Matsunaga et al., 2012; Song and Zhu, 2013). Matsunaga et al. (2012) employed molecular dynamics simulations to calculate the free energy profiles along the transition pathways for the ligand-free and ligand-bound ADK. Their simulations show a coupling between the conformational transition and a highly specific binding of the AMP-moiety. This is expressed by the order of closing in the presence of AP_5A; the AMP lid closes first, enabling interactions between ATP and AMP lid and the subsequent closure of the ATP lid.

Recent experiments and simulations have suggested that the conformational transition of the ATP lid involves a so called "cracking" mechanism (Olsson and Wolf-Watz, 2010; Whitford et al., 2007). During the reaction significant strain energy is build up in the

helices at the hinge of the ATP lid. During a local unfolding event this energy is released and enables the rearrangement of molecular interactions and subsequent refolding of the helices in the closed conformation.

Despite numerous experimental as well as computational approaches to study the conformational transition of adenylate kinase, the linkage between substrate binding and the conformational change is still not fully understood.

4.2 Enzymatic activity of ADK

For single molecule force spectroscopy measurements multiple adenylate kinase variants from different organisms were expressed. To ensure that the different variants are active, their enzymatic activity was tested. For this purpose a coupled spectrophotometric assay was used (Saint Girons et al., 1987). The production of ADP by adenylate kinase in the presence of ATP and AMP is coupled to the oxidation of $NADH/H^+$ by the enzymes pyruvat kinase and lactate dehydrogenase. The decrease in $NADH/H^+$ can be monitored at 334 nm and thereby also the adenylate kinase activity. To obtain the right enzymatic activity it has to be ensured, that the reaction catalyzed by adenylate kinase is the rate limiting step. In this case the coupled enzymatic assay enables the measurement of the Michaelis-Menten constant K_m and the catalytic rate k_{cat}. Tab. 4.2 shows a summary of the obtained values for thADK and mesoADK.

It can be clearly seen from Tab. 4.2, that the different cystein mutants affect neither the Michaelis-Menten constant nor the catalytic rate strongly. Therefore, the mutations sites are well chosen and enable further single molecule experiments without the interference of the mutations.

4.3 Single molecule force spectroscopy of the thermophilic variant of ADK

As described in chapter 4.1, adenylate kinase undergoes a large conformational change during catalysis. This makes it a good candidate to study conformational transitions with an optical trap. When looking at the opening and closing rates of the thermophilic variant of adenylate kinase from *Aquifex aeolicus*, the equilibrium lies further towards the closed configuration at saturating substrate conditions than it does for the mesophilic variant from *E. coli* (see Tab. 4.1). If we want to study the conformational change with our optical trap setup we have to attach our handles at position where the distance change between open and closed state is maximized. We will call this the active geometry. In the active geometry, the enzyme does not only have to spend the energy for the conformational change itself but also has to work against the force of the optical trap. This additional energy contribution will shift the equilibrium between open and

	$K_{M,app}$ [µM]			k_{cat} [s^{-1}]
	Mg^{2+}-ATP	AMP	Mg^{2+}-ADP/ADP	
E.coli				
WT*	51	26±3	90±10	330
N-C	48±15	21±3	170±70	470±30
A.aeolicus				
WT*	35	21		30±10
N-C	18±6	~20	250±80	25±2
42-144	41±11	~10	360±80	25±7

Table 4.2 **Kinetic constants of ADK:** Michaelis-Menten constant K_m and the catalytic rate k_{cat} for different adenylate kinase mutants from *E.coli* and *A.aeolicus* measured using the coupled spectrophotometric assay. WT is the wild type, N-C a mutant with cysteines inserted at the N- and C-terminus and 42-144 a mutant with cysteines inserted at positions 42 and 144. *The values for the wild type proteins from *E.coli* and *A.aeolicus* are taken from (Reinstein et al., 1990a) and (Wolf-Watz et al., 2004) respectively.

closed state at saturating substrate conditions towards the open conformation. This shift depends on the force we are applying. On the other hand, we have to be in a force range where the resolution is good enough to observe the expected transition of about 1.7 nm. Therefore, we decided to study the thermophilic variant of adenylate kinase, where the equilibrium lies further towards the closed, allowing us to exert higher forces and still be in a region where the enzyme undergoes conformational transitions.

4.3.1 Unfolding of thADK in NC direction

In addition to the observation of conformational transitions, adenylate kinase shows an interesting folding behavior shown by single molecule FRET measurements. Pirchi et al. (2011) labeled adenylate kinase from *E.coli* at positions 73 and 203 with fluophores and encapsulated the labeled adenylate kinase in surface-tethered lipid vesicles. They performed single molecule experiments with varying concentrations of the denaturant guanidinium chloride. From their analysis, they postulate that ADK folding incorporates up to six distinct states. To gain further insight in the folding of adenylate kinase we also performed folding and unfolding experiments with the optical trap on thADK. For this purpose, we added a cystein at the N- and at the C-terminus. DNA handles were attached as described in chapter 2.5.1. For the experiment, one fluorescently labeled and one unlabeled bead were trapped and it was checked if a dumbbell

could be formed by touching both beads. If a dumbbell was formed, the relative distance between the beads was increased with constant velocity and thereby force applied on the protein. If the force is high enough the protein unfolds and the distance between the traps is decreased again until no force acts on the unfolded protein and the protein can refold. A typical unfolding transition is shown in Fig. 4.2.

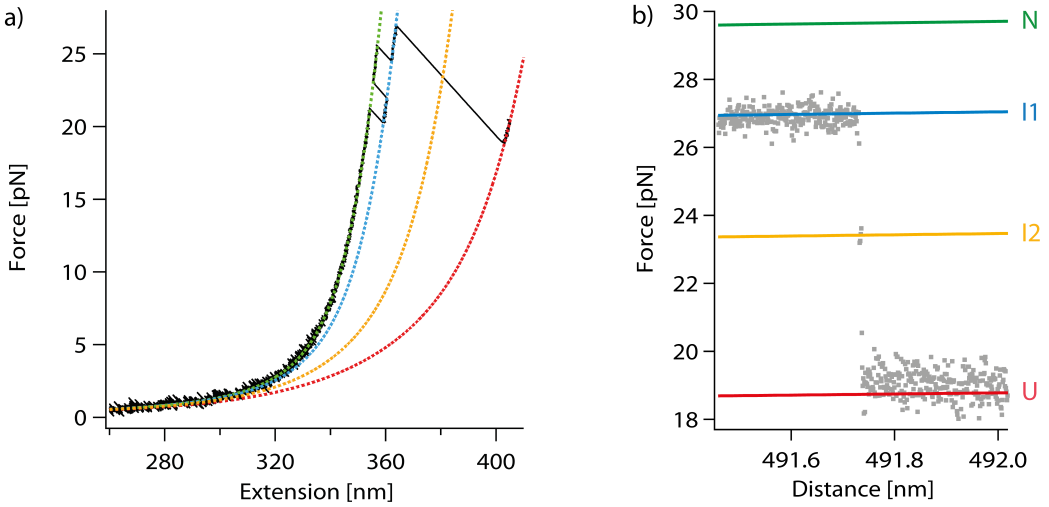

Figure 4.2 **Unfolding of thADK:** a) Force extension trace of the unfolding of thADK pulling at the N- and C-terminus. The black curve shows the data filtered to 160 Hz. The colored curves are fits of a combined WLC model to the data. The green curve shows the force extension behavior of the dsDNA handles. Two unfolding intermediates are present (blue, orange.) The completely unfolded thADK is marked in red. b) Force distance graph of the unfolding of thADK at the raw sample frequency of 20 kHz (dark gray dots). Colored lines are WLC fits from a).

Upon stretching the protein to a force of about 21 pN, one can observe, a first unfolding transition with a contour length gain of 7.5 nm. This part of the protein is able to refold again at a higher force and ultimately unfolds around 25 pN. Shortly afterwards, a large unfolding event at 27 pN with a contour length gain of 60.9 nm can be observed. Whereas Fig. 4.2a) shows the unfolding of thADK in the force extension representation, a zoom into the large unfolding event is shown in Fig. 4.2b) in force distance representation. Here the x-axis does not describe the actual extension of the construct as in a), but the distance between the trap centers. This allows for a better inspection of the unfolding event and a short lived intermediate at a contour length increase of 26 nm can be observed. The lifetime of the intermediate is (0.6 ± 0.2) ms on average (N=102). The overall contour length gain in the observed unfolding transition is 68.5 nm. The expected length gain can be calculated by the total number of amino acids between the two cysteins $N = 201$, each contributing to the unfolding with a length gain of $d_{\mathrm{aa}} = 3.65$ Å.

The calculated length has to be corrected for the end to end distance in the folded state, which is in this case 0.9 nm. From this calculation we obtain an expected contour length increase of 72.4 nm.

The histograms of the contour length increases and the average values are given in Fig. 4.3.

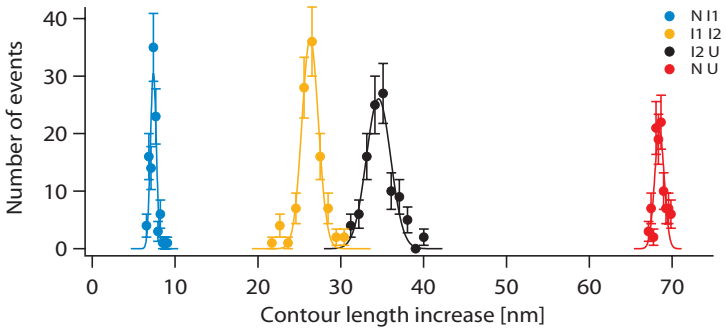

(a)

	Contour length increase $[nm]$
$N \rightarrow I1$	7.4 ± 0.5
$I1 \rightarrow I2$	26.3 ± 1.4
$I2 \rightarrow U$	34.6 ± 2.1
$N \rightarrow U$	68.5 ± 0.9

(b)

Figure 4.3 **Contour length increases:** a) Contour length histograms of the unfolding transitions of thADK pulling at N- and C-terminus. The contour lengths are extracted from WLC fits to force extension traces. (104 events; 9 different molecules) b) Average contour length increases and standard deviation for the different intermediates from the histograms in a).

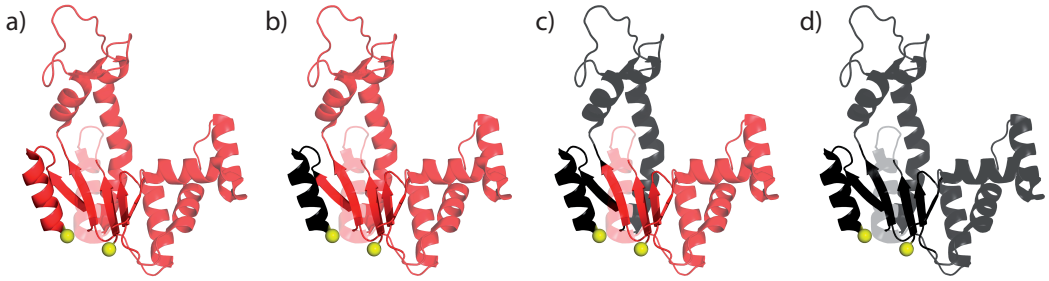

Figure 4.4 **Model for the unfolding intermediates:** Crystal structures of thADK showing the different unfolding intermediates. Red colored parts show the folded structure, black colored parts unfolded structures. The cysteins at N- and C-terminus are shown as yellow spheres. a) shows the native folded form, b) the first unfolding intermediate, where the α-helix of the C-terminus unfolds (I202-D186). c) For the second intermediate the unfolding continues at the C-terminus and the ATP lid unfolds (I202-E111). d) shows the completely unfolded structure.

To map the structure of the folded portion of the intermediate, one has to determine if the unfolding starts from the N- or the C-terminus of the protein. A look at the crystal

structure strongly suggests that the unfolding will start from the C-terminus. After a few amino acids, the N-terminus leads into the β-sheet forming the CORE domain, and therefore is probably quite stable. The C-terminus on the other hand starts with a 12 amino acid long α-helix, followed by a 4 amino acid long loop before it continues into the β-sheet of the CORE domain. From the unfolding of the C-terminal α-helix, including the loop, one would expect a length gain of 7.1 nm, which corresponds well to the observed contour length increase of the first unfolding intermediate of (7.4 ± 0.5) nm. Continuing from the C-terminus, an unfolding of the complete ATP lid up to the CORE domain would lead to an expected length gain of 34.5 nm. This again agrees well with the observed contour length increase for the second short lived intermediate of around 34 nm from the native state. The last unfolding step from the second intermediate with a contour length increase of 34.6 nm will then correspond to a complete unfolding of the protein. Mapping the observed contour length increases on potential unfolding intermediates give a first model for the unfolding pathway starting from the C-terminus, which is shown in Fig. 4.4. To confirm the model additional experiments have to be performed. Two techniques have proven to be very useful in this respect. One is the design of crosslinked mutants, where part of the structure is crosslinked by disulfide bonds between two inserted cysteines (Bertz and Rief, 2008; Bertz et al., 2009). The other one is the insertion of unstructured loops in the protein, which have been successfully used to identify intermediates and folding pathways in single molecule experiments (Schwaiger et al., 2004; Carrion-Vazquez et al., 1999). A similar approach can be used in the future to confirm and refine the proposed unfolding model.

4.3.2 Refolding of thADK

The previous chapter was only concerned with the unfolding behavior of thADK using force. However, the optical trap experiments also allow the observation of the refolding of a protein. After complete unfolding, the protein is relaxed again by bringing the beads together. This reduces the force on the protein and allows it to refold. A typical refolding trajectory is shown in Fig. 4.5a). If one approaches the beads with a speed of 20 nm s^{-1}, the first refolding intermediate can be observed around a force of 7 pN. The first refolding intermediate is followed by several more refolding intermediates. Rapid flipping between the different intermediates can be observed Fig. 4.5b). At least four different intermediates can be seen in constant velocity, as well as constant distance traces. This is confirmed by the deflection histogram of the constant distance trace, which is best fit by four gaussians. The fourth intermediate (magenta) is not visible in the histogram, because it occurs only rarely and is therefore hidden by the other more frequently occurring intermediates. Due to the high exchange between the different states at these low forces a reliable state assignment using Hidden Markov Models is difficult. Therefore we will limit the analysis of the intermediate positions to the values obtained by the WLC fits and the histogram positions. The first two refolding

intermediates have a contour length gain around 14 nm and 25 nm, respectively. The third refolding intermediate has a contour length gain of about 34 nm, i.e. half of the protein is refolded. The contour length of the third refolding intermediate is close to the one of the short lived unfolding intermediate observed in the unfolding of thADK. If these intermediates have similar structural origins, the third refolding intermediate would incorporate the folded AMP lid as well as most of the CORE domain. The fourth refolding intermediate has a contour length gain of around 43 nm.

If the protein is relaxed further, around a force of 5 pN a refolding transition of around 26 nm to the native contour length can be observed. The observation of at least four refolding intermediates is in good agreement with the six states, including fully folded and unfolded state, observed in single molecule FRET folding measurements by Pirchi et al. (2011). Their experiments, however, were done with *E.coli* adenylate kinase, which in our hands shows a quite different refolding behavior, as it will be described later in chapter 4.11.

To identify the structural origin of the refolding intermediates of thADK further experiments have to be performed. Similar techniques as proposed for the characterization of the unfolding intermediates, like crosslinked mutants or the insertion of unstructured loops, can be used.

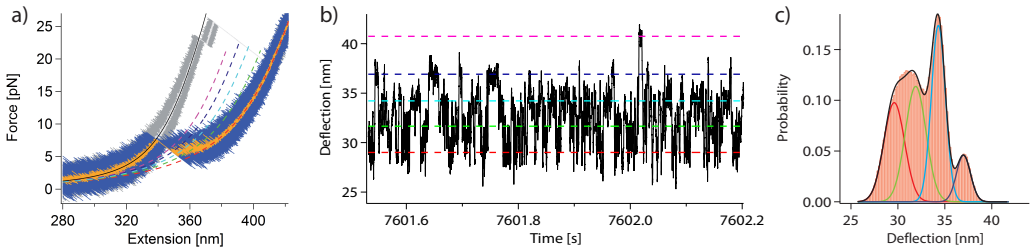

Figure 4.5 **Refolding of thADK:** a) Force extension trace of the relaxation at 20 nm s^{-1} of thADK pulling at N- and C-terminus. The raw data (30 kHz) is shown in blue, with the filtered data at 240 Hz in orange. The previous stretch trace is shown in gray. b) Constant distance trace of the four refolding intermediates filtered to 1.5 kHz at a force around 7 pN. The refolding intermediates are indicated with colored dashed lines. The position of the completely unfolded state is shown with the dashed red line. c) Histogram of the constant distance trace shown in b). The histogram is fit with four Gaussians for the unfolded state and the first three refolding intermediates.

In the last refolding step, thADK attained native compactness. Since this is not always the case, further relaxation to zero-force, allows the protein to fold completely. To test if the protein has completely refolded, it is probed again using a constant velocity ramp. In most cases thADK completely refolded and in the next pull one could observe the previously described unfolding pattern. In some cases, however, thADK was not able to refold and different unfolding patterns could be observed. Fig. 4.6 shows the

sequence of successful or partial refolding events for 68 consecutive pulling traces. The experiment was performed with a constant velocity of 100 nm s^{-1} and no waiting time at zero force. One can see that, in most cases, thADK is in the native conformation after relaxation to zero force. However, in two segments from pull 10 to 16 and 46 to 57 no complete refolding could be observed. For the rest of pulls the probability for complete refolding is 85 %. A stretch of six, respectively eleven consecutive unsuccessful refolding is, therefore, very unlikely.

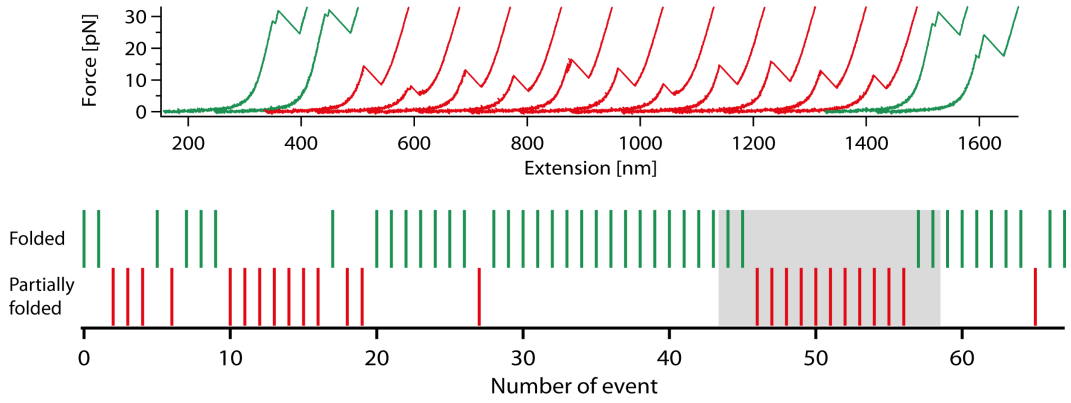

Figure 4.6 **Partial refolding of thADK:** a) Consecutive force extension traces of pulling thADK at N- and C-terminus with 100 nm s^{-1} and no wait times at zero force. Green labeled traces are regular unfolding curves, red labeled traces unfolding curves of a partially folded state. b) Order of completely folded states (green) and partially folded states (red) for 68 consecutive force extension pulls. The 15 traces in a) are taken out of the grey labeled region.

An explanation for this change in the folding kinetics can be cis-trans isomerization of prolines. The cis-trans isomerization of prolines has been shown to be a critical step in protein folding in bulk as well as single molecule studies (Brandts et al., 1975, 1977; Rognoni, 2014). The delocalisation of the lone pair of the nitrogen in a peptide bond gives the group a partial double bond character. The partial double bond character leads to planar configuration of the amide group, which can occur in either trans or cis state (Lu et al., 2007). In an unfolded peptide chain, the peptide can freely isomerize and adopt either cis or trans configuration. In the folded peptide chain, on the other hand, most peptide bonds adopt the trans configuration with a ratio of about 1000:1 trans:cis (Stewart et al., 1990). One exception is the amino acid proline, it adopts the cis configuration in a peptide bond with a fraction of 10 % to 40 %, depending on the preceding amino acid. The cis trans proline isomerization is a rather slow process, it occurs on the time scale of minutes (Wedemeyer et al., 2002). This can slow down the folding process, if the proline has to be in a certain configuration for the protein to fold properly.

thADK contains 15 prolines, of which PHE83-PRO84 occurs as a cis isomer in the native structure. PRO84 is in a loop connecting an α-helix with the β-sheet in the CORE domain of thADK. Assuming the configuration of this proline is essential for proper folding of thADK, extended periods of misfolded states could be observed in optical trap measurements. If PRO84 adopts the trans configuration in the unfolded state, trans-cis isomerization has to occur before thADK can fold. Because proline isomerization is a slow process, minutes of partially folded or unfolded thADK could be observed before thADK completely refolds, as it is seen in Fig. 4.6.

A similar behavior has been reported for mesoADK. mesoADK contains a cis-proline at position 87, which is in a very similar position in the crystal structure as in thADK. Ratner et al. (2002) have shown in bulk FRET measurements that the refolding of mesoADK consists of a fast folding species ($0.7\,s^{-1}$) and a slow folding one ($0.004\,s^{-1}$). The relative contribution of the slow refolding species increased with increasing time in the denatured state. From the timescales of the transition from fast to slow-folding species, as well as the equilibrium content of the fast-folding species, they argued that the isomerization of PRO87 is responsible for the existence of the two species. Therefore, it is very likely that the observation of extended periods of partially folded states in our optical trap measurements of thADK is due to the isomerization of PRO84. To test this hypothesis, one could mutate the proline at position 84 to a glycine and check if the switch in folding kinetics still occurs. Alternatively, proline isomerases can be used to alter the cis-trans proline isomerization kinetics (Fischer and Aumüller, 2003). This has been successfully used in single molecule optical trap experiments to change the folding kinetics of domain 20 of Filamin A (Rognoni, 2014).

4.4 thADK in the active geometry

The N-C pulling geometry is very unfavorable for observing the conformational transitions of adenylate kinase during the enzymatic reaction. By comparing the crystal structure of the open and closed enzyme, no significant length change between N- and C-terminus upon closing is expected. To enable the observation of the conformational change, we removed the cysteins at the N- and C-terminus and inserted new cysteins at positions 42 and 144. The positions were chosen to maximize the observable length change between the closed and open conformation. Additional care was taken to chose positions, where the cysteines are accessible and the insertions minimize the interference with the secondary and tertiary structure of thADK. The expected length change between the open and closed form for these two positions is 1.7 nm, inferred from the crystal structures 2RGX and 2RH5, see Fig. 4.7 a) and Tab. 4.3.

The approach for studying thADK in the active geometry is similar to the NC-pulling direction. The maleimide modified oligos are attached to the cysteines, and the dsDNA handles are hybridized to the oligos. A dumbbell is formed with thADK in the active

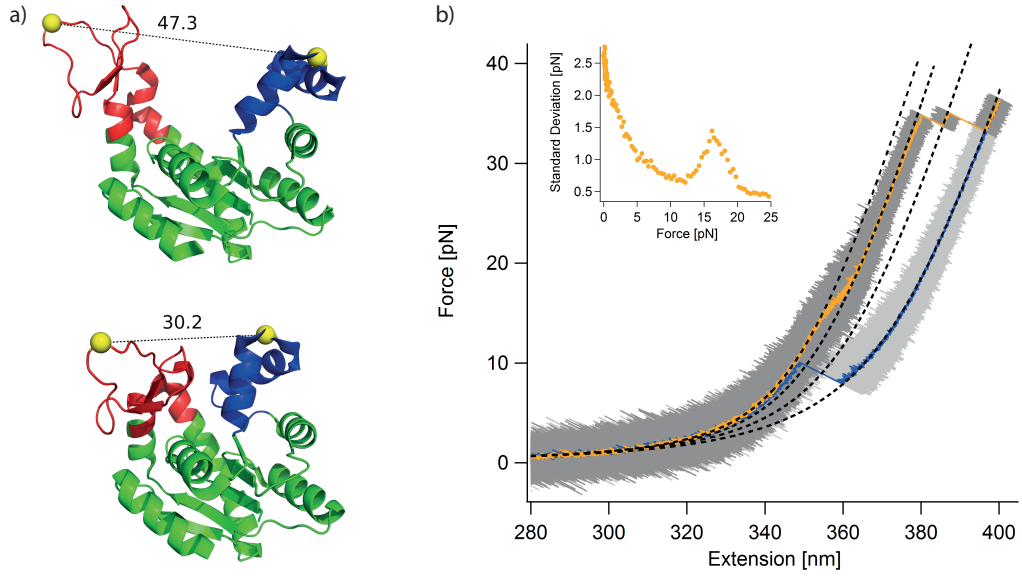

Figure 4.7 **thADK in the active geometry:** a) Crystal structure of thADK in the open state (top) and closed state (bottom). The yellow spheres indicate at the positions where the cysteines are inserted. The distance between the cysteines is given in Å. b) Force extension measurement of thADK pulling at positions 42 and 144. The raw data (30 kHz) is shown in grey. The smoothed traces (120 Hz) are shown in orange (strech) and blue (relax). The dotted lines are fits of a combined WLC model to the data. The insert shows a running standard deviation plot from the force distance data.

AMP lid	ATP lid	Distance	Relative distance to open state
open	open	4.7 nm	0 nm
open	closed	3.8 nm	0.9 nm
closed	open	3.7 nm	1.0 nm
closed	closed	3.0 nm	1.7 nm

Table 4.3 **Distances in thADK:** Distances between the two cysteines at position 42 and 144 for different conformations of thADK. The distances are measured from the crystal structures 2RGX and 2RH5. For single lid closed conformations the open and the fully closed structure is aligned by the CORE domain using PyMol and its built-in function *super*.

geometry and two beads. Before studying thADK in the active geometry in presence of nucleotides or inhibitors, experiments under apo conditions were performed. Like in the NC-terminal experiments, exerting force on the construct will eventually lead to unfolding of the protein. A typical force extension measurement is shown in Fig. 4.7 b). In the trace filtered to 120 Hz a continuous humplike equilibrium transition can be observed around 17 pN. The shape of the transition remained unchanged at all pulling velocities used (10–1,000 nm/s). This demonstrates that the system is in equilibrium at our experimental conditions. A calculation of the standard deviation of the raw signal sampled at 30 kHz is shown in Fig. 4.7 b). Starting around 13 pN, a clear increase from the otherwise monotonic decrease in the standard deviation can be seen. It has its maximum around the midpoint force of 17 pN and decreases again until it reaches a level, expected for just the DNA linker, around 20 pN. The increase in standard deviation can be rationalized by fast unfolding and folding transitions, expected for an equilibrium like transition.

Increasing the force further beyond 20 pN shows two additional unfolding events around 35 pN with a contour length increase of 8.4 nm and 14.1 nm respectively. A precise analysis of the length of these unfolding events is difficult, because they happen at relatively high forces. At these high forces, nonlinearities of the optical trap as well as DNA mechanics complicate the determination of contour length increases. The deviation of the WLC fits from the force extension traces can be seen in Fig. 4.7 b) above a force of 30 pN. The overall length gain of the unfolding of thADK pulling at position 42 and 144, on the other hand, can be measured without these complications. Therefore the relaxation trace of the fully unfolded construct is fit at a force range between 10 pN and 20 pN, where neither refolding nor nonlinearities can be observed. Using this procedure the overall contour length increase upon complete unfolding of thADK in the 42-144 direction can be determined and is (28.7 ± 0.8) nm. The expected contour length increase for complete unfolding in this pulling direction is 32.5 nm. The observed contour length increase is slightly smaller than the expected one. The deviation from the expected contour length, could be due to additional flexibility of the open structure. Especially at the ATP-lid the cystein is surrounded by loop regions which could already be partially unfolded and thereby explain the shorter measured contour length. However, despite the small discrepancy, we are sure that nearly all of thADK is properly folded and the cysteines are inserted at the right positions.

To study the equilibrium transition at 17 pN in more detail, a worm like chain model using a serial combination of DNA and polypeptide elasticity is fit to the data. The fit yields a contour length increase between folded and unfolded state of (5.4 ± 0.3) nm. An equilibrium folding/unfolding model allows the determination of the equilibrium free energy of the folding/unfolding as well as the degree of cooperativity (Zoldák et al., 2013). Fig. 4.8 shows that a two state model with full cooperativity describes the equilibrium transition best. For a three state model, where the protein unfolds in two steps

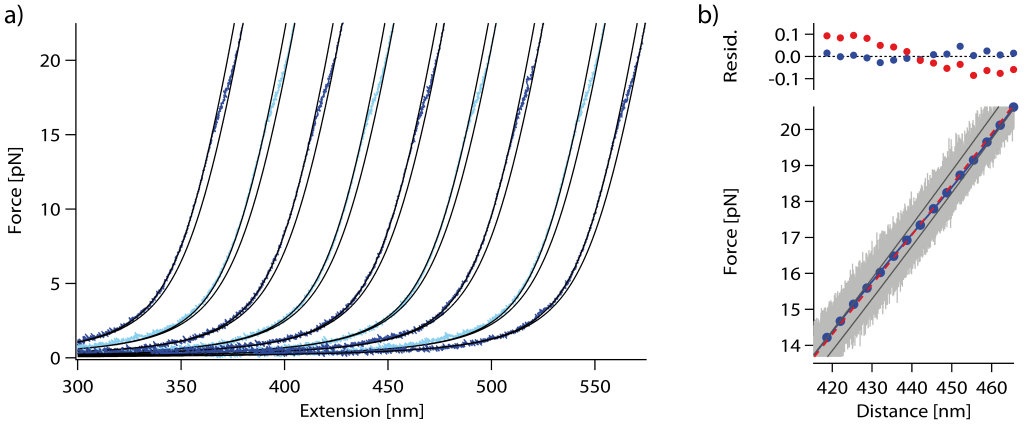

Figure 4.8 **Equilibrium folding/unfolding transition of thADK in the active geometry:** a) Five consecutive stretch (dark blue) and relax (light blue) force extension traces of the equilibrium unfolding/folding transition of thADK in the active geometry. The data is filtered to 60 Hz. Solid black lines are fits of a combined WLC model to the folded, respectively unfolded state. b) Force distance trace of the first unfolding/folding transition at 30 kHz (gray) and filtered to 15 Hz (blue dots). The dark grey lines are fits of a combined WLC model to the folded and unfolded state. The solid blue line is a fit of an equilibrium folding/unfolding model assuming two states to the data. The red dashed line is a fit with a three state model assuming the unfolding occurs in two steps with equal length and free energy. Residual plots for the two state model (red dots) and three state model (blue dots) are shown above.

of equal length and free energies, significant deviations from the measured behavior can be observed. The fit of the two state model to the data yields a folding free energy of (11.9 ± 1.1) kT.

Previous studies have shown that the ATP and AMP lid of adenylate kinase have a lower thermodynamic stability than the CORE domain (Rundqvist et al., 2009). Furthermore Schrank et al. (2009) have shown, that the ATP lid of mesoADK begins to unfold at temperatures over 35 °C. Together with unfolding and folding experiments in presence of nucleotides discussed in chapter 4.8 these results suggest that the observed equilibrium transition is caused by folding and unfolding of the ATP lid.

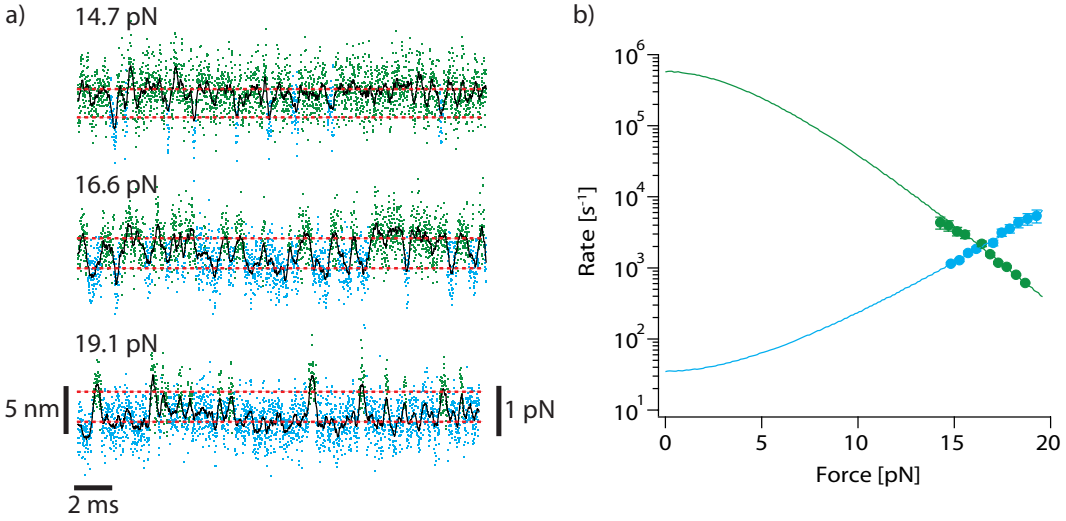

Figure 4.9 **Unfolding and folding of the ATP lid:** a) Constance distant traces at different forces of thADK, pulling at positions 42 and 144, recorded at 150 kHz (dots) and smoothed to 5 kHz (black line). The green and blue points are Hidden Markov Model assigned folded and unfolded states, respectively. The red dotted lines indicate the position of folded and unfolded state from the HMM analysis. b) Folding (green) and unfolding (blue) rates extracted from the lifetimes of the HMM assigned states. Solid lines are fits of the Berkemeier-Schlierf model to the data.

The stretch and relax cycles of the equilibrium transition around 17 pN sampled at 30 kHz show enhanced thermal fluctuations indicating that direct information about the folding and unfolding kinetics under load can be gathered. For this purpose, folding and unfolding transitions were sampled at a frequency of 150 kHz. Additional to stretch and relax cycles, constant distance measurements were performed. To this end, the protein was held at a constant trap separation and the transitions between unfolded and folded state were observed. This was done at different trap separations, as seen in Fig. 4.9 a). Individual transitions between the folded and unfolded state can still be detected. This is in contrast to optical trap experiments on villin headpiece HP35 (Zoldák et al., 2013).

There an assignment of folded and unfolded state could not be reliably made any more, due to the quick exchange between folded and unfolded state. An assignment of the states using Hidden Markov Models can only reliably made if the lifetimes of the states are not comparable to the timescale of the bead motion.

In the case of thADK, transition frequencies are low enough and therefore, the folded and unfolded states can be analyzed using Hidden Markov Models. The assignment of the data sampled at 150 kHz can be seen in Fig. 4.9 a), green for the folded state and blue for the unfolded state. An analysis of the lifetime distribution of the two states allows the determination of the folding and unfolding rate at a specific force. If this is done for different pretensions, the folding and unfolding rate at different forces can be measured. Due to the high rate of folding and unfolding at the measured forces, transitions between the two states will be missed and have to be corrected for, as described by Stigler and Rief (2012). The corrected rates are then fit to the Berkemeier-Schlierf model (see chapter 3.4.1, which allows extrapolation of the folding and unfolding rate to zero force Fig. 4.9 b). The extrapolated zero force unfolding rate is $(29 \pm 5)\ s^{-1}$ and the zero force folding rate $(6.6 \pm 0.8) \times 10^5\ s^{-1}$. Additional to the zero-force rates, also the folding free energy of this transition can be extracted by a global fit to the probability distribution. We obtain a value of (11.1 ± 1.1) kT, which is in close agreement with the free energy obtained from fitting an equilibrium folding/unfolding model to the constant velocity data.

4.5 The effect of the inhibitor AP_5A

The previous experiments performed under apo conditions did not show any sign of a conformational change on the order of 1.7 nm, which would indicate a closure of the lid domains. Henzler-Wildman et al. (2007b) have shown that adenylate kinase undergoes full opening and closing transitions even in the absence of substrates. However, the equilibrium of this transition lies towards the open state (opening:closing rate, $6500\ s^{-1}$:$2000\ s^{-1}$) and one would not expect to be able to observe these transitions under force in our optical trap experiments.

The addition of the inhibitor AP_5A, though, shifts the equilibrium far towards the closed state. If 100 nM of the inhibitor AP_5A is added in solution and stretch relax experiments are performed with thADK, the force extension curves show additional transitions between two distinct states. These transitions can be observed, starting at 4 pN up to the start of the first unfolding intermediate at 13 pN, as seen in Fig. 4.10 a). Note that these transitions occur also at forces higher than 13 pN. However, at these high forces, a mixture between the fast folding/unfolding equilibrium of the first intermediate and the AP_5A-induced transitions will be observed. For further analysis of the AP_5A-induced transitions only forces up to around 12 pN are considered. The equilibrium folding/unfolding transition, as well as the two high-force unfolding events have

the same unfolding forces and contour length increases as the ones at apo conditions. One can, therefore, align the force extension trace in presence of AP_5A (blue) to the one at apo conditions (orange) by using these unfolding events. It becomes clear that the observed transitions in presence of AP_5A take place from a more compact state of thADK to the fully folded one in apo conditions.

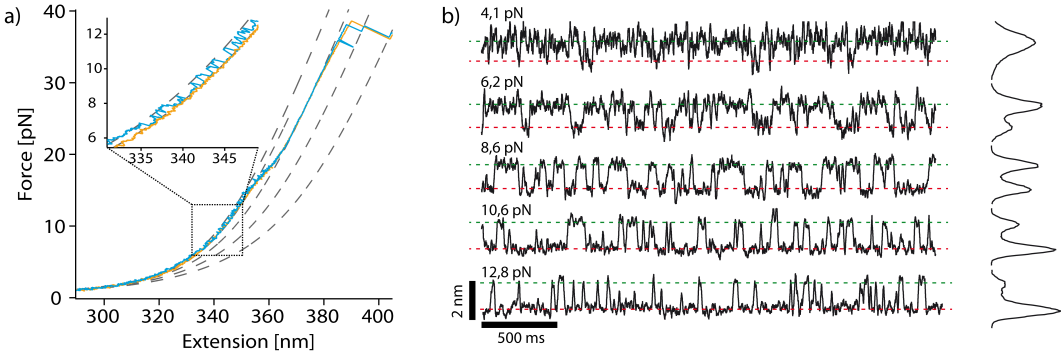

Figure 4.10 **thADK in the presence of AP_5A:** a) Force extension trace (60 Hz) of the unfolding of thADK pulling at residues 42 and 144 in apo conditions (orange) and in the presence of 100 nM AP_5A and 2 mM $MgCl_2$ (blue). b) Constant distance traces with increasing mean forces from top to bottom smoothed to 100 Hz. The upper state (blue) represents the closed state and the lower one (red) the open one. The state positions are obtained by HMM analysis. The histograms on the right side show the population of the two states.

A WLC fit to the two states of this transition yields a contour length difference of around 1.8 nm, which corresponds well to the expected length difference between open and closed state. However, one has to note that, due to the small length difference, a reliable fit to the data is difficult.

To circumvent this problem and to collect more data, experiments with constant trap separation were performed in the relevant force region. Fig. 4.10 b) shows exemplary traces of the conformational transitions of thADK in the presence of 100 nM AP_5A at different pretensions. For all pretensions two distinct states can be observed, a high force and a low force state. Previously the low force state corresponded to the unfolded state of a protein and the high force state to the native conformation. Because we are now not looking at an unfolding transition anymore, but a conformational transition, the nature of the states are different. In the high force state, the enzyme is in a more compact conformation, pulling the beads slightly out of the trap centers. This state, therefore, corresponds to the closed conformation of thADK. At the low force state, on the other hand, the protein adopts a more elongated form, allowing the beads to relax in direction of the trap center; thADK is in the open state. The population of these states shifts with force as it can be seen in the force extension and more clearly in the constant distance data. At low pretensions thADK is mostly in the closed conformation with

short transitions to the open state. At a force of about 9 pN both states are about equally populated, whereas at 13 pN, adenylate kinase is primarily in the open conformation with short spikes to the closed state.

The constant distance data does not show any intermediate states. In particular a state in the middle of open and closed conformation could not be observed. From the crystal structures of open and closed state, one would expect a state with a contour length of around 1 nm, if only one lid closes, see Tab. 4.3. The absence of this state indicates that in the presence of AP_5A a partially closed states does not exist or at least can't be observed within the resolution of the instrument.

As described in chapter 3.2 the constant distance data can be analyzed using Hidden Markov Models, which enables the assignment of each data point to either open or closed conformation. From this assignment, the lifetime of each state can be evaluated and fit to single exponential distributions in an integrated lifetime histogram. The calculated opening and closing rates are shown in Fig. 4.11b). As expected, the opening rate increases with force. Whereas, the closing rate is almost constant over the measured force range and decreases only very slightly with force. The probability that adenylate kinase closes, is, therefore, independent of the force applied by the optical trap. This can already be seen nicely, in the constant distance data itself. The dwell times, of the open state, are proportional to the closing rate and remain constant over the probed force range. The dwell times of the closed state, which are proportional to the opening rate, however, decrease significantly with increasing force.

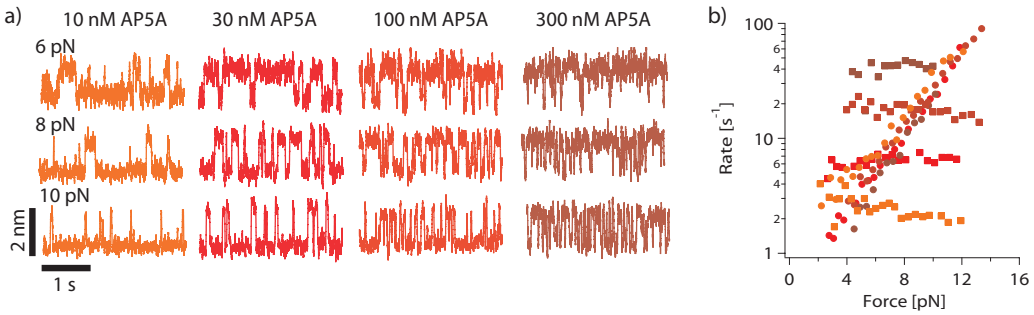

Figure 4.11 **Closing and opening of thADK with different AP_5A concentrations:** a) Constant distance trajectories of the conformational transition of the thADK 42-144 mutant in the presence of different concentrations of AP_5A smoothed to 100 Hz. b) Corresponding closing (squares) and opening (circles) rates extracted from Hidden Markov Model analysis of the data. The color in a) represents the same AP_5A concentration as in b).

All the data of closing and opening discussed so far has been collected at a concentration of AP_5A of 100 nM. How will the opening and closing of adenylate kinase be affected by different AP_5A concentrations?

To answer this question, measurements at different AP_5A concentrations have been performed. Figure 4.11 a) shows typical constant distance trajectories of the opening and closing of thADK at four different concentrations of AP_5A. At a concentration of 10 nM only a few closing events can be observed in the displayed segment. The number of closing events increases with increasing AP_5A concentration. The dwell time of the closed state at a given force, however, remains unchanged between the different concentrations. The opening and closing rate from Hidden Markov Model analysis for the different AP_5A concentrations in Fig. 4.11 b) illustrate this behavior nicely. With increasing AP_5A concentrations the closing rate is shifted higher, but for each concentration it remains constant over the measured force range.

The dependence of the closing rate on the AP_5A concentration indicates that closing is a binding dependent process. Increasing the concentration of AP_5A, increases the probability of thADK finding an AP_5A molecule and inducing the closing event. The independence of the opening rate on AP_5A, suggest that opening itself is AP_5A independent.

To examine the concentration dependence of the closing further, the zero-force closing rate is determined for different AP_5A concentrations by fitting a Bell model to the force dependent rates. The zero-force closing rates are plotted against the concentration in Fig. 4.12a). The zero-force closing rate follows a linear dependence over the whole measured AP_5A concentration range from 3 nM to 10 µM, spanning almost four orders of magnitude. A linear fit to the data, yields a slope of $(1.8 \pm 0.1) \times 10^8\ \mathrm{s^{-1}\ M^{-1}}$. This is in good agreement with the on-rate of AP_5A to human adenylate kinase $1 \times 10^8\ \mathrm{s^{-1}\ M^{-1}}$ estimated by Kalbitzer et al. (1982) from NMR measurements and the expected binding rate of a diffusion limited process. Therefore, AP_5A binding to adenylate kinase is diffusion limited. Our data additionally shows, that AP_5A does not only bind in a diffusion limited manner, but this binding process also induces the conformational change from open to closed state.

The dissociation constant of AP_5A can also be extracted from the data obtained by the optical trap experiments. For the simple reaction of $thADK_{\mathrm{apo}} + AP_5A \rightleftarrows thADK \cdot AP5A$, the dissociation constant K_d is defined as the AP_5A concentration, at which the concentration of apo thADK $[thADK_{\mathrm{apo}}]$ is equal to the concentration of AP_5A bound thADK $[thADK_{\mathrm{AP5A}}]$. For our single molecule experiment, this is fulfilled when the opening and closing rates at zero force are equal. Here, the additional equilibrium free energy due to AP_5A binding is zero. A plot of the equilibrium free energy due to AP_5A binding against the AP_5A concentration is shown in Fig. 4.12b). The additional equilibrium free energy given by binding of a substrate for a conformational transition has been described in chapter 3.5. A fit of $-\Delta G = -ln\left(\frac{x}{K_D}\right)$ to the data yields a dissociation constant of AP_5A (3.3 ± 0.3) nM. Since the dissociation constant is defined as $K_d = \frac{k_{off}}{k_{on}}$, the on-rate k_{on} is known from the closing rate, the off-rate k_{off} can be calculated. With a dissociation constant of 3.3 nM and an on-rate of $1.8 \times 10^8\ \mathrm{s^{-1}\ M^{-1}}$, we obtain an off-rate

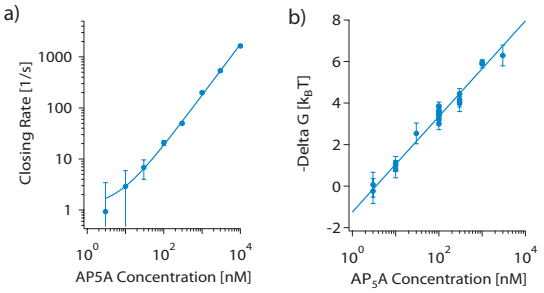

Figure 4.12 **Closing dynamics of thADK with different AP_5A concentrations:** a) Zero-force closing rate of the conformational transition of thADK in the presence of different AP_5A concentrations. The solid line is a linear fit to the data. b) Free energy of the AP_5A-induced conformational transition at different AP_5A concentrations. The solid line is a fit to the data.

of $(0.6 \pm 0.1)\,\mathrm{s}^{-1}$.

Since no literature values for the dissociation constant of nucleotides or inhibitors of thADK exist, the dissociation constants of the Q28H mutant of *e.Coli* ADK reported by Reinstein et al. (1990a) will be used throughout this thesis. The Q28H mutant is used instead of native mesoADK, since the histidine at position 28 is conserved in most adenylate structures, including thADK from *A. aeolicus*. The mutation increases the binding affinities of substrates and inhibitors to the *E. coli* variant of ADK and is, due to the conservation in thADK, a better reference as the native variant.

The reported dissociation constant of AP_5A of the Q28H mutant of mesoADK is 0.9 nM and agrees well with the dissociaton constant obtained from our single molecule optical trap experiments. The low dissociation constant indicates a very high affinity of AP_5A to the enzyme. One of the reasons is the diffusion limited binding of AP_5A. Another reason for the strong binding of AP_5A to adenylate kinase, could be the interplay between binding and closing of the enzyme. Due to the closing of thADK upon binding of AP_5A, thADK has to open up before AP_5A can be released again. This dramatically reduces the off-rate from thADK. Full affinity binding of AP_5A is, therefore, most likely only possible with the conformational change.

The binding process of AP_5A to thADK with a subsequent conformational change, explains the dependence of the closing rate on the AP_5A concentration. However, the independence of the closing rate on force has, so far, not been explained. This only very minor dependence of the closing rate on force results in a small Δx in Bell model fits to the data. What does the small Δx imply for the conformational change? The Δx denotes the distance of the open state to the transition state of the reaction. The enzyme, therefore, has to move this far to reach the transition state and can then continue down the energy landscape. Because the Δx is small, only a small movement of thADK against force is needed, before it is destined for closing in the presence of AP_5A.

As mentioned before, extracting the length of the conformational transition from force extension measurements by using WLC fits is difficult. Due to the small size of the conformational change, fitting errors are unproportionally high. The length can be far better determined from the previously shown constant distance measurements. For each constant distance segment the open and closed states are assigned by Hidden

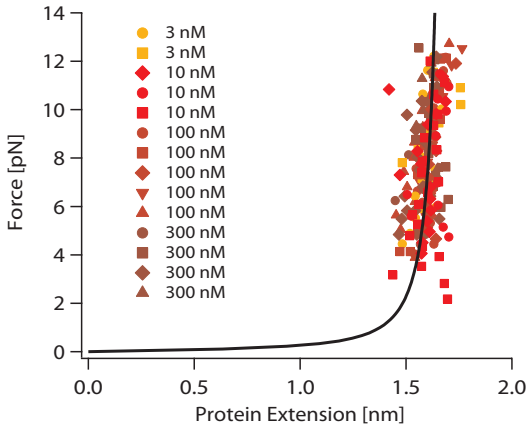

Figure 4.13 **Size of the conformational change of thADK in the presence of different AP_5A concentrations:** Size of the AP_5A-induced conformational transition from Hidden Markov Model analysis transformed into contour length space. Each symbol and color represents a different experiment. A global fit of a WLC model to the data is shown as a black solid line.

Markov Models. The size of the conformational change is calculated by the difference between the position of closed and open state. The resulting lengths have to be corrected for the change in DNA extension due to the difference in force between open and closed state. In Fig. 4.13 the size of the conformational transition is plotted against the average force between open and closed state. As one can see the size of the conformational transition is almost independent of force. There is also no difference in the size visible between the different AP_5A concentrations. The unchanged behavior between the AP_5A concentrations confirms that different AP_5A concentrations don't change the conformational transition itself. Fitting a WLC model to the data yields a contour length of (1.72 ± 0.02) nm and persistence length of (28 ± 9) nm. Opposed to the observation of a transition from folded to unfolded state, the persistence length of the low force state in this conformational change is not significantly lower than the one of the high force state. This is expected, because the nature of the the conformational change is not an order to disorder transition, as it is in unfolding, but an order to order transition. The closed as well as the open state are properly folded states, as can be seen from the crystal structures. As the size of the conformational transition shows a small dependence on force, the open and closed state appear to have slightly different rigidities with the open state being more flexible.

Due to the high persistence length in comparison with the size of the transition and the origin of this order to order transition, a worm like chain model is most likely not the best model to describe the data. But it will be used as an approximation for now.

All of the previously described measurements of thADK in the presence of AP_5A were done with saturating amounts of Mg^{2+}. For mesoADK Reinstein et al. (1990a) have reported that the K_d of AP_5A is about 20 times lower in the absence of Mg^{2+}. If we perform single molecule measurements of thADK with AP_5A in the presence of 2 mM EDTA, opening and closing of the enzyme can still be observed. However the dynamics of the conformational transition are much faster. A comparison of force dependent opening and closing rates in presence and absence of Mg^{2+} is shown for 100 nM AP_5A

in Fig. 4.14a). The closing rate agrees well for the two experiments over the whole force range. The opening rate, on the other hand, does have a similar force dependence in presence and absence of Mg^{2+}, but is shifted upwards in the Mg^{2+} free experiment by a factor of around 5 to a zero-force opening rate of $(5.4 \pm 0.2)\,s^{-1}$. Experiments at different AP_5A concentrations with EDTA show that the closing rate is always similar in presence and absence of Mg^{2+} and that the opening rate remains increased in the presence of EDTA. Therefore, the K_d for Mg^{2+}-free AP_5A is 17.8 nM, which is given by the increase in the off rate. This is in accordance with the lower K_d in presence of EDTA reported by Reinstein et al. (1990a) for mesoADK.

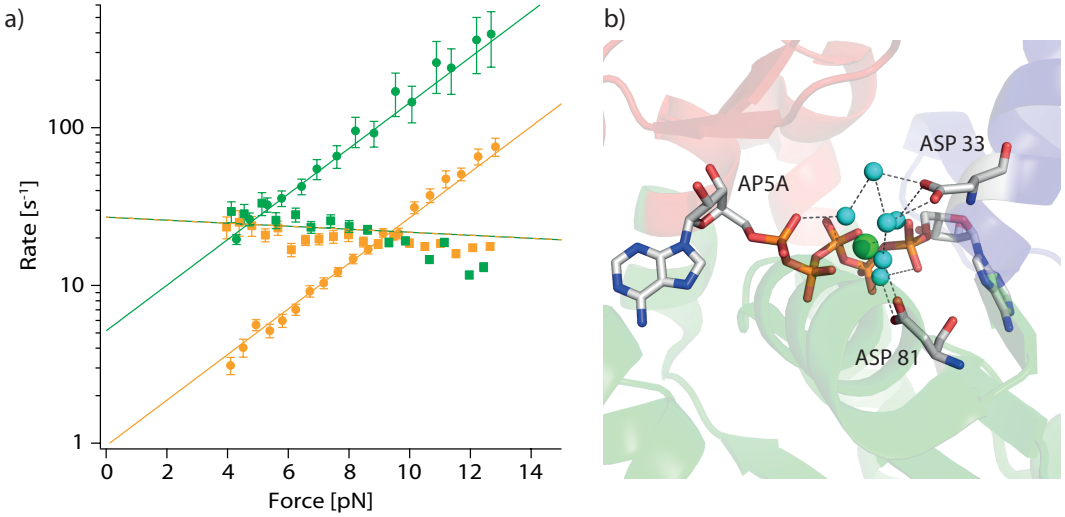

Figure 4.14 **Effect of Mg^{2+} on the AP_5A-induced conformational transition:** a) Opening (circles) and closing (squares) rates of thADK at 100 nM of AP_5A in the presence (orange) and absence (green) of Mg^{2+}. Solid lines are fits of the Bell model to the opening rate. Δx has been fixed for Mg^{2+} and Mg^{2+} free conditions. The dashed line is a fit to the closing rate in presence as well as absence of Mg^{2+}. b) Coordination of Zn^{2+} (green sphere) by ASP33 and ASP81 in the AP_5A closed crystal structure of thADK (PDB 2RGX). Water molecules are shown as blue spheres. Dashed lines are polar contacts between atoms.

The unchanged closing behavior suggests that the binding process is not altered in the absence of Mg^{2+}. With the same on-rate for Mg^{2+}-free AP_5A, the binding process is still diffusion limited and the binding induces closing of adenylate kinase. The change in the opening rate, indicates that the Mg^{2+} plays an important role in the stabilization of the closed complex.

The crystal structure of the AP_5A-bound closed state of thADK was crystallized in presence of Zn^{2+} instead of Mg^{2+}. Therefore, statements about the coordination of Mg^{2+} can only be made with the Zn^{2+} substitute. Zn^{2+} is mainly coordinated by Asp33 of the NMP lid and Asp81 of the core domain, see Fig. 4.14b). These interactions of thADK

with Zn^{2+} and AP_5A stabilize AP_5A in the binding pocket as well as the closed state of thADK overall. One can assume that Mg^{2+} will adopt a similar position, therefore information obtained from the crystal structure fit well with the observation from our single molecule optical trap experiments.

4.5.1 Switching kinetics

Occasionally, thADK shows different opening and closing kinetics during single molecule optical experiments. An exemplary switch in the kinetics in the presence of AP_5A is shown in a constant distance trace in Fig. 4.15a). The beginning of the trace shows the usually observed opening and closing of thADK. At this force the enzyme is mostly in the open state. This changes at a time of 6477.2 s. Now thADK is mostly in the closed state. Therefore, a change in the opening and closing kinetics must have taken place. The dwell times of the open state is similar in both cases. The dwell times of the closed state, however, are now longer. The apparent shift in equlibrium towards the closed state is, therefore, not due to an increase in the number of closing events, but an enhanced lifetime of the closed state. This can be clearly seen in the extracted closing and opening rates Fig. 4.15b). The closing rate is unchanged, AP_5A still binds in a diffusion limited manner and induces the conformational change. The opening rate, however, is decreased by a factor of about six. There is no change in the size of the conformational change visible. The open and closed state remain at the same positions, as it can be seen in Fig. 4.15a).

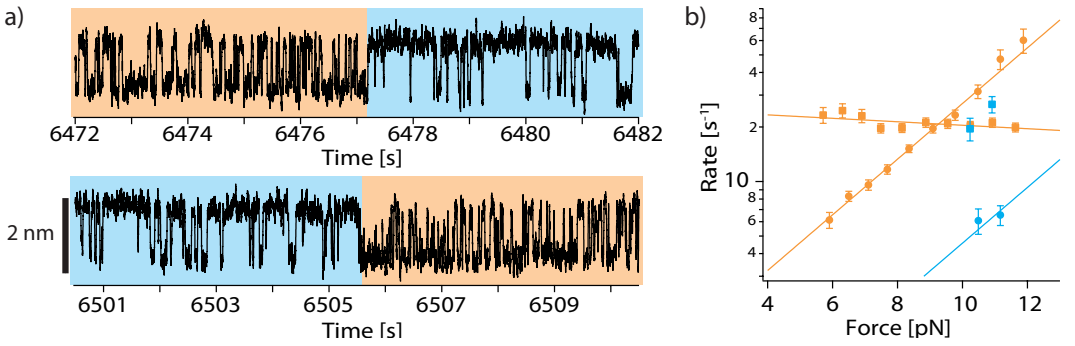

Figure 4.15 **Switching of opening kinetics of AP_5A-induced conformational change:** a) Opening and closing of thADK in the presence of 100 nM AP_5A and 2 mM Mg^{2+} sampled at 100 Hz. The typical opening and closing is shaded in orange, the slowed down kinetics in blue. b) Opening (circles) and closing (squares) rates of the conformational change. The kinetics extracted from the blue shaded region in a) is shown in blue. The regular kinetics of the transition is extracted from the rest of the data of the experiment and shown in orange. The solid lines are fits of the Bell model to the data. The blue opening rate was fit with the Δx obtained by fitting the orange data.

This switch in kinetics of the conformational change is reversible, after 28 s the previous opening and closing rates are attained again Fig. 4.15a). Due to the stepping protocol, the switch occured at a slightly higher force as the first one. In the cases, where one could observe this switch in kinetics, force didn't seem to have played a role in the time frame in which the switch occurred. However, to confirm this, further experiments have to be performed.

Because this switch in kinetics happened without apparent external influence, it most likely originates from the protein itself. One possible explanation could be proline isomerization within the folded structure. Proline isomerization can be a critical step in protein folding, as already mentioned, but since proline isomerization affects the structure of a protein, it can also have an influence on conformational changes. As mentioned before, adenylate kinase from *Aquifex aeolicus* contains 15 prolines. Of these, PRO84 is in the cis conformation and the rest in the trans conformation.

The timescales of the observed switch in opening kinetics are in good agreement with the known values for proline isomerization (Wedemeyer et al., 2002). In *E.coli* proline 87 also adopts the cis configuration and is in a very similar position as proline 84 in thADK. A mutation of PRO87 in mesoADK to serine showed a decrease in the catalytic activity (Gilles et al., 1986). For the forward reaction two ADPs to ATP and AMP, the catalytic activity is reduced by a factor of 7. Although the conserved proline at this position does not have any direct contact with the substrates, it appears to affect conformational transition of the enzyme and with this the catalytic activity. Because the opening rate is the rate limiting step in the enzyme catalysis as shown by Wolf-Watz et al. (2004), a decrease in the opening rate will lead to a decrease in catalytic activity. If our hypothesis is true, that the trans configuration of PRO84 decreases the opening rate of the enzyme, it could explain the decreased catalytic activity of the P87S mutant in *E.coli*. The serine at position 87 will adopt the trans configuration, therefore, the enzyme will have a reduced opening rate and since opening is rate limiting, a reduced catalytic activity. To test this hypothesis, one could mutate proline 84 to a serine or glycine and check if the switch in kinetics in the single molecule experiments still occurs. One would expect to see a permanent decrease in the opening kinetics. If the proline isomerization is responsible for the switching in opening and closing kinetics, we can show in our single molecule experiment, that proline isomerization can not only change the folding kinetics of a protein but also the kinetics of a conformational change of an enzyme.

All the previously shown experiments and the following experiments are done in the more unstable state. The switch to the more stable conformation only occured in very few experiments. For the rest of the analysis in this thesis, the more stable state was not considered.

4.6 Observing single lid motion

To confirm that the conformational transitions seen in the presence of AP_5A are indeed opening and closing transitions of the enzyme, a mutant with a different pulling geometry was designed. For this mutant the observed conformational change was restricted to one of the two lids, the ATP lid. This enables us to study the enzyme in a different geometry and additionally more information about the interplay between the two lids can be obtained. For a suitable mutant, we kept the cysteine at position 144 in the ATP lid, as it had been proven to affect the enzyme activity only slightly and enabled us to see the conformational transition in the 42-144 mutant. As the second attachment point we used the N-terminus. The N-C terminal pulling experiments have shown, that the α-helix at the C-terminus already starts to unfold at low forces. Therefore, the C-terminus is not a good choice, because the unfolding of the α-helix would interfere with the observation of the conformational transition. For that reason, we inserted a cysteine at the N-terminus as the second attachment point of the handles. A comparison of the distance between the two positions in the open and closed crystal structure, yields an expected size of the conformational transition of 1.2 nm, see Fig. 4.16a).

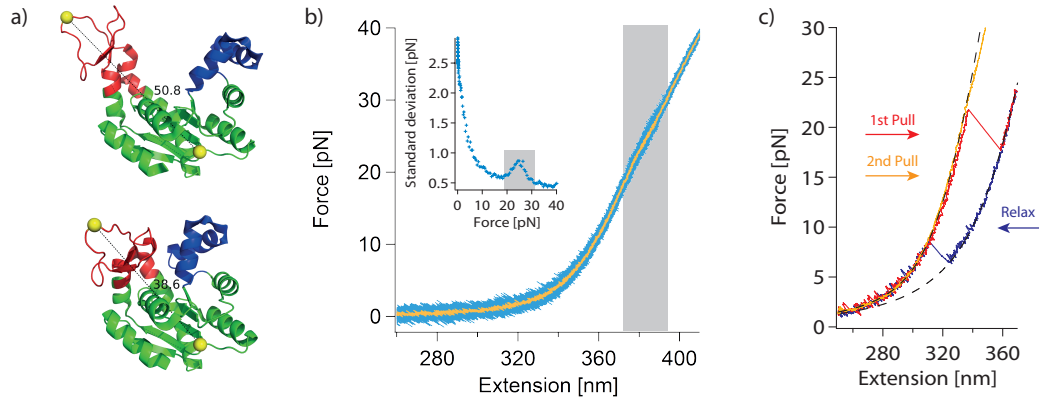

Figure 4.16 **Observing single lid motion:** a) Crystal structure of thADK in the open state (top) and closed state (bottom). Yellow spheres indicate the inserted cysteines at the N-terminus and position 144. The distance between the cysteines is shown in Å. b) Constant velocity experiment pulling at the N-terminus and position 144 with a fast unfolding/folding transition (gray area). The data is recorded at 30 kHz (blue) and smoothed to 60 Hz (orange). The insert shows a running standard deviation plot of the force signal with a significant increase of the standard deviation in the fast unfolding/folding regime. c) Constant velocity experiment of thADK N-144 at 500 nm s^{-1} of two consecutive stretch cycles (red and orange) with the interjacent relax cycle (blue). Dashed lines are fits of a combined WLC model to the data.

A typical constant velocity measurement of the N-144C mutant is shown in Fig. 4.16b). The enzyme in this pulling direction shows high stability against force. A fast unfold-

ing/folding transition can be seen at forces around 25 pN. Analyzing this unfolding event is complicated by the fact that this transition already lies in the nonlinear regime of the trap and the DNA tethers. However, a running standard deviation analysis of the force signal, shows an increase in the standard deviation between 20 pN and 30 pN Fig. 4.16b) (Insert). This increase in the standard deviation, indicates a similar equilibrium like transition, as it can be observed for the 42-144 mutant. This strengthens the hypothesis, that the first unfolding transition observed in the 42-144 mutant is, indeed, the unfolding of the ATP lid. Unfolding of the rest of the protein in the N-144 pulling direction could not be observed before the DNA handles detach. However on rare occasions the protein was not properly folded upon the first stretch cycle. Unfolding was then possible, during the relax cycles thADK was able to refold and attained the stable state again. Comparison of the previous unfolded stretch cycle with the refolded curve yields a contour length increase of 40.6 nm upon unfolding. The observed contour length increase from the unfolding transition is shorter than the expected contour length increase of 47.5 nm from the unfolding of the 144 AA. However, since this is an indirect way of determining the unfolded contour length, parts of the structure could still be folded and explain the discrepancy to the expected contour length increase. The presence of the equilibrium folding/unfolding transition as well as the approximate agreement of the measured and expected contour length increases show that we are probing thADK from N-terminus to the ATP-lid.

Addition of AP_5A results in a similar behavior as seen in the previous mutant, pulling at position 42 and 144. Starting at low forces of 3 pN to 4 pN up to around 20 pN, small closing and opening transitions can be observed. The accessible force range is larger due to the fact, that the first unfolding transition doesn't start until a force of 20 pN.

To acquire more detailed information about the closing and opening of the ATP lid, constant distance measurements at different AP_5A concentrations were performed. Sample traces at different force biases and an AP_5A concentration of 30 nM are shown in Fig. 4.17a).

The constant distance traces show a similar behavior, as it has been observed for the 42-144 mutant. At low forces, thADK is mostly in the closed state and the population of the open state increases with increasing force. However, the constant distance traces already show a smaller distance between the closed and open state. This is expected, because we're now only looking at the conformational change of one of the two lids. To quantify the size of the conformational transition in more detail, we used the same approach as it has been described for the two lid construct. For each constant distance trajectory, the distance between the closed and open state of the Hidden Markov Model assigned state was calculated and transformed to contour length space. A plot of the size of the AP_5A-induced conformational transition for the N-144C mutant is shown in Fig. 4.17b). Similar to the 42-144 construct no difference in the size of the conformational change is seen for different AP_5A concentration. However, the dependence of the

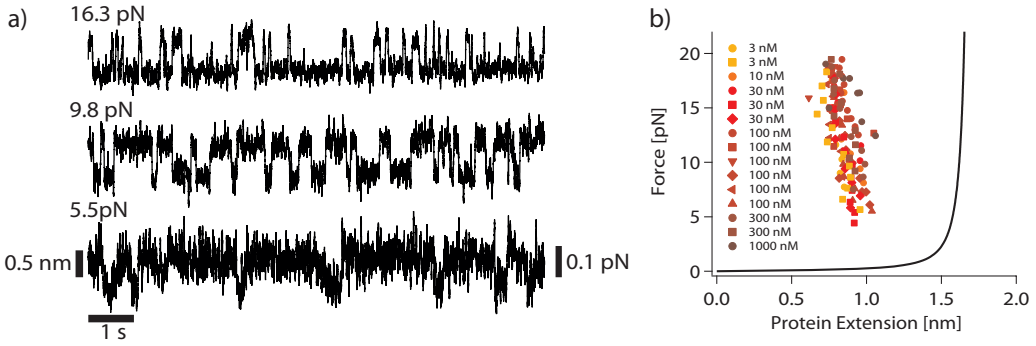

Figure 4.17 **Closing and opening of the N-144 mutant in the presence of AP_5A:** a) Constant distance trajectories of the opening and closing of thADK N-144 in the presence of 30 nM AP_5A and 2 mM Mg^{2+} at different forces smoothed to 30 Hz. b) Size of the AP_5A-induced conformational transition from Hidden Markov Model analysis transformed into contour length space. Each symbol and color represents a different experiment. For comparison the fit of the WLC model to the data of the 42-144 mutant is shown as a black solid line.

size of the conformational transition on force is different for the two mutants. For the N-144C mutant the observed size of the conformational transition is higher at low forces than it is at higher forces. Even though the dependence on force is not large, at a force of 5 pN the size is on average 0.95 nm and 0.8 nm at 20 pN. From the crystal structure of open and closed state one would expect a difference in length between open and closed ATP lid of around 1.2 nm Fig. 4.16b). This is very close to the observed size of the conformational transition, indicating that we are able to observe the closing of thADK by looking at only one of the two lids. The nonintuitive size-force behavior could be explained again by the nature of the transition. Also for the N-144C mutant opening and closing are order to order transitions. If, for this pulling direction, the open state is the more rigid state compared to the closed state, an inverse force dependence of the size of the conformational transition would be expected. It has to be noted, that the difference in the size of the conformational change, is only around 1.5 Å. Due to the overall small size of the transition itself, misassignments of states cannot be excluded and this force dependent behavior should be considered with care. Nevertheless, the overall size of the conformational transition induced by AP_5A is very close to the expected one.

The dynamics of the conformational transition between the 42-144 and the N-144 mutant agree very well. Fig. 4.18 shows the closing and opening rates of both pulling directions, extracted from Hidden Markov Model analysis, for different AP_5A concentrations. There is no significant difference in the closing rates observable between the 42-144 (filled symbols) and N-144 (unfilled symbols) mutant for the same AP_5A concentration. A global fit of a Bell model to the data yields a distance to the transition state Δx_{O-TS} of (-0.09 ± 0.01) nm and concentration dependent closing rates (Fig. 4.18). The

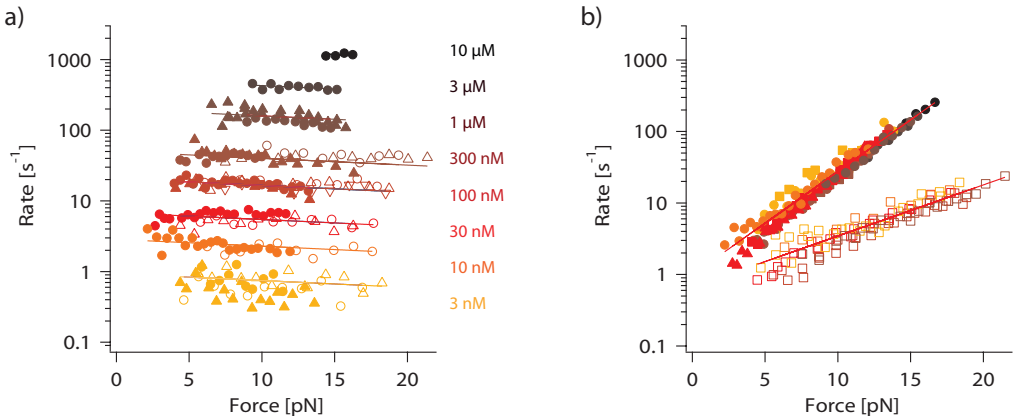

Figure 4.18 **Closing and opening rates in the presence of AP_5A:** Closing (a)) and opening (b)) rates of thADK in the presence of AP_5A and Mg^{2+}. Opening and closing rates were calculated from constant distance trajectories by Hidden Markov Model analysis. Filled symbols represent data of the 42-144 mutant and unfilled symbols of the N-144 mutant. Solid lines are global fits of the Bell model to the data. For a) the fit parameter Δx is linked between all concentrations and the mutants and k_0 for the same AP_5A concentrations and the two mutants. For b) Δx and k_0 are linked for all concentrations but not between the two mutants.

force dependent opening rates of the N-144 mutant are independent of the AP_5A concentration in the tested concentration range. This is in very good agreement with the behavior of thADK for the 42-144 direction.

The response of the opening rate to force, though, is different for the two constructs. Because the conformational transition, which is probed, is significantly smaller in the N-144 direction, the opening rate is not as force dependent, as it is in the 42-144 direction. This can be clearly seen, by fitting a Bell model to the opening rate of both mutants. The $\Delta x_{\mathrm{C-TS}}$ of the 42-144 mutant with $\Delta x_{\mathrm{C-TS}}^{42-144} = (1.36 \pm 0.02)\,\mathrm{nm}$ is about twice as big as the one from the N-144 mutant $\Delta x_{\mathrm{C-TS}}^{\mathrm{N-144}} = (0.67 \pm 0.03)\,\mathrm{nm}$. However, if one looks at the zero-force opening rates for the two, $k_{0,\mathrm{open}}^{42-144} = (0.99 \pm 0.07)\,\mathrm{s}^{-1}$ and $k_{0,\mathrm{open}}^{\mathrm{N-144}} = (0.67 \pm 0.07)\,\mathrm{s}^{-1}$, it becomes clear, that the difference in the opening-rate plot is only due to a different response to force. The opening rates at zero-force agree very well.

The data, obtained by single molecule optical trap measurements on the N-144 mutant, confirms that we are, indeed, observing the conformational transition of thADK in the presence of AP_5A. Additionally we know that the lid-closing and opening due to AP_5A is a cooperative motion. The measurements with the 42-144 mutant did not show any intermediate states. This is confirmed by the measurements of the N-144 mutant. If the lid-opening would not be cooperative, one would also expect a different closing behavior of the N-144 mutant. For a non-cooperative opening, an opening of the ATP-lid would not lead to an opening of the AMP lid and AP_5A could remain bound in the

AMP binding pocket. This, on the other hand, would dramatically increase the local concentration of AP_5A and lead to rebinding to the ATP binding site and subsequent closing of the ATP lid again. One would, therefore, expect an increase in the closing rate for the N-144 mutant compared to the 42-144 one at the same AP_5A concentration. Since this cannot be observed, the lid-closing as well as lid-opening are cooperative.

4.6.1 Induced fit vs. conformational selection

The optical trap data of the conformational change in presence of AP_5A can help to understand, how ligands can induce or modulate the conformational transition of a protein. Two theoretical models have been proposed to describe the conformational change of a protein and its interplay with ligand binding, the "induced fit" and the "population shift" model.

The first model describes the conformational change as a direct consequence of the binding of the ligand to the protein. The interaction between the binding partner and the protein "induce" the conformational change of the protein and drive it from the ligand-free state to ligand-bound conformation (Koshland, 1958). In this model the protein is described as a rigid structure, which is only able to attain the closed state in the presence of the ligand. In the "population shift" model or conformational selection model the protein, on the other hand, is seen as a dynamic molecule, which is able to sample different geometries (Bosshard, 2001; Boehr et al., 2009). The protein is able to undergo transient motions in the apo state from open to closed conformation. Thus, the apo protein exists in many conformations, including open and closed state and the ligand binds selectively to the binding competent state along the reaction pathway from open to closed conformation. Thereby, the population is shifted from the open to the closed form.

Both models have been suggested for conformational changes of proteins involving the binding of ligands. The induced fit model has been used to explain DNA-protein and protein-protein interaction (Bui and McCammon, 2006; Levy et al., 2007; Sugase et al., 2007), where as the population shift model has been described for antigen-antibody interaction or small ligand binding systems (Kumar et al., 2000; James et al., 2003; Bakan and Bahar, 2009). However, these models are not mutually exclusive and a combination of the two might be helpful to understand protein ligand interactions (Wlodarski and Zagrovic, 2009; Silva et al., 2011).

It has been shown experimentally (Hanson et al., 2007; Henzler-Wildman et al., 2007b), as well as computationally (Arora and Brooks, 2007; Matsunaga et al., 2012; Song and Zhu, 2013), that adenylate kinase undergoes transitions from open to closed conformation even in the absence of substrates. This would at first glance favor the "population shift" model, which requires these transient motions along the reaction coordinate. The data obtained by our optical trap experiments, however, show that the conformational change of thADK caused by AP_5A follows the "induced fit" mecha-

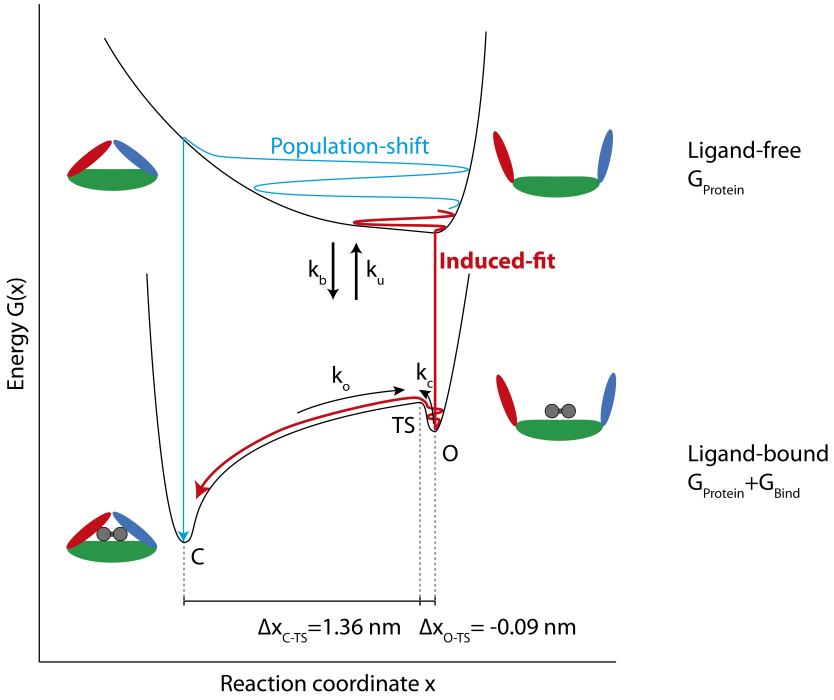

Figure 4.19 **AP_5A binding and closing model:** Schematic view of the binding and closing of adenylate kinase to AP_5A with two energy landscapes for the ligand-free and ligand-bound form of adenylate kinase. Adenylate kinase can exist in the open and closed conformation in bound and unbound form. It can jump between the two energy landscapes by ligand binding and unbinding with the rate k_b and k_u, respectively. For the ligand-bound energy landscape, distances from open and closed state to the transition state are shown from optical trap experiments. Exemplary routes from open ligand-free to closed ligand-bound form are shown for the the population-shift and induced-fit model.

nism and not a conformational selection process. This can be nicely illustrated by the model shown in Fig. 4.19, which has been adapted from Okazaki and Takada (2008). The binding and release of the ligand is modeled as a jump between two energy landscapes, one in the ligand-free form and the other in the presence of ligand. Here, the energy landscape of the ligand free form is an adaptation of the one shown in molecular dynamics simulations by Arora and Brooks (2007), because we are not able to make a statement about the ligand-free energy landscape from our optical trap experiments. In this energy landscape, no significant energy barrier between open and closed state can be observed and adenylate kinase is able to sample all conformations from open to closed state, however the energy minimum is at the open state and subsequently the equilibrium. Binding of the ligand changes the energy landscape, so that the energy minimum is now at the closed state and an energy barrier is present between open and closed state. The two mechanisms, population shift and induced fit, can be represented as two specific routes on the two energy landscapes. In the population shift mechanism of binding and closing, adenylate kinase exists with a small probability in the closed unbound form and with binding of the ligand this conformation is stabilized and the closed bound form is reached directly. For the induced fit mechanism, adenylate kinase resides in the open unbound form and upon ligand binding jumps to the ligand bound energy landscape. Subsequently the conformational change from open to closed ligand bound form occurs.

Depending on the model, which describes the binding and closing of adenylate kinase in presence of AP_5A, a difference in the force dependence of the closing rate in optical trap experiments is expected. The force dependence of the closing rate is proportional to the distance from the open state to the transition state Δx_{O-TS}. This distance needs to be crossed by the enzyme to reach the transition state from where closing readily occurs. Assuming the binding and closing follows the conformational selection model, adenylate kinase has to exist in the closed and yet unbound form before AP_5A binding can occur, resulting in a large distance from the open state to the transition state. Here, the closing rate will be highly force dependent and will decrease with increasing force. If, on the other hand, the binding and closing follows the induced fit model, the ligand binds to the open state of adenylate kinase and "induces" the conformational change. For this model, a small distance from the open state to the transition state is expected, resulting in a small force dependence of the closing rate. Our optical trap data of thADK in presence of AP_5A shows, that the closing rate is almost independent of force, the distance from the open state to the transition state is very small Δx_{O-TS}=−0.09 nm. This is in stark contrast to the expected force dependence of the conformational selection model. In the process of binding and closing, adenylate kinase has to undergo only small rearrangements before AP_5A can bind and the protein closes, consistent with the induced fit model. This provides very strong evidence that the closing of thADK in presence of AP_5A follows the induced fit model.

The experiments at different AP_5A concentrations have shown, that the closing of thADK is a diffusion limited process. The rate-limiting step in the pathway from the open ligand-free form to the closed ligand-bound form is the binding rate k_b. The closing rate k_c, depicted in Fig. 4.19, must, therefore, be higher than the binding rate k_b. In the optical trap experiments, one cannot observe the actual closing process, but rather the binding rate of AP_5A as the rate limiting step in closing of the enzyme.

4.6.2 The AMP lid

The N-144 mutant enabled us to observe the motion of a single lid, the ATP lid, during the conformational change induced by AP_5A. Additionally, it provided further evidence that the fast folding/unfolding transition of 5.4 nm, observed in the 42-144 mutant, is caused by the ATP lid. To confirm this assumption, we created a mutant, with one cysteine at the N-terminus and one in the AMP lid at position 42. This allows the observation of folding and unfolding behavior of the AMP lid independent of the ATP lid.

Constant velocity experiments on the N-42 mutant under apo conditions did not show any unfolding events in the accessible force range up to 40 pN-45 pN before the construct detaches from the beads. The contour length from WLC fits to the data, agrees with the expected contour length of the construct of 370 nm. This indicates that we are, indeed, probing single constructs and not multiple in parallel tethered constructs. Repeated experiments never showed unfolding events with this construct. However, we cannot fully exclude, that the observed events are DNA only events, where the handles are cross-linked by oligo-dimers. To minimize the probability of this to happen, special care has been taken during the attachment of the maleimide modified oligos to the construct. An additional Ni^{2+}-column purification step is performed after the reaction of the oligos to the protein, to remove any unreacted oligos, as well as oligo-dimers. For the other construct, this helped to reduce the appearance of DNA only events to a bare minimum. If we are, indeed, probing the N-42 mutant, the stability of the mutant against force is high and the AMP lid can't be unfolded in the force regime accessible with our setup. This strengthens our hypothesis that the first unfolding transition seen in the 42-144 mutant is the unfolding of the ATP lid. Additionally, this indicates, that the protein continues unfolding near the ATP lid, after the lid has been unfolded.

Optical trap experiments of the N-42 mutant in the presence of AP_5A did not show any conformational transitions, as we have seen for the 42-144 as well as the N-144 mutant. This observation is already expected from the comparison of the crystal structure of open and closed thADK. During the conformational transition the AMP lid flips over the N-terminus and the absolute distance of the cysteine at position 42 to the N-terminus between open and closed state is only 2.3 Å. A possible alternative pulling direction could be between position 42 and 189. Position 189 is located at the C-terminus after the terminal α-helix. In the N-C terminal pulling direction, the terminal α-helix un-

folded at relatively low forces. Attaching the handle after the α-helix should ensure that the α-helix won't be unfolded during the experiment. The expected length change for the position 42 and 189 is 5.2 Å between open and closed state. As shown for the simulated conformational transition of 4.8 Å in chapter 2.4.4, this should be within the resolution of our instrument.

4.7 Binding of the inhibitor AP_4A and AP_6A

Reinstein et al. (1990a) have shown in their binding studies of adenylate kinase that not only the bisubstrate mimic AP_5A binds to adenylate kinase, but also the inhibitors AP_4A and AP_6A. The order of the dissociation constants is given as follows: $K_D^{AP_5A} < K_D^{AP_6A} < K_D^{AP_4A}$. Surprisingly AP_4A shows the lowest affinity of the three inhibitors, despite its structure, which resembles the four phosphates in the natural substrates the most. Even AP_6A which has two additional phosphates shows higher binding affinity than AP_4A. This binding study however does not show if the inhibitors AP_4A and AP_6A also trigger the closing of adenylate kinase or if they just bind to the enzyme. To address this issue, we measured the behavior of thADK in the presence of AP_4A and AP_6A in our single molecule optical trap assay.

4.7.1 AP_4A

Constant velocity measurements of the 42-144 thADK mutant in the presence of AP_4A showed a similar behavior, as in the presence of AP_5A. Again small transitions with a contour length of around 1.8 nm can be observed between 4 pN and the start of the unfolding of the ATP lid around 13 pN. To obtain more detailed information about the closing and opening, constant distance measurements in the presence of AP_4A were performed.

Fig. 4.20a) shows exemplary constant distance traces of the opening and closing due to AP_4A at three different force biases. Frequent transitions between the open and closed state can be observed. There is no difference in the size of the conformational change visible for different AP_4A concentrations and a global fit of a WLC model to the data results in a contour length of (1.67 ± 0.01) nm, see Fig. 4.20b). This is very close to the measured size of the conformational transition in presence of AP_5A of 1.72 nm. The similar sizes of the conformational change suggest that the closed state is the same in the presence of AP_4A and AP_5A. The dynamics of the conformational transition for different AP_4A concentrations Fig. 4.21a) confirm this hypothesis. No difference in the opening rates of thADK at different concentrations of AP_4A can be observed and the zero-force opening rate k_0 is extrapolated to $(1.0 \pm 0.2)\ s^{-1}$ with a Δx of (1.4 ± 0.1) nm. These values agree very well with the ones obtained for the conformational change in presence of AP_5A (k_0 of $1\ s^{-1}$ and Δx of 1.36 nm). Because the opening rates are

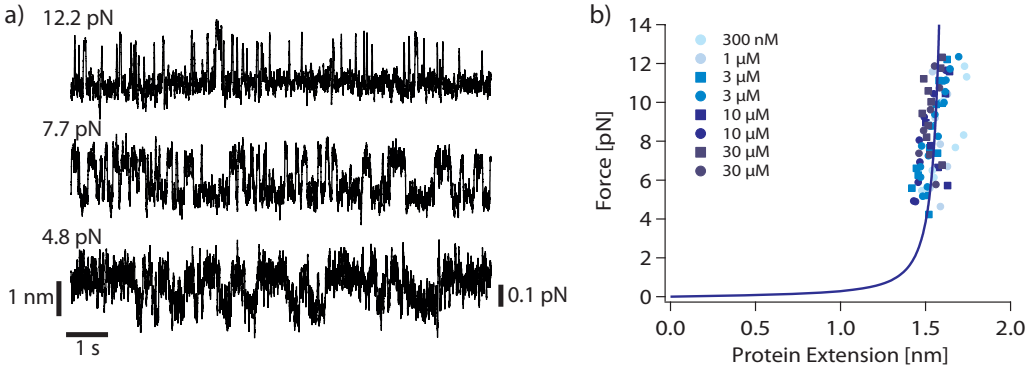

Figure 4.20 **Closing and opening of thADK in the presence of AP_4A:** a) Constant distance trajectories of the opening and closing of thADK 42-144 in the presence of 3 µM AP_4A and 2 mM Mg^{2+} smoothed to 75 Hz. b) Size of the AP_4A-induced conformational transition from Hidden Markov Model analysis transformed into contour length space. Each symbol and color represents a different experiment. A global fit of a WLC model to the data is shown as a blue solid line.

the same in both cases, the closed state has the same stability for the two inhibitors, demonstrating that the structure of the closed state is very similar.

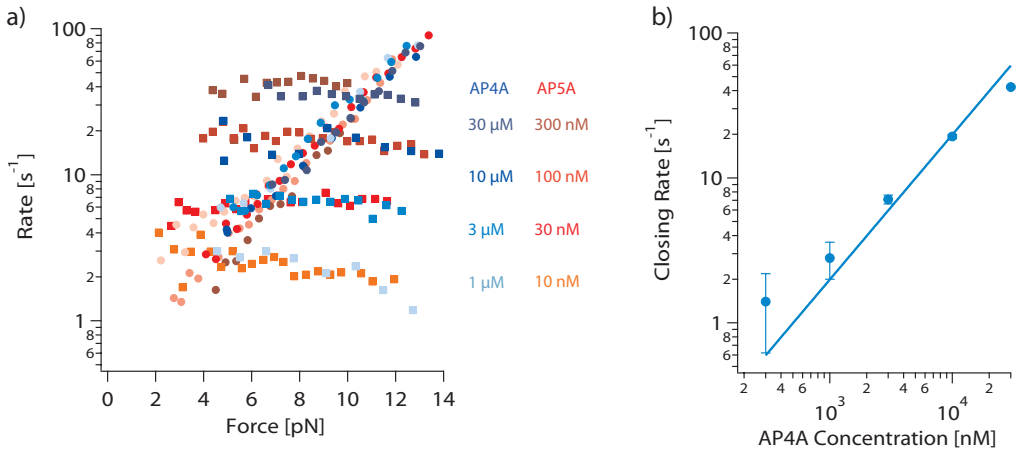

Figure 4.21 **Dynamics of the conformational change of thADK in the presence of AP_4A:** a) Closing (squares) and opening (circles) rates of thADK in the presence of different concentrations of AP_4A (blue). For comparison the closing and opening rates of thADK in the presence of different AP_5A concentrations (red) is shown as well. b) Zero-force opening rates of the conformational transition in presence of different AP_4A concentrations. The solid line is a linear fit to the data.

The closing rates are, again, almost independent of force. However for the observation of the same closing rate as with AP_5A about 100 times more AP_4A is needed. By

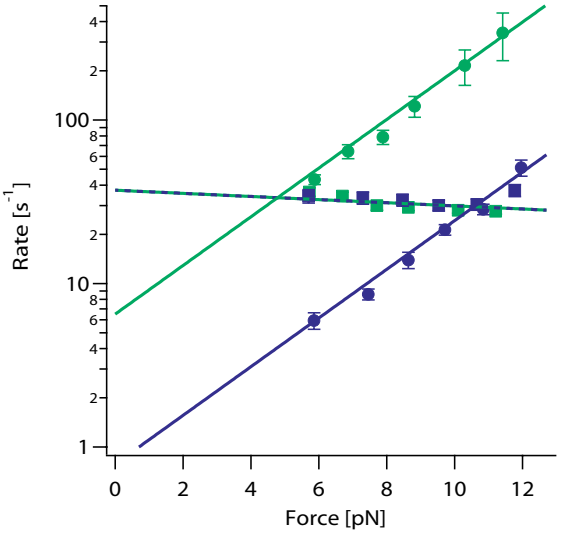

Figure 4.22 **Effect of Mg^{2+} on the AP_4A-induced conformational change:** Opening (circles) and closing (squares) rates of thADK at 30 µM of AP_4A in the presence (blue) and absence (green) of Mg^{2+}. Solid lines are fits of the Bell model to the opening rate. Δx has been fixed for Mg^{2+} and Mg^{2+} free conditions. The dashed line is a fit to the closing rate in presence as well as absence of Mg^{2+}.

fitting a Bell model to the data, the zero force closing rate can be extrapolated and it is plotted against the AP_4A concentration in Fig. 4.21. As with AP_5A, the closing rate is linearly correlated with the concentration. This indicates that the closing is a binding dependent process. In contrast to the diffusion limited binding of AP_5A, the on-rate of AP_4A is with $(2.0 \pm 0.1) \times 10^6\,\mathrm{M^{-1}\,s^{-1}}$ about a factor 100 lower. AP_4A, therefore, does not bind in a diffusion limited manner. The dissociation constant K_d of AP_4A in the presence of Mg^{2+} is (421 ± 58) nM.

Experiments with thADK and AP_4A in the absence of Mg^{2+} showed a similar behavior, as has been observed for AP_5A and EDTA, see Fig. 4.22. The opening rate is increased by a factor of around five to $(6.1 \pm 0.3)\,\mathrm{s^{-1}}$. The closing rate, on the other hand, remains unchanged. Therefore, the dissociation constant for AP_4A in the absence of Mg^{2+} is increased to around (2100 ± 300) nM. This is additional evidence, that the closed conformation is very similar for the two inhibitors AP_4A and AP_5A and that Mg^{2+} stabilizes the closed conformation. This is in contrast to the observations of Reinstein et al. (1990b), who reported dissociation constants of AP_4A of 0.7 µM in the presence of Mg^{2+} and 1.3 µM in the absence of Mg^{2+}. Their experiments suggested that Mg^{2+} does not have a strong effect on opening and closing for AP_4A. However, the single molecule experiments showed that Mg^{2+} is indeed needed for AP_4A to bind with full affinity.

The unchanged contour length as well as the slope of the opening and closing rates suggest that the opening and closing takes place in a similar fashion in the presence of AP_4A, as it does in the presence of AP_5A. However the binding of AP_4A to adenylate kinase seems to be hindered, which results in the lower on-rate. The closing behavior of thADK in presence of AP_4A fits well to the reported crystal structure of human adenylate kinase 1 in the presence of AP_4A (PDB 2C95). The crystal structure shows a closed

state which resembles closely the one of human adenylate kinase 1 in the presence of AP_5A (PDB 1Z83). Only minor differences of the protein structure between the two closed states can be observed. To compare the distance between the two adenine groups between the AP_4A and the AP_5A structure the distance of the ring oxygen of the ribose in the adenosine is chosen. The distance is with 15 Å only 1.2 Å smaller in the AP_4A structure compared to the AP_5A structure. Because the additional phosphate in AP_5A adds about 3 Å more spacer length between the adenine groups. AP_4A has to take on a more stretched configuration to compensate for the fifth phosphate. Due to its shorter length AP_4A has to be in this more stretched conformation, before it can bind properly in the two binding pockets of adenylate kinase and induce closing of the enzyme. This might be the reason for the reduced on-rate of AP_4A. The attained closed structure is similar to the one of AP_5A, therefore no difference in the size of the conformational change or opening behavior is expected, which is confirmed by the single molecule optical trap data.

4.7.2 AP_6A

Bulk experiments have shown that AP_6A is also a strong inhibitor of adenylate kinase. This is quite surprising, because AP_6A has two more phosphates than the natural substrates, ATP and AMP, combined. It is, however, unknown, if the inhibition process of AP_6A includes closing of adenylate kinase or if the steric hindrance of the additional phosphates prevents closing of the enzyme.

Initial constant velocity experiments of thADK in the presence of AP_6A indicated that closing and opening take place, however with a reduced size. To characterize the closing and opening transition in more detail, constant distance experiments were performed. Fig. 4.23a) shows exemplary constant distance traces at three different force biases in the presence of AP_6A. Similar to the other inhibitors, opening and closing transitions can be observed. The difference between open and closed state is smaller than the one observed in the presence of AP_4A and AP_5A. An analysis of the length difference between the open and closed state is shown in Fig. 4.23b). It can be clearly seen that the size of the conformational change is much smaller compared to the one in presence of AP_5A. For the different AP_6A concentrations, no difference in the size of the conformational change can be observed. A global fit of a WLC model to the data, with the same persistence length as in the AP_5A case, yields a contour length of (6.4 ± 0.1) Å. Compared to the size of the conformational change in presence of AP_4A and AP_5A adenylate kinase only closes to around 40 %.

Due to the small size of the conformational change an assignment of the open and closed state is difficult, potential misassignments of states cannot be excluded. Nonetheless the closing and opening dynamics are shown in Fig. 4.24. With the exception of 30 nM, the closing rate of thADK in presence of AP_6A is very similar to the one at the same AP_5A concentration. The difference for the 30 nM condition is most likely due to

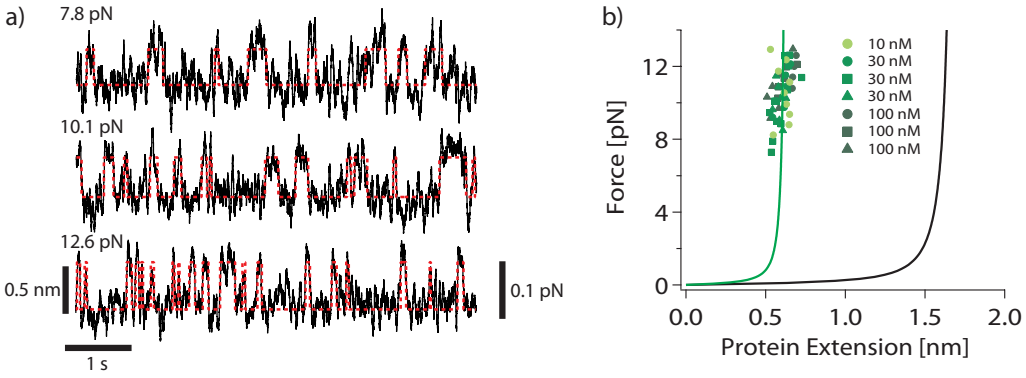

Figure 4.23 **Closing and opening of thADK 42-144 in the presence of AP_6A:** a) Constant distance trajectories of the opening and closing of thADK 42-144 in the presence of 30 nM AP_6A and 2 mM Mg^{2+} smoothed to 50 Hz. The dashed red lines indicate the state assignment by Hidden Markov Model analysis. b) Size of the AP_6A-induced conformational transition from Hidden Markov Model analysis transformed into contour length space. Each symbol and color represents a different experiment. A global fit of a WLC model to the data is shown as a green solid line. For comparison, the WLC fit to the data of the conformational changed induced by AP_5A is shown in black.

a pipetting error for this AP_6A concentration.

If we exclude the experiments at 30 nM, the AP_6A-induced conformational change shows the same concentration dependent closing behavior, as it has been observed in presence of AP_5A. Also the conformational transition due to AP_6A must, therefore, be a binding dependent process with a diffusion limited on-rate. This is in contrast to the binding of AP_4A to adenylate kinase which shows an on-rate which is reduced by a factor of 100 compared to AP_5A and AP_6A. Not only is the concentration dependence of AP_5A and AP_6A the same, but also the force dependence of the closing rate is very similar. It can be fit with the Bell model using the same Δx of -0.09 nm. Despite the difference in the size of the conformational change, the initial closing step appears to be the same.

How does the partial closing in presence of AP_6A influence the stability of the closed state? The stability of the closed state is given by the opening rate at zero force. If we fit the force dependent opening rate to the Bell model we obtain a Δx of (0.7 ± 0.1) nm and a zero-force opening rate of $(2.0 \pm 0.6)\ s^{-1}$. The zero-force opening rate is surprisingly close to the one obtained in the presence of AP_5A of around $1\ s^{-1}$. The extrapolated opening rate shows only a small decrease in the stability of the closed complex. This suggests that even the partly closed adenylate kinase already forms a rather stable conformation. However, one has to note, that the force range over which the extrapolation to zero force can be made for AP_6A is relatively small, because the resolution at lower

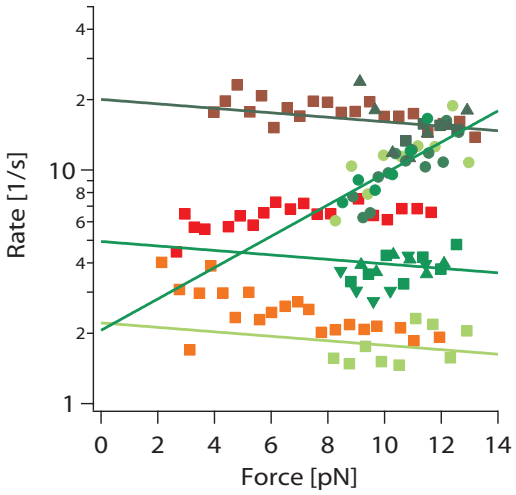

Figure 4.24 **Closing and opening rates of thADK 42-144 in the presence of AP_6A:** Closing (squares and triangles) and opening (circles) rates of thADK 42-144 in the presence of different concentrations of AP_6A (10 nM light green, 30 nM green, 100 nM dark green). For comparison the closing and opening rates of thADK in the presence of different AP_5A concentrations (10 nM orange, 30 nM red, 100 nM dark red) is shown as well. Solid lines are fits of the Bell model to the data.

forces is not high enough to reliably assign the open and closed state. This likely affects the precision of the zero-force estimate.

The question remains, how the reduced size of the conformational change can be explained. Most likely, it is caused by the additional sixth phosphate. Adenylate kinase is able to tolerate the fifth phosphate of AP_5A and fully close. Early experiments by Kupriyanov et al. (1986) have shown that adenylate kinase 1 from rabbit can tolerate additional phosphates even for the natural substrates. They were able to observe the generation of AP_4 by adenylate kinase catalyzing the reaction from ATP and ADP to AMP and AP_4. This shows, that the binding pocket is large enough to accommodate a fifth phosphate and the phosphotransfer can still be catalyzed. Therefore, water has to be excluded from the reaction volume to prevent nonproductive ATP hydrolysis. This, on the other hand, requires the closure of the two lid domains. However, with AP_6A this is not possible anymore. The six phosphates are apparently to big to fit entirely in the binding pocket and sterical hindrances prevent thADK from closing completely.

To address the question if the reduced conformational transition of adenylate kinase in the presence of AP_6A is due to the hinderance of either the AMP or ADP lid, or if both lids are affected, experiments with the N-144C mutant in presence of AP_6A were performed.

Also in this pulling direction conformational transitions in the presence of AP_6A can be observed. Representative constant distance traces are shown in Fig. 4.25a). The size of the conformational change is reduced even further, which can be clearly seen in Fig. 4.25b). The small size of the conformational transitions limits the force range, in which an assignment of open and closed state can be made. Therefore, a reliable statement about the force dependence of the size of the conformational change cannot be made. Because the force dependent behavior of the size of the conformational change in the presence of AP_6A is not clear, we will give an average value of the size of the

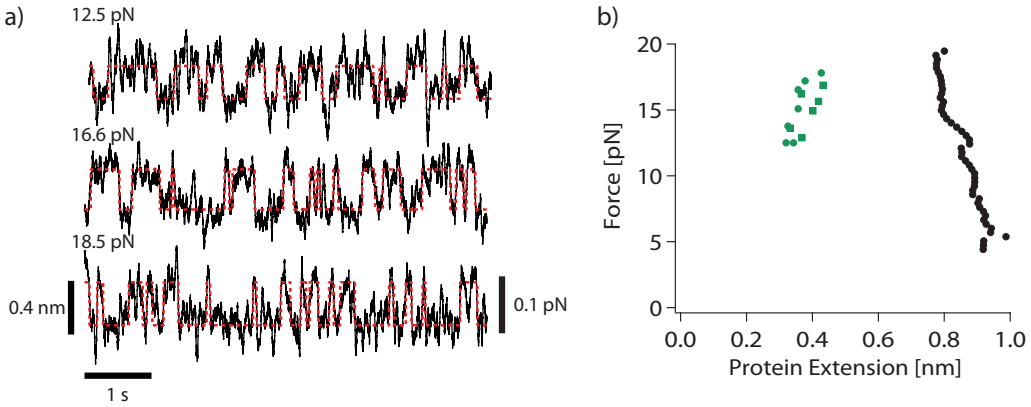

Figure 4.25 **Closing and opening of thADK N-144 in the presence of AP_6A:** a) Constant distance trajectories of the opening and closing of thADK N-144 in the presence of 30 nM AP_6A and 2 mM Mg^{2+} smoothed to 30 Hz. The dashed red lines indicate the state assignment by Hidden Markov Model analysis. b) Size of the AP_6A-induced conformational transition from Hidden Markov Model analysis transformed into contour length space at 30 nM AP_6A. Each symbol and color represents a different experiment. For comparison, the average values of the conformational change of thADK N-144 in presence of AP_5A is shown in black.

conformational change of (3.7 ± 0.4) Å for the measured force range. For comparison the average size of the conformational transition due to AP_5A is (8.0 ± 0.6) Å in this force range. In the presence of AP_6A the ATP lid closes only to about 45 %.

For the conformational change observed in the 42-144 direction due to AP_5A, both lids contribute about equally to the overall size of the conformational change, as it can be seen in Tab. 4.3. If the hindrance effect of AP_6A was limited to the ATP lid, a 45 % closure of the ATP lid and a full closure of the AMP lid would, therefore, lead to an overall closure of adenylate kinase of approximately 70 %, around 20 % from the ATP lid and 50 % from the AMP lid. Since we observe only 40 % closure in the 42-144 direction the hindrance effect of AP_6A cannot be limited to the ATP lid alone. The steric hinderance of the additional phosphate is therefore not limited to one of the two lids, but it affects them both approximately to the same extent.

4.7.3 Discussion

In addition to the experiments with AP_5A, the experiments with the two other bisubstrate inhibitors AP_4A and AP_6A show important aspects of the conformational change of adenylate kinase. Interestingly AP_4A and AP_6A behave differently than AP_5A but each of them shares a common characteristic with AP_5A. AP_4A and AP_5A both induce a conformational change of the same size and stability. Whereas AP_6A and AP_5A have

the same association rate to adenylate kinase.

The on-rate of the different inhibitor provides important information about the initial binding process of the bisubstrate inhibitors to adenylate kinase. The two adenine groups have to span a minimum distance to be able to bind into their respective binding pockets. AP_5A and AP_6A, both have enough spacer length between the two adenine groups, as well as flexibility to cover the distance between the binding sites. This enables them to bind in a diffusion limited process. AP_4A, on the other hand, has to undergo structural rearrangements to compensate for the missing length of one phosphate, about 3 Å in bond length. These rearrangements reduce the on-rate of AP_4A by a factor of about 100. The spacer length between the two binding moieties is, therefore, critical for efficient binding to the enzyme.

However, if AP_4A is bound to thADK, it triggers the same conformational change as it can be observed for AP_5A. This in contrast to AP_6A, which binds in a diffusion limited manner, but the induced conformational change itself, is significantly smaller. These experiments show that thADK cannot only populate the fully open or closed state, but also a partially closed state. Surprisingly, this intermediate state shows a stability which is close to the one observed for the fully closed conformation. The reduced closing of thADK in presence of AP_6A is most likely caused by steric hinderance of the sixth phosphate. The partial closing is also not limited to the closing of only one of the two lids, but an intermediate position of each lid. These observations are in accordance with previous experiments, which have shown that substates along the reaction trajectory can be populated by adenylate kinase (Henzler-Wildman et al., 2007b).

Interestingly, for all three bisubstrate inhibitors AP_4A, AP_5A and AP_6A the closing rate is almost independent of force. Fits of a Bell model to the closing data show a similar force dependence of $\Delta x = -0.09\,\mathrm{nm}$ for all three inhibitors. The distance from the open state to the transition state is very small. Despite different binding kinetics and different closed states, the initial part of the conformational change is the same for the three different inhibitors. Therefore, the binding and closing of thADK in presence of all three inhibitors can be explained by the induced fit model.

4.8 Binding of the nucleotides AMP, ADP and ATP

The previous chapters showed that the optical trap setup enables us to observe the conformational transition of adenylate kinase upon binding to different kind of bisubstrate inhibitors. What happens to adenylate kinase in the presence of the real substrates AMP, ADP or ATP? This question will be adressed in the following chapters.

4.8.1 AMP, ADP and ATP

To investigate the behavior of thADK in the presence of substrates, optical trap experiments with different nucleotide conditions were performed. Fig. 4.26 shows an exemplary trace of thADK in the presence of 1 mM ADP and 2 mM Mg^{2+}. Unlike the experiments with AP_5A no clear conformational transitions can be seen in the force range from 4 pN to 13 pN. The trace in this force region is very similar to the one at apo conditions. However, the equilibrium folding/unfolding transition is now shifted to higher forces. WLC fits to the data show a contour length increase for the first unfolding transition of 5.4 nm, which is in agreement with the contour length increase at apo conditions. Therefore, the enzyme does not unfold when it is in the closed state but rather in the open state. An unfolding from the closed state would result in a larger contour length increase, accounting for the opening transition of 1.7 nm.

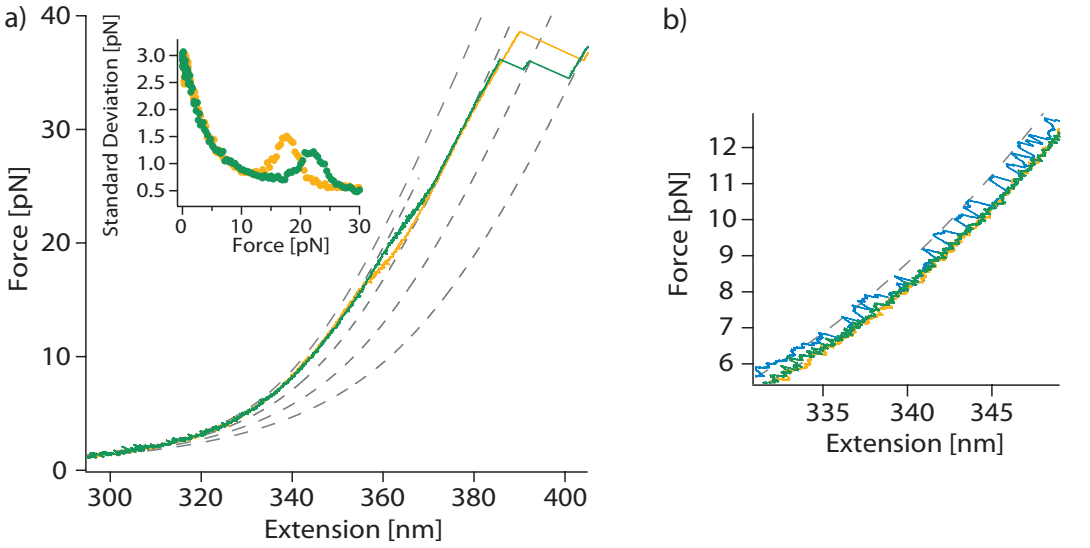

Figure 4.26 **The effect of the nucleotide ADP on thADK:** a) Force extension trace of the 42-144 mutant of thADK in the presence (green) and absence (orange) of 1 mM ADP and 2 mM Mg^{2+} filtered to 60 Hz. Dashed lines are fits of a combined WLC model to the different folded and unfolded states of thADK. The inset shows a running standard deviation plot of the force extension traces with a significant increase of the standard deviation in the fast unfolding/folding regime of the ATP-lid. In presence of ADP, this transition regime gets shifted to higher forces. b) Magnified section of a) with an additional trace showing the opening and closing of thADK in presence of 100 nM AP_5A (blue). No conformational changes can be observed for thADK in apo conditions and in the presence of ADP.

To exclude influences caused by the enzymatic turnover of the substrates AMP and ATP as well as ADP, nonhydrolyzable analogues of ADP and ATP were tested as well.

The nonhydrolyzable ATP analogues AMPPNP and AMPPCP were shown to induce conformational transitions in thADK in NMR experiments (Wolf-Watz et al., 2004). However, in our measurements neither ADPβ-s, AMPCP, nor AMPPCP with AMP showed any distinct conformational transitions, of the kind observable in the presence of AP_5A. AMPPNP on the other hand, was able to induce these kind of conformational transitions, even in the absence of AMP. This special case will be discussed in chapter 4.10. Because all nucleotides and most of the nonhydrolyzable analogues do not show any conformational transitions of thADK, the question arises if the nucleotides bind to thADK. If they indeed bind, why are we not able to observe conformational fluctuations of thADK in their presence? To address these questions, we used an AP_5A competition assay in the optical trap, which is described in the next chapter.

4.8.2 AP_5A competition assay

The competition assay shown here, is based on similar principles as the one used by Reinstein et al. (1990a) to determine the affinities of nucleotides to *E.coli* ADK. Instead of using the fluorescence enhancement of the fluorescently labeled mant-AP_5A-mant (mAP_5Am) upon binding to ADK, we use the conformational transition in the optical trap as our reporter. Bound nucleotides will prevent AP_5A binding, leading to altered kinetics of the opening and closing. Exemplary traces of the AP_5A competition at different ATP conditions are shown in Fig. 4.27a). The number of closing events decreases with increasing ATP concentration. Furthermore, the dwell times of the open state increases, while the dwell times of the closed events stay approximately the same. At the shown ATP concentrations, ATP binds to thADK and thus blocks the binding site. This prevents AP_5A binding along with the induced conformational transition. The higher the ATP concentration, the more likely it is for ATP and less likely for AP_5A to bind, thereby, increasing the dwell times of the open state. This shows that ATP can indeed bind to thADK and that the closing due to AP_5A, or better the absence of it, can serve as a reporter for nucleotide binding.

The opening and closing rate of thADK due to AP_5A binding in the presence of different nucleotides and concentrations is shown in Fig. 4.27b). Above a certain concentration all nucleotides reduce the closing rate of thADK. However, the concentration needed to observe the same effect varies between the different nucleotides, due to their different affinities to thADK. A slight increase in the opening rates can be observed as well, which is most prominent for AMP. To address the combined effect of nucleotide binding on the closing as well as the opening rate, the free energy of the conformational change is calculated. By looking at the effect on the free energy, one can easily compare competition experiments with different AP_5A concentrations. Especially at high nucleotide concentrations, only very few closing events can be observed at low AP_5A concentrations. Therefore, the AP_5A concentration was increased for high nucleotide concentrations. To be able to compare the AP_5A competition experiments stemming

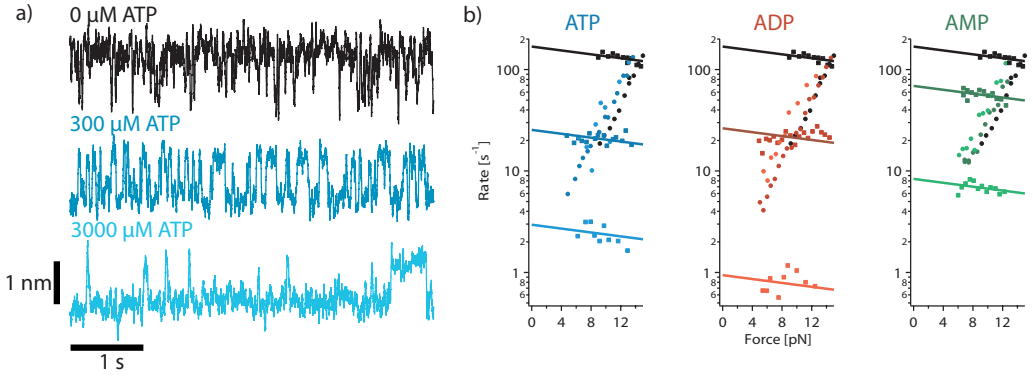

Figure 4.27 **AP_5A nucleotide competition experiments:** a) Constant distance trajectories of the opening and closing of thADK 42-144 in the presence of 1 µM AP_5A, Mg^{2+} and varying concentrations of ATP smoothed to 75 Hz. b) Opening (circles) and closing (squares) rates of the conformational transition in the presence of 1 µM AP_5A, Mg^{2+} and varying nucleotide concentrations (300 µM ATP dark blue, 3 mM ATP blue, 30 µM ADP dark red, 1 mM ADP red, 3 mM AMP dark green, 16 mM AMP green). For reference the opening and closing rate in the absence of nucleotides is shown in black.

from different AP_5A concentrations, only the decrease in free energy due to nucleotide binding from the nucleotide free case is evaluated. The AP_5A concentrations used in the competition assay were either 100 nM or 1000 nM.

The free energy difference between the AP_5A only experiments and the ones in presence of nucleotides and AP_5A is plotted in Fig. 4.28. For all three nucleotides, one can see a decrease in free energy upon reaching a certain concentration. ADP in the absence of Mg^{2+} is the first nucleotide to show a decrease in free energy, followed by ADP in presence of Mg^{2+}, ATP and AMP. ADP in presence and absence of Mg^{2+} and ATP, all show a similar behavior at higher concentrations. AMP, on the other hand, shows a steeper decrease in free energy at higher concentrations than the other nucleotides. The decrease in free energy can be modeled as described in chapter 3.5. For ADP and ATP, the data is fit best with a model, assuming the binding of one molecule. For higher concentrations, the free energy is decreased by 2.3 kT for every ten-fold increase in nucleotide concentration. In case of AMP, a two-molecule binding model reproduces the data best. For the AMP competition experiments at higher concentrations, the free energy is decreased by 4.6 kT for every ten-fold increase in AMP concentration. The resulting fits of the two models are shown in Fig. 4.28.

From the fits we obtain the corresponding dissociation constant K_d for the different nucleotides. The K_d value for ATP in the presence of Mg^{2+} is (17 ± 2) µM, which corresponds well to the values obtained by Reinstein et al. (1990a) for the Q28H mutant of *E.coli* ADK with 20 µM. For ADP in the absence and presence of Mg^{2+} we obtain

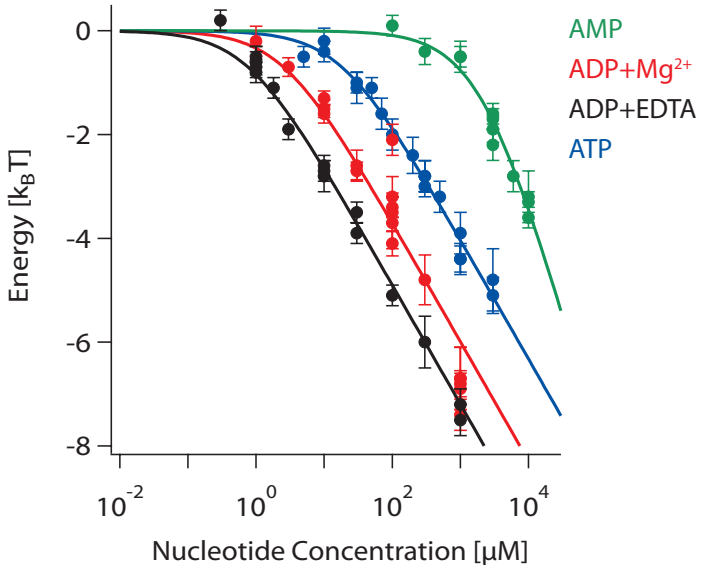

Figure 4.28 **AP_5A nucleotide competition:** Decrease in the free energy of the conformational change induced by AP_5A due to the binding of nucleotides to thADK. The effect is shown for the nucleotides AMP (green), ADP+Mg^{2+} (red), ADP+EDTA (black) and ATP+Mg^{2+} (blue). Solid lines are fits to the data.

a dissociation constant K_d of (0.8 ± 0.1) µM and (2.0 ± 0.1) µM, respectively. This is again in good agreement with the literature value for the ADP in absence of Mg^{2+} of 2.6 µM.

The effective dissociation constant for AMP of (2180 ± 130) µM is about ten-fold higher than the one reported for the AMP binding site (186 µM). Apparently, AMP is not able to bind to the AMP binding site and prevent AP_5A from binding. However, it has been reported that AMP can bind nonspecifically to the ATP binding site. This unspecific AMP binding has been suggested to cause the substrate inhibition of adenylate kinase by AMP (Sinev et al., 1996), which is also observed in our own enzymatic activity assays. Adén and Wolf-Watz (2007) have reported a dissociation constant of AMP for the ATP binding site of mesoADK of (1700 ± 400) µM from NMR experiments. This agrees well with the dissociation constant for AMP, observed in our competition experiments. As the AMP data can only be fit by a model, assuming the binding of two molecules, AMP binding even to the ATP binding site alone is not enough to prevent AP_5A from binding. Therefore, AMP has to bind to the AMP, as well as, the ATP binding site to abolish the binding of AP_5A. This is in contrast to the other two nucleotides ADP and ATP. Here, the free energy difference decreased by 2.3 kT for every ten-fold increase in nucleotide concentration, indicating that the binding of only one nucleotide molecule is enough to prevent AP_5A from binding.

A similar behavior has been observed by Reinstein et al. (1990a), who claim that binding of AMP to the AMP binding site alone is not enough to replace mAP_5Am from adenylate kinase. They explain this by improper binding of the fluorescently modified AP_5A to the AMP binding site. However, from their experiments, it is not clear, whether the binding of one or two AMP molecules is needed to observe the decrease in fluorescence. Our single molecule optical trap competition experiments show that AMP binding to the AMP binding site alone, is also not enough to prevent unmodified AP_5A from binding or AP_5A is able to displace the bound AMP.

Upon close inspection of the constant distance traces of the ATP competition experiment, one can see that the distance between the open and closed state decreases with increasing ATP concentration. This observation will be discussed in detail in the next chapter.

4.8.3 Conformational transition due to nucleotides.

The nucleotide competition experiments with AP_5A have shown that binding of the nucleotides to thADK occurs with expected affinities. In addition to the decrease of the number of AP_5A-induced conformational changes, the constant distance data also shows a shrinking size of the conformational transition with increasing nucleotide concentration. To study this behavior in more detail, the size of the conformational change is shown in Fig. 4.29 for different ATP concentrations. At low ATP concentrations (10 µM), the size of the conformational change with 1.6 nm is very close to the one in AP_5A only conditions. With increasing ATP concentrations, the size drops to 1.4 nm at 30 µM and levels off at around 1.3 nm above a concentration of 300 µM. No further decrease in size can be observed at even higher concentrations.

One would not expect a change in the measured size of the conformational transition, if ATP just blocks the binding site for AP_5A in the competition assay. Either the binding site is unoccupied (AP_5A can bind and induce the full conformational transition) or ATP is bound and AP_5A cannot bind and, therefore, not trigger the conformational transition and thADK remains in the open state. However, the measured size of the conformational transitions decreases with increasing ATP concentration. This cannot be explained by just a simple binding process of ATP, but the binding must also trigger a conformational change. However, the question remains why conformational transitions cannot be observed in the optical trap experiments of thADK in presence of ATP alone.

To address this issue, one can do the following gedankenexperiment: Henzler-Wildman et al. (2007b) have shown in NMR experiments, that thADK closes with a rate of $1571\,s^{-1}$ and opens with a rate of $44\,s^{-1}$ under saturating nucleotide concentrations. If one assumes for now, that the conformational transition in the presence of nucleotides couples to force in the same way, as it does for AP_5A, the opening rate, at a force of 10 pN, with a $\Delta x = 1.4$ nm would be around $1200\,s^{-1}$. Together with a closing rate of around $1600\,s^{-1}$, observing the full conformational transition, which at a force of

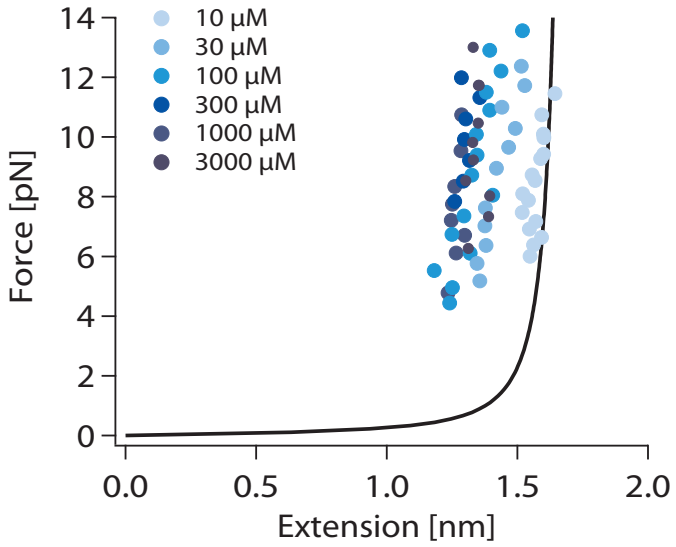

Figure 4.29 **Size of conformational change in presence of AP_5A and ATP:** Size of the conformational change in presence of AP_5A, Mg^{2+} and different ATP concentrations. The size is extracted from Hidden Markov Model analysis of constant distance traces and transformed to contour length space. For comparison, the WLC fit to the data of the conformational change induced by AP_5A only is shown in black.

10 pN has a length of 1.6 nm, is not within the resolution of the instrument. One would not expect to be able to fully resolve the conformational transitions as it was possible for AP_5A.

However, if the individual conformational transitions induced by the nucleotides cannot be resolved there would still be a difference from the fully open or fully closed state expected. Due to the fast exchange between open and closed state, one would observe an average between the two states as depicted in Fig. 4.30. The average position will depend on the equilibrium between open and closed state of the conformational change. For low nucleotide concentrations, thADK would be mostly in the open state with short excursions to the closed state. Due to the comparably low time resolution of the optical trap, one would expect an average state position close to the open state. By increasing the nucleotide concentration the equilibrium will be shifted further towards the closed state. If both states are equally populated, a low time resolution would give an average state position at a deflection, equaling half the full conformational transition.

The subtle change from a fully open state to a partially closed state is not visible in a nucleotide only experiment. However, in a competition experiment with AP_5A this change in the position of the open state should be observable. Fig. 4.30c) shows the expected effect of the previously described closing of adenylate kinase due to nucleotides in an AP_5A competition experiment. If AP_5A binds, adenylate kinase fully

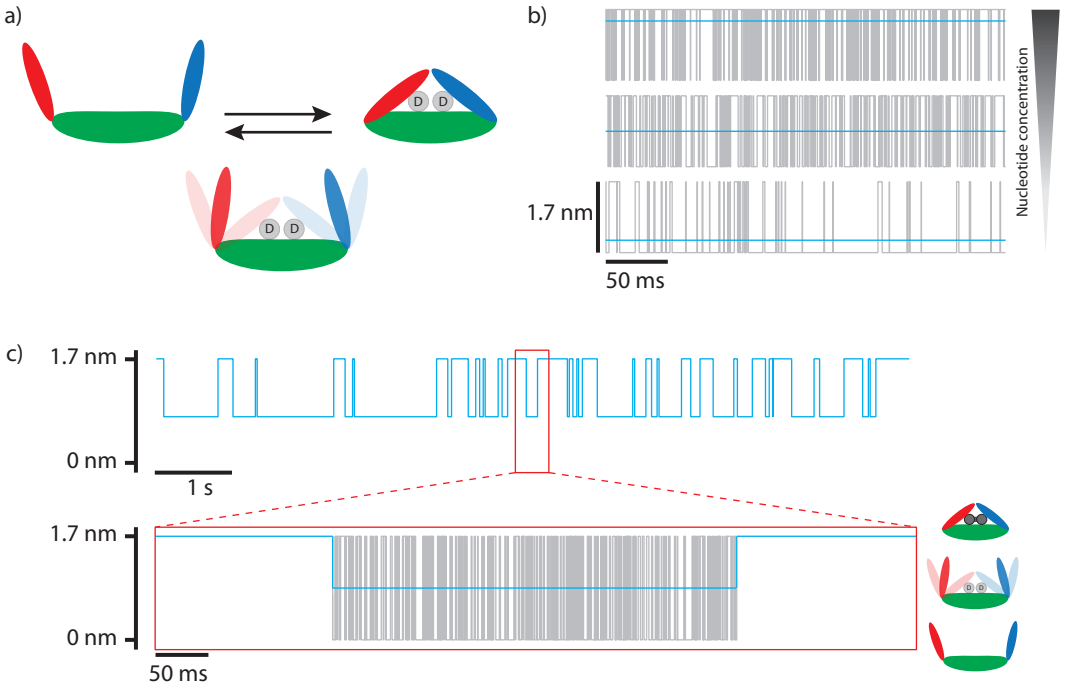

Figure 4.30 **Model for nucleotide induced conformational change:** a) Sketch of fast flipping between nucleotide free open (left) and nucleotide bound closed (right) state. Due to the limited time resolution, one can only observe an average between the two states (lower). b) Exemplary constant distance traces for three different arbitrary nucleotide concentrations. The nucleotide concentration increases from bottom to top. Gray lines show the flipping between the fully open and fully closed state. Blue lines indicate the average state position for the respective nucleotide concentration. c) Exemplary constant distance trace for an AP_5A competition experiment with a nucleotide concentration which causes open and closed state to be equally populated. Blue lines indicate the observed flipping between fully closed state and partially closed state (upper). The lower trace shows a zoom of the upper constant distance trace. Gray lines indicate the fast transitions between fully open and closed, which would be observable with higher time resolution. The middle blue line is the actual observed open state position, caused by averaging of the fast transitions.

closes, the position of the closed state, therefore, remains the same. The open state, however, is now not the fully open state, as in an AP_5A only experiments, but the average value of the fast flipping between open and closed state due to the nucleotides. In an AP_5A nucleotide competition, we will only observe the transition between the fully closed state and the average value of the fast flipping between open and closed state. For the previously described case, equal population of open and closed state due to nucleotides, the measured distance would be half of the full conformational change (see Fig. 4.30c)). Changing the nucleotide concentration will shift the equilibrium between open and closed state and thereby the observed size of the conformational change. This is the behavior, we can observe for the AP_5A competition experiments with ATP shown in Fig. 4.29.

For a better characterization of the conformational change, which is caused by the nucleotides, the difference between the expected size of the conformational change for AP_5A only experiments and the measured size in an AP_5A nucleotide competition experiment is calculated. This difference is normalized by the expected size for AP_5A only experiments and yields a fraction of closing due to the nucleotides at each force F as follows

$$Frac(F) = \frac{L_{\mathrm{AP5Aonly}}(F) - L_{\mathrm{NuclComp}}(F)}{L_{\mathrm{AP5Aonly}}(F)}, \tag{4.1}$$

where $L_{\mathrm{AP5Aonly}}(F)$ is the size of the full conformational change for AP_5A only, which is calculated for each force using a WLC model with a persistence length of 27.8 nm and a contour length of 1.72 nm, $L_{\mathrm{NuclComp}}(F)$ the distance between the open and closed state in the competition experiment, transformed into contour length space. Fig. 4.31 shows the fraction of full closing for different ATP concentrations. As it could already be seen from Fig. 4.29 closing due to ATP starts at an ATP concentration of 30 µM and stops around 300 µM at a fraction of full closing of about 0.2.

Fig. 4.31a) shows a slight force dependence of the fraction of closing, which depends on the ATP concentration and is highest for the ATP concentration of 30 µM. Because we are not able to resolve the individual closing and opening transitions of thADK in presence of nucleotides, the system can be described by the probability to find the protein in either the open or closed state. The force dependent probability for the closed state is given by

$$P_{\mathrm{closed}}(F) = \frac{k_{\mathrm{close}}(F)}{k_{\mathrm{close}}(F) + k_{\mathrm{open}}(F)} = \frac{1}{1 + \frac{k_{\mathrm{open}}(F)}{k_{\mathrm{close}}(F)}}, \tag{4.2}$$

where $k_{\mathrm{open}}(F)$ and $k_{\mathrm{close}}(F)$ are the force dependent opening and closing rates at a specific nucleotide concentration. Assuming the Bell model, with a zero force rate $k_{0,\mathrm{i}}$

and a distance to the transition state Δx_i, the force dependence of the rates is given by

$$k_\mathrm{i}(F) = k_{0,\mathrm{i}} * exp\left(\frac{\Delta x_\mathrm{i} F}{k_\mathrm{B} T}\right) \tag{4.3}$$

and with this a force dependence of the probability to find adenylate kinase in the closed state can be rewritten as

$$P_\mathrm{closed}(F) = \frac{1}{1 + \frac{k_{0,\mathrm{open}}}{k_{0,\mathrm{close}}} * exp\left(\frac{\Delta x F}{k_\mathrm{B} T}\right)}. \tag{4.4}$$

Here $k_{0,\mathrm{open}}$ and $k_{0,\mathrm{close}}$ are the zero-force opening and closing rates and Δx the size of the conformational change, that adenylate kinase undergoes in presence of nucleotides. Because the fraction of closing is normalized by the full conformational change of 1.72 nm, the probability has to be extended by $A = \frac{\Delta x}{1.72\,\mathrm{nm}}$ to give the force dependent fraction of closing

$$Frac(F) = \frac{A}{1 + \frac{k_{0,\mathrm{open}}}{k_{0,\mathrm{close}}} * exp\left(\frac{\Delta x F}{k_\mathrm{B} T}\right)}. \tag{4.5}$$

A global fit of this model is performed on the data shown in Fig. 4.31a) with Δx and $\frac{k_{0,\mathrm{open}}}{k_{0,\mathrm{close}}}$ as fit parameters. The size of the conformational change is expected to be the same for all nucleotide concentrations and only the ratio $\frac{k_{0,\mathrm{open}}}{k_{0,\mathrm{close}}}$ changes, therefore Δx is linked for the global fit. The fit yields a size of the conformational change in presence of ATP of $\Delta x = (0.5 \pm 0.1)\,\mathrm{nm}$ and a concentration dependent $\frac{k_{0,\mathrm{open}}}{k_{0,\mathrm{close}}}$. For better comparison the extrapolated zero-force fraction of closing at different ATP concentrations is plotted from the corresponding fit values in Fig. 4.31b).

In the presence of nucleotides thADK can assume four different conformations, the ligand-unbound open (UO) and closed state (UC) as well as the ligand-bound open (BO) and closed (BC) state. To describe the concentration dependent behavior of the fraction of closing, one has to take into account that the nucleotides will have a dissociation constant to the closed state of thADK K_close, as well as one to the open state K_open. No significant closing of thADK in presence of ATP will be expected, when the ATP concentration is below the dissociation constant to the closed state. For ATP concentrations above K_close, the fraction of closing will increase until the dissociation constant to the open state is reached and will level off. In equilibrium terms, the probability to find the enzyme in the closed conformation in the presence of a ligand is given by

$$P_\mathrm{closed} = \frac{[BC] + [UC]}{[BC] + [UC] + [BO] + [UO]}, \tag{4.6}$$

where $[BC]$ and $[UC]$ are the concentrations of ligand-bound and ligand-unbound closed state, $[BO]$ and $[UO]$ the concentrations of ligand-bound and ligand-unbound

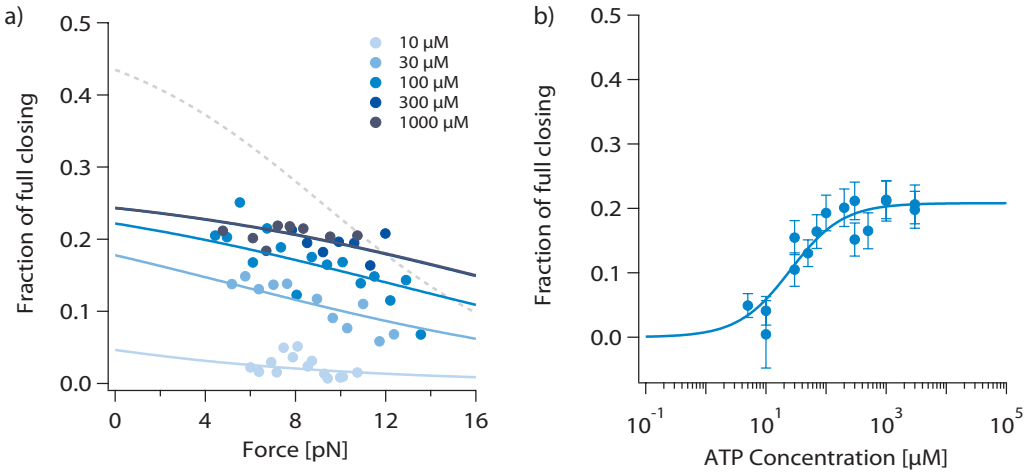

Figure 4.31 **ATP-induced closing of thADK:** a) Fraction of full closing from AP_5A competition experiments for different ATP concentrations against force. Solid lines are global fits of the force dependent closing model to the data with a linked Δx fit parameter. For comparison, the grey dashed line shows an expected closing dependence for a size of the conformational change of $\Delta x = 0.85\,\text{nm}$, half the full closing, and $\frac{k_{0,\text{open}}}{k_{0,\text{close}}}$ of 0.15. b) Extrapolated zero-force closing fractions from fits of the model to a) for different ATP concentrations. Solid line is a fit of equation 4.10 to the data.

open state. The dissociation constants of the ligand to the open and closed state are defined by

$$K_{\text{open}} = \frac{[UO] * c}{[BO]} \tag{4.7}$$

and

$$K_{\text{close}} = \frac{[UO] * c}{[BC]}. \tag{4.8}$$

Measurements by Henzler-Wildman et al. (2007b) have shown that the equilibrium between open and closed state in the absence of nucleotides lies on the open side (opening:closing rate, $6500\,\text{s}^{-1}$:$2000\,\text{s}^{-1}$). Assuming a similar Δx for full closing as in the AP_5A case, force will shift the equilibrium further towards the open side. At our measurement forces, the concentration $[UC]$ will be negligible compared to the other concentrations. Together with equation 4.7 and 4.8, equation 4.6 can be simplified to

$$P_{\text{closed}}(c) = \frac{1}{1 + K_{\text{close}} * \left(\frac{1}{c} + \frac{1}{K_{\text{open}}}\right)}. \tag{4.9}$$

Because the size of the conformational change caused by the nucleotides is known from the fits of the force dependent closing data, the concentration dependent fraction of

closing can be written as

$$Frac(c) = \frac{A}{1 + K_{\text{close}} * \left(\frac{1}{c} + \frac{1}{K_{\text{open}}}\right)}. \tag{4.10}$$

The fit of equation 4.10 to the data shown in Fig. 4.31b) yields a dissociation constant to the closed state K_{close} of (34 ± 8) µM and to the open state of K_{open} of (103 ± 40) µM.

The affinity of ATP to the closed state is comparable to the affinity, we obtained from the AP_5A competition experiments in chapter 4.8.2, of 17 µM. In the AP_5A competition experiments, however, we cannot discriminate between the affinity of ATP to the closed or open state of thADK. The closing behavior of thADK in presence of ATP suggest, that the affinity measured in the competition experiment is the one to the closed state. A precise determination of the affinity to the open state is difficult, because the fraction of closing at these ATP concentrations approaches the maximum expected value, obtained from the force dependence of closing.

The competition assay with ADP also shows a decrease in the size of the AP_5A-induced conformational change (Fig. 4.32). Here, significant differences between ADP in presence and and absence of Mg^{2+} can be observed. For the experiments with EDTA, in a concentration range of ADP between 10 µM and 1 mM, the fraction of closing due to ADP is very similar and the force dependence is very small. This is most likely due to the fact that the dissociation constant of Mg^{2+}-free ADP to the open state lies below the tested concentrations. The competition experiments have shown a dissociation constant of ADP in presence of EDTA of 0.8 µM. Because the force dependence is very small in the measured ADP concentration range, fits to the data don't yield reliable values for the size of the conformational change. The zero-force estimates for the fraction of closing are plotted in Fig. 4.32b) and show a constant fraction of closing around 0.2. To get a better estimate for the size of the conformational change in presence of Mg^{2+}-free ADP, future experiments should be done in a concentration range between 0.8 µM and 10 µM. In this concentration range, one expects to be more sensitive for the force dependence of the closing.

To test if the closing due to Mg^{2+}-free ADP is caused by closing of the AMP lid or the ATP lid, Mg^{2+}-free ADP competition experiments with the N-144 mutant were performed. At a concentration of 30 µM of ADP with 2 mM EDTA, a significant decrease in the number AP_5A-induced conformational changes could be observed. The conformational transitions, however, had the full length of around 0.85 nm, indicating that Mg^{2+}-free ADP causes closing of the AMP lid and not the ATP lid.

Mg^{2+}-free ADP showed a maximum closing of about 0.2. ADP in presence of Mg^{2+}, on the other hand, shows a significant increase in the fraction of closing. In Fig. 4.32a) the force dependent closing behavior for different ADP concentrations in presence of Mg^{2+} is shown. A fit of the force dependent closing model to the data yields a size of the conformational change of (0.7 ± 0.1) nm. One has to note, that at high ADP concentrations of 10 mM, the fit shows large deviations from the data. Possible reasons will be

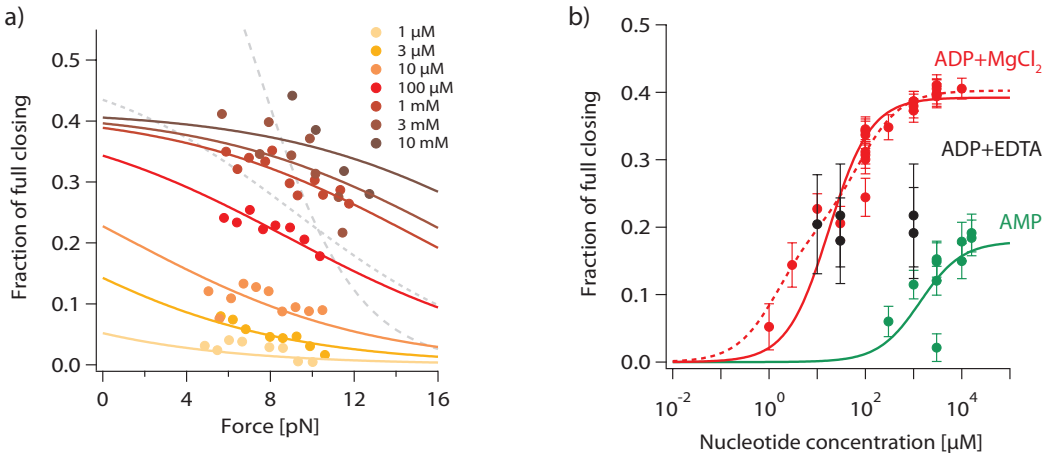

Figure 4.32 **AMP- and ADP-induced closing of thADK:** a) Fraction of full closing from AP_5A competition experiments for different ADP concentrations in the presence of Mg^{2+} against force. Solid lines are global fits of the force dependent closing model to the data with a linked Δx fit parameter. For comparison, the grey dashed lines show an expected closing dependence for a size of the conformational change of Δx = 0.85 nm (short dash) and Δx = 1.7 nm (long dash) and $\frac{k_{0,\text{open}}}{k_{0,\text{close}}}$ of 0.15, respectively 0.05. b) Extrapolated zero-force closing fractions from fits of the force dependent closing model for different AMP (green), Mg^{2+}-ADP (red) and EDTA-ADP (black) concentrations. Solid lines are fits of equation 4.10 to the data. The dashed line shows a model consisting of the sum of two binding sites, each described by 4.10 and contributing equally to the overall conformational change.

discussed in the next chapter. From the fits, the zero-force extrapolations of the fraction of full closing are shown in Fig. 4.32b). The fraction of closing increases at an ADP concentration of 1 µM and levels off at the highest concentrations of 3 mM and 10 mM. A fit of equation 4.10 with a Δx of 0.7 nm to the data yields a dissociation constant to the closed state K_{close} of (19 ± 2) µM and to the open state of K_{open} of (290 ± 80) µM. However, the fit of the model, assuming a single binding site, does not properly describe the data. Due to the fact, that adenylate kinase has two binding sites for ADP, a model with two binding sites and respective dissociation constants for the open and closed state might be needed to reproduce the data better. A plot for a model consisting of the sum of two binding sites, each described by equation 4.10 and contributing equally to the overall conformational change, is shown in Fig. 4.32b) as the red dashed line. Here we assume the following dissociation constants $K_{close,1}$ = 2 µM, $K_{open,1}$ = 50 µM, $K_{close,2}$ = 80 µM and $K_{open,2}$ = 5000 µM. The lowest dissociation constant for the closed state is taken from the data obtained by AP_5A competition experiments. A proper fit is difficult because there is not enough data over the whole range of ADP concentrations. The model assuming two binding sites with different affinities for ADP describes the data better than the simple model with only one binding site. For a better discrimination between the two models and the ability to fit the data with the two-binding-site model, more experiments have to be done, especially, at low ADP concentrations.

Also the AP_5A competition experiments in presence of AMP showed closing at high AMP concentrations. A fit of the force dependent closing model to the data yields a size of the conformational change of (0.5 ± 0.1) nm. The resulting zero-force closing fraction is shown in Fig. 4.32b) and fit with equation 4.10. The fit yields a dissociation constant to the closed state K_{close} of (2260 ± 770) µM and to the open state of K_{open} of (3500 ± 2000) µM. The affinity of AMP to the closed state is similar to the affinity, we obtained from the AP_5A competition experiments in chapter 4.8.2, of 2200 µM.

4.8.4 Discussion

Even though the initial experiments in presence of nucleotides did not show signs of closing of thADK, we could demonstrate in the AP_5A competition experiments, that they, indeed, cause closing of thADK. The conformational transitions from the open to a closed state induced by the nucleotides happen on a timescale, which is too fast to resolve individual opening or closing transitions with the optical trap setup. However, the AP_5A competition experiments in presence of nucleotides allowed the observation of a gradual shift of thADK from the open to more closed state. From the force dependence of the closing induced by the nucleotides, it was possible to extract the size of the conformational change. The size of the conformational change is smaller than one would expect for all nucleotides, AMP, Mg^{2+}-ADP, ADP and ATP. For ATP it has been shown, that it only binds to the ATP binding site (Adén and Wolf-Watz, 2007) and induces closing of the ATP lid (Schlauderer et al., 1996). The complete closure of the

ATP lid has been inferred from the crystal structure of yeast ADK in presence of the nonhydrolyzable ATP analogue AMPPCF$_2$P. Therefore, one would expect a closing-distance between 0.8 nm to 1 nm. Our experiments, however, only show a closing of around 0.5 nm. One has to note, that the determination of the size of the conformational change is difficult, because the observed force dependence is small. In the case of ATP, a concentration of 10 µM showed the largest force dependence in the observable force range. Here, the difference between the largest and smallest size of the conformational change at low, respectively, high forces is only around 2 Å. Due to the small differences, an exact determination of the size of the conformational size is challenging. Although the absolute value obtained might be error prone, it still gives a good estimate for the size of the conformational change. In Fig. 4.31a), the expected force dependency for a conformational change of the size of 0.8 nm is shown, which corresponds to the full closing of one lid. One can clearly see, that the force dependency is much higher than the one we observe in our experiments. Therefore, a full closing of the ATP lid cannot be brought into agreement with our measurements. Similar observations have been made by Adén and Wolf-Watz (2007) in NMR experiments. They only observe a partial closing of the ATP lid in presence of 20 mM of ATP and conclude that this is caused by a dynamic equilibrium between open and completely closed state with both states populated equally. The reduced size of the conformational change in our competition experiments is also explained by a dynamic equilibrium. However, our data shows an equilibrium between the open and a half-closed state. A shift of the equilibrium to the half-closed state, as it can be seen for the highest ATP concentrations in our experiments, could also describe the observations made by Adén and Wolf-Watz (2007).

But not only ATP induces a partial closing of its respective lid, also in the presence of ADP or Mg^{2+}-ADP a full closing of thADK is not observed. ADP is expected to cause a full closure of adenylate kinase, because it can bind to both binding sites and thereby induce closing of the two lids. Even though a larger conformational change of 0.7 nm in presence of Mg^{2+}-ADP can be seen, the observed closing still accounts only for about half the expected length. Fig. 4.32a) shows the expected force dependence for half and full closing of thADK. The full closing shows a much higher force dependence than the one observed in our experiments. However, as already mentioned, the fits to the force dependent closing data showed substantial deviations for the highest Mg^{2+}-ADP concentrations of 3 mM and especially 10 mM. The model fit to the data assumes the presence of only one binding site and hence, only one Δx. However, ADP binds to both binding sites and the conformational change should be described as a sum of the conformational change of both lids. One of the lids starts to close at lower ADP concentrations and the conformational change of the second lid sets in at higher ADP concentrations. An appropriate model would consist of the sum of two conformational changes, each having an independent Δx. A fit of such a model to the data is difficult, because the amount of data points especially at high ADP concentrations is not sufficient.

An additional closing at concentrations above 3 mM would require one of the binding sites to have an affinity in this concentration range, but so far all reported dissociation constants for ADP are much lower. However, Fujii et al. (2013) have reported a similar closing behavior of adenylate kinase in bulk FRET experiments. By increasing the Mg^{2+}-ADP concentration, they observe a steady increase in the population of the closed state, which can be rationalized by binding of one ADP molecule to adenylate kinase. Above a concentration of 3 mM ADP, an additional increase in the population of the closed state can be observed, which cannot be described anymore by binding of a single ADP molecule to adenylate kinase alone. They explain this by the lack of Mg^{2+}-free ADP at low ADP concentrations and an increase of the concentration of Mg^{2+}-free ADP at high ADP concentrations, leading to a gradual occupancy of the AMP binding site by Mg^{2+}-free ADP. If the relation of Mg^{2+}-bound and Mg^{2+}-free ADP plays a role in the shift from open to fully closed state, future optical trap experiments with varying amounts of Mg^{2+}-bound and Mg^{2+}-free ADP can help to address this issue. For the ADP experiments an additional issue complicates the interpretation of the results. In these experiments it is always possible that catalysis of ADP takes place. The catalysis from ADP into ATP and AMP will lower the ADP concentration and additionally add ATP and AMP in solution. Similar experiments in presence of nonhydrolyzable ADP analogues can prevent catalysis. Alternatively, the use of a fluidic measurement chamber to the optical trap setup with a steady stream of fresh nucleotides would guarantee the presence of the right nucleotide concentration.

Even though we were not able to extract the size of the conformational change in presence of Mg^{2+}-free ADP, the experiments showed an equilibrium between open and closed state lying on the open side. This is in contrast to the results from Adén and Wolf-Watz (2007), who showed in their NMR experiments, that saturating amounts of Mg^{2+}-free ADP cause a similar closing behavior as AP_5A. In the experiments by Fujii et al. (2013), on the other hand, Mg^{2+}-free ADP up to a concentration of around 3 mM showed less closing than Mg^{2+}-ADP. In our experiments, the equilibrium between open and closed conformation was constant in a concentration range between 10 µM to 1000 µM. Further experiments above 1000 µM will show, whether an additional closing can be observed at these concentrations. However, from the reported affinities of ADP to adenylate kinase, one would not expect this to occur.

Overall, our experiments showed that the closing of adenylate kinase caused by the nucleotides AMP, ADP and ATP can be measured using our optical trap setup. The closing behavior in presence of nucleotides is substantially different from the one observed in the presence of AP_5A. Where, the AP_5A-induced closing showed a strong coupling between ligand binding and closing over a wide concentration range, the nucleotides show a much more dynamic picture. Here, an increase in the concentration shifts the equilibrium from the open state to a more closed state, but adenylate kinase remains very dynamic and undergoes many transitions between open and closed state. Unlike

AP_5A, which can force the enzyme to be predominantly in the closed state at high concentrations, even very high nucleotide concentrations do not shift the equilibrium above an equal population of open and closed state. Focusing on the role of the conformational change for adenylate kinase as an enzyme, this makes sense. To efficiently catalyze the reaction, especially at high substrate concentrations, opening and closing have to occur rapidly. If the enzyme would be shifted to the completely closed state at high substrate concentrations, it would not be able to release the products which is crucial to achieve a high substrate turnover. Potentially, this is achieved by a relatively high affinity of the substrates to the open state of adenylate kinase, as it is suggested by the concentration dependent binding model used to fit the closing data. In the next chapter, the binding to the open state will be studied in more detail.

4.9 Stabilization of the ATP lid

The competition assay with AP_5A and the nucleotides AMP, ADP and ATP showed that they are able to bind to thADK and can also induce a partial closing of adenylate kinase in our optical trap experiments. However, not all of the binding energy goes into the conformational transition. Above an ATP concentration of around 300 µM no further increase in the fraction of closing could be observed. However, increasing the ATP concentration further still decreased the probability of binding of AP_5A to thADK. The proposed model explains this by the affinity of ATP to the open state of thADK. When the ATP concentration reaches the affinity of ATP to the open state, a further increase in the concentration will not shift the equilibrium further towards the closed state.

An independent measurement of the affinity of nucleotides to the open state of thADK would help to support this model. The force extension measurement of thADK in the presence of 1 mM ADP and 2 mM of Mg^{2+} in Fig. 4.26 has already shown, how this measurement could be done. Compared to apo conditions, the fast folding/unfolding equilibrium transition is shifted from a mean unfolding force of 17 pN to 22 pN in the presence of 1 mM ADP. Binding of ADP, therefore, does not only induce a closing of thADK but it also stabilizes the folding/unfolding transition and shifts the equilibrium to higher forces. If ADP binds to the open conformation of the ATP lid, it has to be released when the ATP lid unfolds and thereby stabilizes the folded conformation. The unfolding free energy of this transition in apo conditions was determined in chapter 4.4. An analysis of the unfolding/folding transition using an equilibrium folding model yielded a free energy of (11.9 ± 1.1) kT. From Hidden Markov Model analysis of this transition a very similar value of (11.0 ± 1.1) kT could be obtained. The two methods could also be used to analyze the free energy of the transition in presence of nucleotides. However, at higher nucleotide concentrations the folding/unfolding transition is not a two-state process anymore, but an additional state appears. Due to the high folding and unfolding rates, a reliable assignment of three states using Hidden Markov Models can

not be guaranteed. Also the equilibrium folding/unfolding model fails to reproduce the data at high nucleotide concentrations.

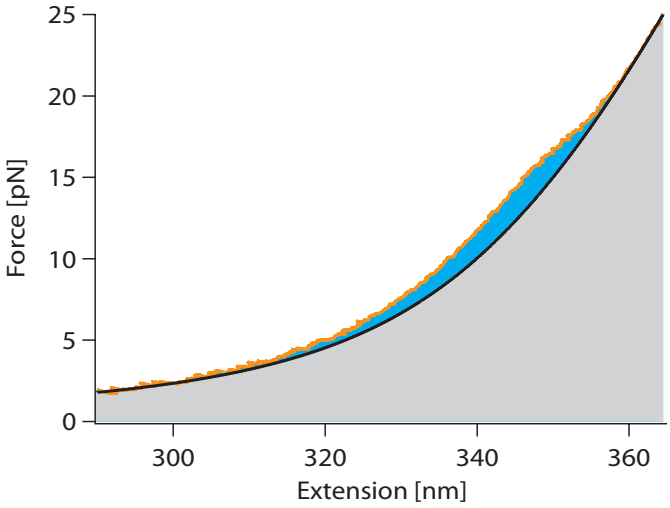

Figure 4.33 **Free energy of the ATP lid:** Force distance curve stretching apo-thADK at position 42 and 144 filtered to 60 Hz (orange). A fit of a combined WLC fit to the unfolded state is shown as a solid black line. The free energy of the folding/unfolding transition of the ATP-lid is given by the area shown in blue. The free energy of the whole system in the unfolded state is given by the area shown in gray.

Therefore, a third very basic approach is taken to analyze the free energy of this transition. For this approach, no assumptions about the number of states involved have to be made. The free energy of the whole system, including the stretching of the DNA linker, is given by the area under the force distance curve of a constant velocity experiment. For a clearer representation Fig. 4.33 shows the corresponding curves as force extension traces, however, the calculations are made using the appropriate force distance data. By subtracting the free energy of the system in the unfolded state (gray area) from the free energy of the whole system, we obtain the free energy of the folding/unfolding equilibrium transition (blue area). To calculate the energy of the system in the unfolded state, a serial combination of DNA and polypeptide elasticity is fit to the data and the energy of the system in the unfolded state is given by the area under the fit. To reduce the influence of noise at low forces, a WLC model is also fit to the folded state. The energy of the whole system is calculated by the sum of the area under the WLC fit to the folded state up to a force of 10 pN and the area under the actual curve (orange) for forces above 10 pN.

Using this method to calculate the free energy of the folding/unfolding equilibrium transition in apo conditions yields a free energy of (11.7 ± 0.7) kT. This is in very good agreement with the values obtained, by the other two methods. An increase in the mean

unfolding force of the transition due to binding of nucleotides to the ATP lid, results in an increase in the area under the curve and thereby a higher free energy. Because this method is independent of the number of states involved in the transition, it can be used at high nucleotide concentrations, where the other two methods fail.

The free energy of the ATP lid in presence of different concentrations AMP, ADP or ATP using the previously described method is shown in Fig. 4.34. All three nucleotides show an increase in the free energy of the ATP lid with increasing concentrations, starting with ADP, followed by ATP and AMP. In contrast to the free energy decrease in the AP_5A competition assay, all three nucleotides have the same slope at higher concentrations.

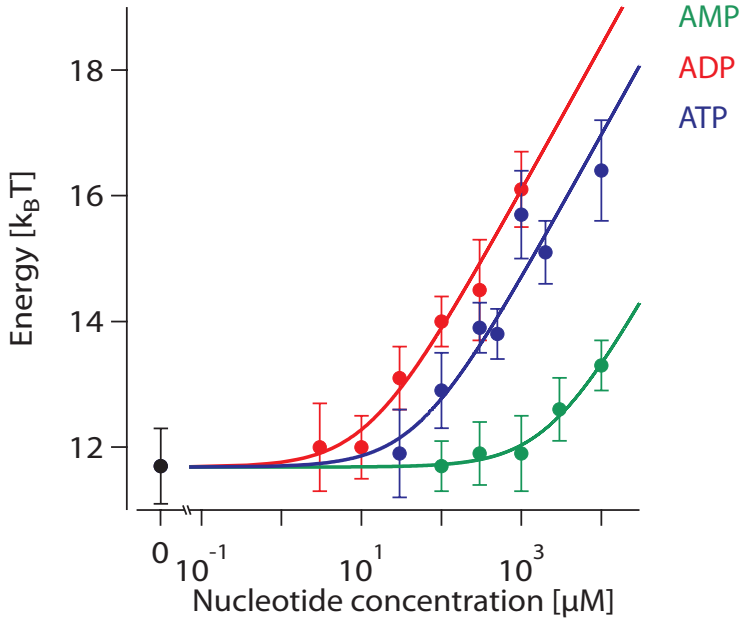

Figure 4.34 **Stabilization of the ATP lid by nucleotides:** Free energy of the fast unfolding/folding transition of the ATP lid for different nucleotide concentrations from area measurements. The stabilization is shown for AMP in green, Mg^{2+}-ADP in red and Mg^{2+}-ATP in blue. Black indicates the free energy of the ATP lid in apo conditions. The free energy for each concentration is an average value from different experiments with the standard deviation as error bars. Solid lines are fits of a ligand binding model to the data.

The increase in free energy can be modeled as described in chapter 3.5. The fits of equation 3.20 to the data yield the dissociation constants of the nucleotides to the open state of the ATP lid. For Mg^{2+}-ADP, the dissociation constant is (12 ± 5) µM, for Mg^{2+}-ATP (51 ± 17) µM and for AMP (2383 ± 1300) µM. For all three nucleotides, the data could be fit with a model, that assumes the binding of one molecule. At higher concen-

trations, the free energy is increased by 2.3 kT for every ten-fold increase in nucleotide concentration. The stabilization of the ATP-lid is, therefore, caused by binding of only one nucleotide molecule.

With this method we are able to determine the affinities of the nucleotides to the open state of the ATP-lid. The K_d of Mg^{2+}-ATP of (51 ± 17) µM fits well to the one obtained from the closing model from chapter 4.8.3 of (122 ± 51) µM. This confirms the hypothesis that a further shift of the equilibrium towards the closed state at higher ATP concentrations is not possible, because ATP starts to bind to the open conformation.

For Mg^{2+}-ADP, the K_d to the open state of the ATP-lid is (12 ± 5) µM. Therefore, one would not expect further closing of thADK by increasing the ADP concentration above 12 µM, if ADP binds only to the ATP-lid. However, the AP_5A competition experiments in presence of Mg^{2+}-ADP have shown, that one can observe an increase of the fraction of closing even up to the highest measured concentration of 10 mM ADP. This can only be explained by binding of ADP to the AMP lid.

Interestingly, a stabilization of the ATP lid cannot be observed by binding of AP_5A. Depending on the AP_5A concentrations, numerous binding events can be seen at forces where a fast exchange between folded and unfolded ATP lid occurs. However, these binding events are linked to a closing of thADK. If thADK opens up again and releases AP_5A, the open state will again be in the equilibrium between folded and unfolded state. High AP_5A concentrations can stabilize the closed state above the mean force of the equilibrium transition but the open state is not affected at the AP_5A concentrations used. A stabilization of the ATP lid, similar to the one observed by the nucleotides AMP, ADP and ATP, by AP_5A is expected when the AP_5A concentration is above the affinity of AP_5A to the open state. For AP_5A concentrations up to 10 µM a stabilization could not be observed, the affinity of AP_5A to the open state must, therefore, be higher.

The measurement of the stabilization of the equilibrium folding/unfolding transition of the ATP-lid provides an independent measure of the affinity of the nucleotides to the open state of the ATP lid. The obtained values are in good agreement with the ones from the AP_5A competition experiments. They provide further evidence that the equilibrium of open and closed conformation cannot be shifted further towards the closed state at higher nucleotide concentrations due to the relative high affinity of the nucleotides to the open conformation of adenylate kinase.

4.10 The case of AMPPNP

thADK did not show AP_5A like conformational transitions in the presence of any of the nonhydrolyzable ADP and ATP analogues ADPβ-s, AMPCP, AMPPN, AMPNP, AMP-PCP with AMP. However, when AMPPNP is added to the solution, conformational transitions of thADK around 1.5 nm can be observed (Fig. 4.35). The concentration needed to observe these transitions is high compared to the one used in AP_5A experiments. The

constant distance traces shown in Fig. 4.35 are recorded at an AMPPNP concentration of 1 mM. At this concentration, thADK is mostly in the open state with short spikes to the closed state. Even increasing the concentration of AMPPNP up to 10 mM does not increase the closing rate, as it can be seen in Fig. 4.36. Over a concentration range from 300 µM to 10 mM the zero-force closing rate is $(23 \pm 2)\ s^{-1}$. Only at a concentration of 100 µM a decrease in the closing rate to (7 ± 2) pers can be observed. This is in stark contrast to the closing behavior induced by AP_5A, where one could observe a linear increase of the closing rate with increasing AP_5A concentration from 3 nM to 10 µM. In this wide concentration range, the closing rate did not level off, even not at high AP_5A concentrations.

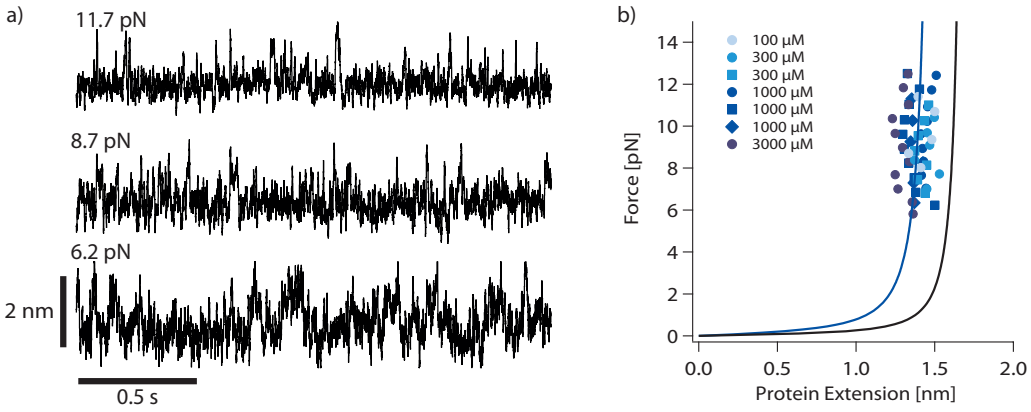

Figure 4.35 **Conformational transition in the presence of AMPPNP:** a) Constant distance trajectories at 300 Hz of the opening and closing of thADK 42-144 in the presence of 1 mM AMPPNP and 2 mM Mg^{2+}. b) Size of the conformational transition in the presence of AMPPNP from Hidden Markov Model analysis transformed to contour length space. Each symbol and color represents a different experiment. A global fit of a WLC model to the data is shown in blue. For comparison, the WLC fit to the data of the conformational changed induced by AP_5A only is shown in black.

However, a linear increase of the closing rate of thADK with increasing substrate concentration is only expected, if the substrate concentration is below the affinity of the substrate to the open state of thADK. If one approaches the affinity of the substrate to the open state, the open state will also start to bind the substrate. Increasing the concentration above the affinity of the open state will not shift the equilibrium between the open and closed state further toward the closed state. This could be the reason, why an increase of the AMPPNP concentration above 300 µM does not shift the equilibrium further toward the closed state. An estimate for the affinity of AMPPNP to the open state of thADK, from the constant distance experiments at different concentrations of AMPPNP, is, therefore, around 300 µM.

To measure the affinity of AMPPNP to the open state of thADK, the potential stabi-

lization of the unfolding/folding equilibrium transition for different AMPPNP concentrations is measured. Fig. 4.36b) shows the free energy of the equilibrium transition for different AMPPNP concentrations. Above an AMPPNP concentration of 300 µM an increase in the free energy can be observed. A fit of a model assuming the binding of one molecule (Equation 3.20) yields a dissociation constant of AMPPNP to the open state of (370 ± 160) µM. This is in good agreement with the observed closing behavior in presence of AMPPNP and explains, why a further increase of the AMPPNP concentration above 300 µM does not increase the closing rate of thADK.

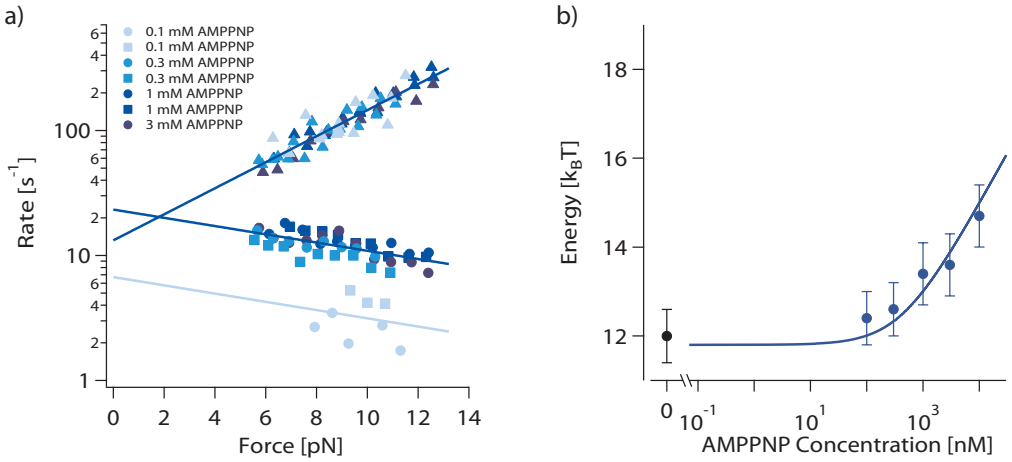

Figure 4.36 **Conformational transition in the presence of AMPPNP and the stabilization of the ATP-lid:** a) Closing (squares, circles) and opening (triangles) rates of thADK in the presence of different concentrations of AMPPNP and Mg^{2+}. Solid lines are global fits of the Bell model to the opening and closing rate. b) Free energy of the fast unfolding/folding transition of the ATP lid of thADK by area measurements in the presence of AMPPNP (blue) and in apo conditions (black). The free energy for each concentration is an average value from different experiments with the standard deviation as error bars. The solid line is a fit of a ligand binding model to the data.

However, the question remains, why AMPPNP by itself can induce closing of thADK in an AP_5A like fashion. Fig. 4.35 shows the size of the conformational change from the different constant distance measurements. Again, no difference between the various AMPPNP concentrations can be observed. A global fit of the data with a persistence length of 27.8 nm yields a size of (1.5 ± 0.1) nm. This is about 85 % of the size of the conformational change in presence of AP_5A.

Additionally to the reduced size of the conformational change, the force dependent opening and closing rates show, that the conformational change itself is different from the one observed in presence of AP_5A. A global fit of the Bell model to the opening rate yields a Δx_{C-TS} of (1.0 ± 0.1) nm and a zero-force opening rate k_{open} of $(13 \pm 2)\,s^{-1}$. The zero-force opening rate in the presence of AMPPNP is about 13 times higher than

the one in presence of AP_5A. Also fits to the closing rate show a significant difference in Δx_{O-TS} from AP_5A. Global fits to the data in presence of AMPPNP yield a Δx_{O-TS} of (-0.31 ± 0.05) nm.

One would expect, that additionally AMP is needed to observe these conformational transitions, since this would be the mimic for ATP and AMP. However, by adding AMP in combination with AMPPNP to the solution, the closing rate of thADK goes down with increasing AMP concentration. AMP competes with AMPPNP in a similar fashion as AMP does with AP_5A.

4.10.1 Discussion

The crystal structure of adenylate kinase from *E.coli* in the presence of AMPPNP and AMP suggest, that AMPPNP and AMP are able to bind in their respective binding pockets and fully close adenylate kinase (Berry et al., 1994). In our optical trap experiments AMPPNP by itself induces a closing of thADK to almost the full extent. One explanation could be that AMPPNP binds to both ATP and AMP binding site and thereby triggers closing of both lids. However, in this configuration six phosphates would be present inside the closed structure. Although adenylate kinase can tolerate additional phosphates inside the closed structure, as it can be seen from the AP_5A and AP_6A data, experiments with AP_6A with its six phosphates have shown that thADK only closes to about 40 %. Even though thADK does not fully close in the presence of AMPPNP, the closing is still twice as big as in the presence of AP_6A. It is, therefore, very unlikely that the binding of an AMPPNP to the ATP binding site, as well as to the AMP binding site, is responsible for the closing of the enzyme.

The stabilization of the unfolding/folding transition of the ATP lid by AMPPNP shows, that AMPPNP binds to the ATP lid. Possibly, this is enough to induce the observed conformational change. The increased off-rate indicates that the closed state is not as stable, as the one observed in the presence of AP_5A and fewer stabilizing contacts between the closed enzyme and AMPPNP are formed.

Similar observations of the full closing of thADK in presence of AMPPNP have been made by Ott (2008) in single molecule FRET experiments. By labeling the AMP and the ATP lid with fluorescent dyes, they could monitor the closing of adenylate kinase by an increase in the FRET signal. They observed the full closing of thADK in presence of AMPPNP without AMP. The energy transfer between acceptor and donor in presence of AP_5A was similar to the one in presence of AMPPNP, indicating a similar conformational change was occurring. Additionally, they saw a decrease in the population of the fully closed state upon addition of AMP in combination with AMPPNP.

Because AMPPNP can hydrolyze to AMPPN, especially at higher temperatures, it would also be possible that the observed effect is caused by AMPPN. However, experiments with thADK in presence of AMPPN did not show any conformational transitions.

It is still possible, that the observed conformational change is caused by a mixture of AMPPNP and AMPPN.

For further experiments with AMPPNP, impurities of the AMPPNP solution should be checked by HPLC analysis. Thereby it can be excluded that contaminants like bisubstrate analogs or hydrolyzed analogs are present in solution. Experiments with AMPPNP from a different supplier (Jena Biosciences) than the one used before (Sigma Aldrich) showed different closing kinetics at the supposedly same AMPPNP concentrations. Therefore, the presented results should be considered with care until further tests show that indeed AMPPNP is causing the conformational change.

The experiments of thADK in presence of AMPPNP can turn out to be very important in the understanding of the conformational change of adenylate kinase, if one can exclude that they are not artifacts e.g. caused by contaminants. The conformational transitions in presence of AMPPNP show similarities both between the ones observed in presence of AP_5A as well as the ones observed with nucleotides. AMPPNP triggers a closing of similar extent as AP_5A with lifetimes which are about ten times lower but still much higher than the ones observed in the presence of nucleotides. However, the conformational transitions do not couple as strongly to the AMPPNP concentration as they do for AP_5A, because the affinity of AMPPNP to the open state of adenylate kinase is reached at AMPPNP concentrations, which show only relatively low closing rates.

The determination of the mechanism which causes the conformational change in presence of AMPPNP might eventually help to understand the difference between conformational change in presence of the bisubstrate inhibitors and the one in presence of the nucleotides.

4.11 Single molecule force spectroscopy of the mesophilic variant of ADK

All the previous experiments were done with the thermophilic variant of adenylate kinase from *Aquifex aeolicus*. The question arises if the observations and models made for thADK would also apply to the mesophilic variant of adenylate kinase. To address this question, we repeated the experiments with adenylate kinase from *E.coli*. A comparison of thADK and mesoADK reveals homology between the two variants from the primary sequence (Henzler-Wildman et al., 2007a) as well as the structure. A structural alignment of the open conformation of both variants is shown in Fig. 4.37a) and displays only minor deviations in two loop regions.

4.11.1 Mechanical stability of mesoADK

The thermophilic variant of adenylate kinase showed high stability against force. Does mesoADK show a similar stability or do the adaptations to lower temperature also result in lower mechanical stability? To address this question we expressed a mutant of mesoADK, where one cysteine was introduced at the N-terminus and one at the C-terminus. A representative force extension measurement is shown in Fig. 4.37. The mesophilic variant of adenylate kinase already starts unfolding at a force of around 11 pN. A large unfolding transition of 69 nm can be observed at this force. A short lived intermediate is present at a contour length increase of around 27 nm. Before the large unfolding transition occurs, a smaller unfolding transition of around 8 nm can be observed. This transition also shows refolding against force. However, it can only be seen if the large unfolding does not occur at forces below 8 pN to 9 pN. The overall unfolding length of (69.3 ± 0.9) nm agrees well with the one observed for thADK of 68.5 nm.

A comparison of the contour length increases of the two unfolding intermediates with the ones observed in force extension measurement of the NC-mutant of thADK also shows very similar contour length increases. Therefore, it is very likely that the two variants of adenylate kinase follow the same unfolding pathway. Similar to thADK, mesoADK has a C-terminal α-helix consisting of 12 AA. This α-helix ends with a short loop in a β-sheet structure, which makes up most of the CORE domain. Following the same arguments as for the thermophilic variant, the unfolding most likely starts with the α-helix at the C-terminus. In the mesophilic variant the flipping between folded and unfolded α-helix is not as pronounced as it is in the thermophilic variant. However, in a few force extension traces of mesoADK, multiple unfolding and folding events of the α-helix against force can be observed. The unfolding probably advances from the C-terminus and the observed second intermediate is the unfolding of the ATP lid. In the last step mesoADK unfolds completely. The proposed sequence of unfolding events is, therefore, the same as for thADK shown in Fig. 4.4.

Although the observed contour length increases of the two variants are quite similiar, the unfolding forces of mesoADK and thADK are very different. mesoADK unfolds at forces around 10 pN to 12 pN, where thADK shows the unfolding of the C-terminal α-helix around 20 pN, followed by the main unfolding event around 27 pN. Despite having the presumably same unfolding pathway, thADK can withstand significantly higher forces than mesoADK. This shows that the thermophilic variant is not only more stable against temperature but also against force as a denaturing agent.

The two variants also show large differences in the refolding behavior. In the relaxation traces of the force extension measurements (Fig. 4.38a)), mesoADK shows predominantly only one refolding intermediate. This refolding intermediate has a contour length increase of around 37 nm i.e. half of the protein is refolded. The refolding intermediate can be observed starting at forces around 4 pN. This is in stark contrast to

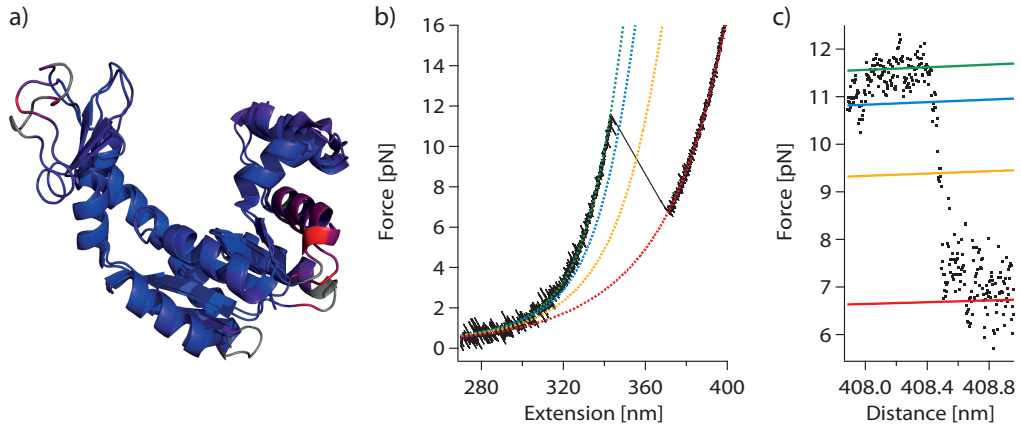

Figure 4.37 **Unfolding of mesoADK:** a) Alignment of the open structure of thADK (PDB 2RH5) and mesoADK (PDB 4AKE) using the PyMOL plugin ColorByRMSD. The colors indicate the deviations of the alignment between the two structures, dark blue for small deviations, higher deviations are in red. b) Force extension graph of the unfolding of mesoADK pulling at the N- and C-terminus. The black curve shows the force signal smoothed to 600 Hz. The colored curves are fits of a combined WLC model to the data. The green curve shows the force extension behavior of the dsDNA handles. Two unfolding intermediates are present (blue, orange). The completely unfolded mesoADK is marked in red. c) Force distance graph of the unfolding of mesoADK. The black dotted points are data sampled at 30 kHz. Solid lines are WLC fits from b).

the refolding behavior of thADK, which shows several refolding intermediates starting at 7 pN, as well as complete refolding against force. A complete refolding of mesoADK against force could not be observed. A relaxation to zero force with a waiting time of two seconds, yielded a refolding rate of around 30 % (Fig. 4.38b)). Similar measurements of thADK without a waiting time resulted in 85 % successful refolding events. These refolding experiments show that thADK does not only withstand higher forces, but it also refolds faster than mesoADK.

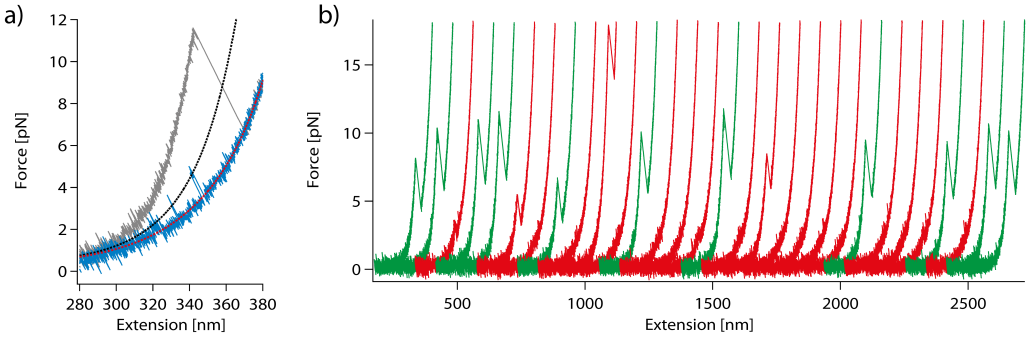

Figure 4.38 **Refolding of mesoADK:** a) Force extension measurement of the refolding of mesoADK pulling at the N- and C-terminus smoothed to 600 Hz. Gray shows the initial pulling curve and blue the following relaxation trace. b) Consecutive pulling traces at 100 nm s^{-1}, between each pulling trace is a 2 s pause at zero force. Green traces indicate complete refolding in the previous pause at zero force. Red curves stretch cycles of unfolded or partially folded mesoADK.

4.11.2 mesoADK in the active geometry

The measurements on the NC terminal mutant of mesoADK already showed significant differences in the unfolding stability and folding behavior compared to thADK. The question arises how these differences influence the closing and opening behavior in the presence of inhibitors or nucleotides. As it is the case for thADK, pulling at the N- and C-terminus of mesoADK is a suboptimal coordinate to observe the conformational change. Similar to the mutation of thADK, we removed the cysteines at the N- and C-terminus and inserted the following sequence CKGS at position 44 and GSCKSG at position 148. This active geometry would allow the observation of the conformational transition.

An exemplary force extension measurements of the 44-148 mutant of mesoADK in apo conditions is shown in Fig. 4.39a). At a force of about 12 pN a 25 nm large unfolding transition can be observed. The expected contour length increase upon unfolding for the positions 44 and 148 is 34 nm. Different from the experiments with thADK pulling at position 42 and 144, no folding/unfolding equilibrium transition can be observed for

mesoADK. This suggests that either the ATP lid has a very different unfolding and folding behavior or that it is already unfolded at our experimental conditions. An unfolded ATP lid would also account for the missing 9 nm in the unfolding transition. Schrank et al. (2009) have reported that the ATP lid of mesoADK starts unfolding above 35 °C. Due to heating of the sample chamber by the infrared trapping laser, the temperature during a regular experiment is around 30 °C. The increase in temperature could destabilize the ATP lid and lower the unfolding forces of the ATP lid to a force range where the unfolding transition cannot be detected.

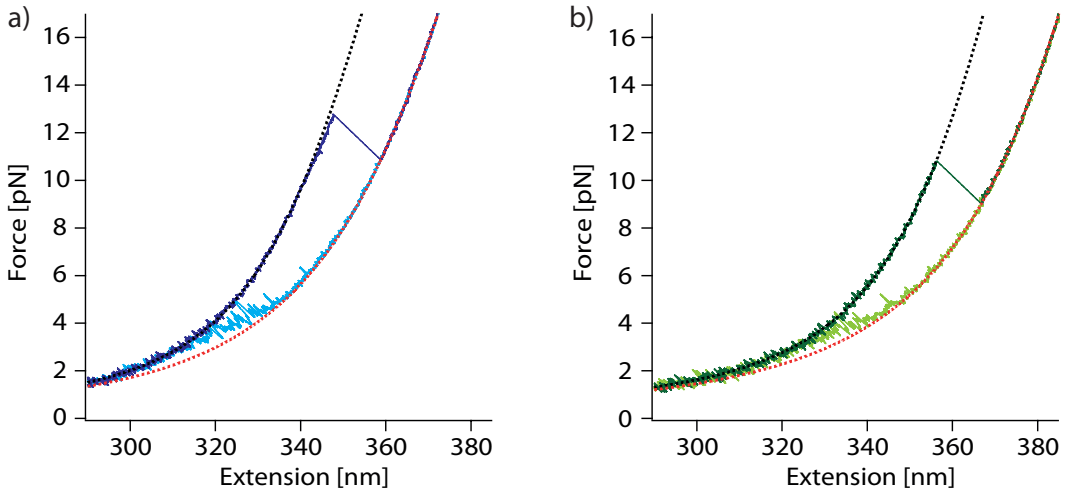

Figure 4.39 **mesoADK in the active geometry:** Force extension measurement of the Q28H mutant of mesoADK pulling at cysteines at position 44 and 148 in apo conditions (a)) and in the presence of 100 nM AP_5A and 2 mM Mg^{2+} (b)) smoothed to 60 Hz. Dark blue, dark green show the pulling and light blue, light green the relaxation trace. The black and red dotted lines are fits of a combined WLC model to the folded and unfolded state respectively.

To observe AP_5A-induced conformational transitions of the 44-148 mesoADK mutant, constant velocity experiments are performed in the presence of AP_5A. Fig. 4.39b) shows a force extension trace of mesoADK in the active geometry in the presence of 100 nM AP_5A and 2 mM Mg^{2+}. The experiments in presence of AP_5A do not show any difference to the ones in absence of AP_5A. No conformational transitions can be seen before mesoADK unfolds at a force of around 10 pN. The unfolding transition has the same contour length increase of 25 nm as the one in apo conditions. Also, measurements at an AP_5A concentration of 1 µM did not show any conformational transitions around 1.7 nm. For the two AP_5A concentrations, as well as the experiments in apo conditions the unfolding forces were in the range of 9 pN to 12 pN. An increase in the unfolding force with increasing AP_5A concentration could not be observed.

4.11.3 Discussion

The experiments on adenylate kinase of *E.coli* showed large differences to the ones on the thermophilic variant from *A.aeolicus*. Not only is mesoADK significantly less stable against force than thADK, but also conformational changes in presence of AP_5A could not be observed. The absence of observable conformational changes, especially, in the presence of AP_5A is quite surprising. The crystal structures of open and closed state of mesoADK, as well as, a wide variety of previously performed experiments suggest that mesoADK undergoes a very similar conformational change as thADK. However, this could not be observed in our optical trap experiments. The tested AP_5A concentrations are well above the reported K_d of this variant of 0.88 nM (Reinstein et al., 1990b). The missing conformational transitions in combination with the absence of a stabilization of mesoADK in presence of AP_5A suggest that mesoADK is not able to bind AP_5A at our experimental conditions. Schrank et al. (2009) have shown that the ATP lid of mesoADK starts to unfold at temperatures of 35 °C and renders the enzyme into a binding incompetent state. The missing contour length increase in the unfolding transition and the absence of a conformational change indicate that the ATP lid is already unfolded and the construct is in the binding incompetent state, observed by Schrank et al. (2009).

In addition to the destabilization of the ATP lid due to the increased temperature in the sample chamber, the insertions of the two cysteines in the AMP and ATP lid could also influence the secondary and tertiary structure of the protein. To test if these mutations further reduce the stability of mesoADK and potentially inactivate the protein, the enzymatic activity of this mutant has to be measured. Furthermore, other mutants with other attachment positions in the two lids could potentially improve the mechanical stability and allow the observation of conformational transitions of mesoADK.

How do nature's evolutionary adaptations to high temperatures of proteins affect the mechanical stability, was one of the questions we asked at the beginning. The single molecule force spectroscopy measurements show clearly that the mesophilic variant unfolds at considerably lower forces than the thermophilic variant. Additionally, the thermophilic variant folds much faster and is able to refold against force, which could not be observed for adenylate kinase from *E.coli*. A higher mechanical stability as well as an increase in folding rate result from the adaptations of thADK to extreme temperatures and show how proteins can attain and preserve their native conformation at these temperatures. To expand the already gathered information about temperature adaptation beyond mesophilic and thermophilic variants, additional experiments on a psychrophile (adapted to cold temperatures) variant can be done. Preliminary tests of the enzymatic activity of adenylate kinase from *Psychroflexus torquis* already showed higher K_M-values and a reduced activity in comparison to the other two variants. Future optical trap measurements of this variant will contribute to the understanding of the correlation between temperature adaption and mechanical stability of proteins.

5 Outlook

The optical trap described here allows the measurement of biological systems with high temporal as well as spatial resolution. Experiments on villin headpiece HP35 expanded the time resolution of force spectroscopy measurements down to the ~10 µs timescale thus approaching the timescales accessible for all atom molecular dynamics simulations (Zoldák et al., 2013). The experiments presented here on adenylate kinase showed that the optical trap is capable of observing conformational transitions of enzymes down to 4 Å. Even though experiments with high resolution and stability are possible already now, future work can further push the limits.

The resolution of the experiment is limited by the thermal noise of the protein-linker-bead system. The noise of the system is reduced by using differential detection as described in chapter 2. Moffitt et al. (2006) have shown that for such a setup the reduction in noise is limited by the stiffness of the linker, in our case the dsDNA handles. The rise of DNA origami technique, which allows the nanofabrication of different structures using DNA (Seeman, 2003; Rothemund, 2006; Dietz et al., 2009), can help to improve the resolution in our optical trap system even further. First experiments using rigid DNA beams as linkers between the two beads have been proven to increase the resolution by a factor of around 1.5 especially at low forces (Pfitzner et al., 2013). This enabled us to observe the folding and unfolding of a short DNA hairpin, which was not possible with standard double stranded DNA linkers. The use of these rigid DNA beams for other biological systems can help to understand these in much more detail. This can be especially helpful for detecting small conformational changes like the ones presented here, which are at the limit of the resolution of an optical trap. Because the decrease in noise with the DNA origami linkers is particularly high at low forces, they will enable us to probe small conformational transitions in the force range below 5 pN which has been inaccessible before.

Not only the protein linker bead system can be improved further, but also the optical trap setup still has room for optimization, especially concerning long term stability. The incorporation of the laser stabilization scheme (see chapter 2.3.3) has already improved on this. Overall, temperature fluctuations are most likely the main cause for residual drifts in the system and affect the long term stability during an experiment. The addition of motorized linear stages for the movement of the sample stage can keep the need for physical interaction with the trap setup to a minimum. Every physical contact with the setup can lead to unwanted drifts in the system. Introducing motorized stages allows the whole setup to be isolated further from the effect of temperature fluctuations in the trap

room by a complete isolating housing.

Furthermore, the addition of a microfluidic device as the sample chamber can enhance the experimental conditions. First, it dispenses the need to change the sample chamber for every experiment. Changing the sample chamber involves the retraction of one of the objectives, which is a potential source of misalignments of the setup. This will also help the overall stability, because the sample chamber and objectives don't have to heat up again after the exchange. Second and maybe more important, a fluidic device allows the observation of a single molecule in the trap under different conditions. By using a fluidic device with multiple laminar flows, consisting of different buffer conditions or nucleotides, one can quickly move the trapped beads, with the construct in between, from one condition to the other. This can greatly help to compare different experimental conditions with each other, because the molecule is the same for the whole experiment. Thereby variations between different bead pairs and sample chambers are reduced and more subtle differences can be detected. This can prove to be very helpful to understand the conformational change of adenylate kinase in more detail. The AP_5A nucleotide competition experiments have relied so far on the comparison of measurements on different molecules in separate sample chambers. A fluidic device allows the measurement in different conditions on the same molecule. Thereby, one can directly compare the conformational change in absence and presence of nucleotides and observe the differences more directly.

Additionally, experiments with different adenylate kinase mutants can be helpful to understand the conformational change in more detail. Specifically, point mutations in the ATP and AMP binding site have shown interesting changes in the the enzymatic activity of the enzyme in preliminary bulk experiments. However, it is not clear how these mutations affect the opening and closing of the enzyme and the binding of the ligands. Optical trap experiments using these mutants will help to gain further insight in the coupling between ligand binding and the conformational transition.

Using the optical trap to study conformational changes of enzymes does not have to be limited to adenylate kinase. The experiments have shown that the optical trap setup is able resolve conformational transitions down to 4 Å and the previously described DNA origami technique will push the limit even further. Since conformational changes have been shown to be very important for biological and enzymatic function, one can use a similar approach to study the conformational change of other enzymes like the heat shock proteins HSP70 and HSP90 with the optical trap. The ability to actively manipulate the native conformation of a protein and simultaneously observe sub-nanometer transitions can shed light on previously unaccessible areas, like domain-domain communication and the interaction of the heat shock proteins with different cochaperones.

6 Appendix

6.1 Construct preparation

Molecular cloning

The gene sequences for the different constructs were synthesized by Genscript or MrGene and inserted in pET11a (thADK constructs) or pET28a(+) (all other constructs) vectors via Nde1 and BamH1 restriction sites. Point mutations were performed using QuikChange Lightning Site-Directed Mutagenesis Kit (Agilent Technologies).

Protein Expression and purification

Proteins were expressed in *E.coli BL21 (DE3)* by lac-promoter controlled overexpression. The cells were disrupted by French press and the protein initially purified by His_6 Ni-NTA affinity columns. In a second purification step, the protein was further purified by size exclusion chromatography using either Superdex 200 columns or Diol 120 columns. To prevent di- or oligomerization of the cis-modified protein, TCEP was added to work in reducing conditions. The buffer conditions were 50 mM MOPS, 200 mM KCl, pH 7. The protein was flash frozen in liquid nitrogen and stored at −80 °C.

Oligo attachment

Short single stranded oligos with a maleimide group at the 3'-end were added to the purified protein in a cysteine:oligo ratio of 1:1. The mixture was incubated in reducing conditions of 1 mM TCEP for one hour at room temperature. To improve the seperation of unreacted oligos and oligo-dimers from the protein, the mixture is initially purified by His_6 Ni-NTA affinity columns. The Ni-NTA column with the bound oligo-protein constructs is then mounted on a Superdex 200 column. The bound protein is eluted with 0.5 M imidazol and subsequently travels through the size exclusion column. Here, the oligo-protein-oligo construct is separated from unreacted protein and protein with only one oligo bound. The oligo-protein-oligo fraction were flash frozen and stored at −80 °C.

The single stranded oligo sequence is

Oligo. GGCAGGGCTGACGTTCAACCAGACCAGCGAGTCG-Maleimide

Handle preparation

The dsDNA handles were prepared using PCR with λ-phage DNA as the template and a 1:1 mixture of digoxigenin and biotin modified sense primers and an anti sense primer containing an abasic site. At the abasic site the polymerase stops and leaves a single stranded overhand complimentary to the protein bound oligo. The PCR product was purified using a Qiagen PCR purification kit.

The primer sequences are

Sense primer. *GGCGA*CTGG*CGTTGATTTG

with * the sites of the biotin and digoxygenin modifications and

Anti sense primer. CGACTCGCTGGTCTGGTTGAACGTCAGCCCTGCCXCCTG CCCGGCTCTGGACAGG

with X the abasic site.

6.2 Protein sequences

The amino acid sequences of the measured proteins are given below.

thADK N-C. MACKGELSGMILVFLGPPGAGKGTQAKRLAKEKGFVHISTGDIL REAVQKGTPLGKKAKEYMERGELVPDDLIIALIEEVFPKHGNVIFDGFPR TVKQAEALDEMLEKKGLKVDHVLLFEVPDEVVIERLSGRRINPETGEVY HVKYNPPPPGVKVIQREDDKPEVIKKRLEVYREQTAPLIEYYKKKGILRII DASKPVEEVYRQVLEVIGDGNGTGSKCLEHHHHHH

thADK 42-144. MAAKGELSGMILVFLGPPGAGKGTQAKRLAKEKGFVHISTGD ILREAVQKGCTPLGKKAKEYMERGELVPDDLIIALIEEVFPKHGNVIFDG FPRTVKQAEALDEMLEKKGLKVDHVLLFEVPDEVVIERLSGRRINPETG EVYHVKYNPPPPGCVKVIQREDDKPEVIKKRLEVYREQTAPLIEYYKKK GILRIIDASKPVEEVYRQVLEVIGDGNGTGSKALEHHHHHH

thADK N-144. MACKGELSGMILVFLGPPGAGKGTQAKRLAKEKGFVHISTGDI LREAVQKGTPLGKKAKEYMERGELVPDDLIIALIEEVFPKHGNVIFDGFP RTVKQAEALDEMLEKKGLKVDHVLLFEVPDEVVIERLSGRRINPETGEV YHVKYNPPPPGVKVIQREDDKPEVIKKRLEVYREQTAPLIEYYKKKGILR IIDASKPVEEVYRQVLEVIGDGNGTGSKALEHHHHHH

thADK N-42. MACKGELSGMILVFLGPPGAGKGTQAKRLAKEKGFVHISTGDIL REAVQKGTPLGKKAKEYMERGELVPDDLIIALIEEVFPKHGNVIFDGFPR TVKQAEALDEMLEKKGLKVDHVLLFEVPDEVVIERLSGRRINPETGEVY HVKYNPPPPGCVKVIQREDDKPEVIKKRLEVYREQTAPLIEYYKKKGILR IIDASKPVEEVYRQVLEVIGDGNGTGSKALEHHHHHH

mesoADK N-C. MACKSSGRIILLGAPGAGKGTQAQFIMEKYGIPQISTGDMLRA
AVKSGSELGKQAKDIMDAGKLVTDELVIALVKERIAQEDSRNGFLLDGF
PRTIPQADAMKEAGINVDYVLEFDVPDELIVDRIVGRRVHAPSGRVYHV
KFNPPKVEGKDDVTGEELTTRKDDQEETVRKRLVEYHQMTAPLIGYYS
KEAEAGNTKYAKVDGTKPVAEVRADLEKILGSSKCLTA

mesoADK N-C Q28H. MACKSSGRIILLGAPGAGKGTQAQFIMEKYGIPHISTGD
MLRAAVKSGSELGKQAKDIMDAGKLVTDELVIALVKERIAQEDSRNGF
LLDGFPRTIPQADAMKEAGINVDYVLEFDVPDELIVDRIVGRRVHAPSGR
VYHVKFNPPKVEGKDDVTGEELTTRKDDQEETVRKRLVEYHQMTAPLI
GYYSKEAEAGNTKYAKVDGTKPVAEVRADLEKILGSSKCLTA

mesoADK 44-148. MRIILLGAPGAGKGTQAQFIMEKYGIPQISTGDMLRAAVKS
GSCKGSELGKQAKDIMDAGKLVTDELVIALVKERIAQEDSRNGFLLDGF
PRTIPQADAMKEAGINVDYVLEFDVPDELIVDRIVGRRVHAPSGRVYHV
KFNPPKVEGKDDGSCKSGVTGEELTTRKDDQEETVRKRLVEYHQMTAP
LIGYYSKEAEAGNTKYAKVDGTKPVAEVRADLEKILGGSHHHHHH

mesoADK 44-148 Q28H. MRIILLGAPGAGKGTQAQFIMEKYGIPHISTGDMLRA
AVKSGSCKGSELGKQAKDIMDAGKLVTDELVIALVKERIAQEDSRNGFL
LDGFPRTIPQADAMKEAGINVDYVLEFDVPDELIVDRIVGRRVHAPSGR
VYHVKFNPPKVEGKDDGSCKSGVTGEELTTRKDDQEETVRKRLVEYHQ
MTAPLIGYYSKEAEAGNTKYAKVDGTKPVAEVRADLEKILGGSHHHHH
H

6.3 Experimental procedures

The oligo-protein-oligo construct was mixed with the dsDNA handles and incubated on ice for one hour. The resulting DNA-protein construct was incubated with silica microsphere (1 µm diameter, Bangs Laboratories), that were previously covalently coated with fluorescent label and anti-digoxigenin Fab fragments. For the final solution streptaviding-coated silica microspheres (1 µm diameter, Bangs Laboratories) and an oxygen scavenger system, consisting of 26 U mL^{-1} glucose oxidase, 17 000 U mL^{-1} catalase, 0.65 % glucose, were added. All measurements were carried out in a buffer containing 50 mM Tris, 200 mM KCl, pH 7.0 with varying amounts of $MgCl_2$, EDTA, nucleotides, non-hydrolyzable nucleotide analogues or bisubstrate inhibitors. The measurement chamber consisted of two 170 µm thick coverslips (Präzizions-Deckgläser, Carl Roth, Germany) attached to each other by Parafilm (Bemis Company, USA). The measurement chamber is passivated with 10 mg mL^{-1} bovine serum albumin (Sigma Aldrich, USA) to prevent the beads from sticking to the surface. Finally the ends of the chamber were sealed with silicon grease. Experiments were carried out at 23 °C, due to

the heating of the sample chamber by the infrared laser the temperature in the sample chamber was typically 30 °C.

Bibliography

Abbondanzieri, E. a., Greenleaf, W. J., Shaevitz, J. W., Landick, R., and Block, S. M. Direct observation of base-pair stepping by RNA polymerase. *Nature*, 438(7067): 460–5, November 2005a. (Cited on page 2)

Abbondanzieri, E. a., Shaevitz, J. W., and Block, S. M. Picocalorimetry of transcription by RNA polymerase. *Biophysical journal*, 89(6):L61–3, December 2005b. (Cited on page 3)

Abele, U. and Schulz, G. E. High-resolution structures of adenylate kinase from yeast ligated with inhibitor Ap5A, showing the pathway of phosphoryl transfer. *Protein science : a publication of the Protein Society*, 4(7):1262–71, July 1995. (Cited on page 1)

Adén, J. and Wolf-Watz, M. NMR identification of transient complexes critical to adenylate kinase catalysis. *Journal of the American Chemical Society*, 129(45): 14003–12, November 2007. (Cited on pages 1, 32, 74, 83, 84, and 85)

Arora, K. and Brooks, C. L. Large-scale allosteric conformational transitions of adenylate kinase appear to involve a population-shift mechanism. *Proceedings of the National Academy of Sciences of the United States of America*, 104(47):18496–501, November 2007. (Cited on pages 33, 59, and 61)

Asbury, C. L., Fehr, A. N., and Block, S. M. Kinesin moves by an asymmetric hand-over-hand mechanism. *Science (New York, N.Y.)*, 302(5653):2130–4, December 2003. (Cited on page 18)

Ashkin, A. and Dziedzic, J. M. Optical trapping and manipulation of viruses and bacteria. *Science (New York, N.Y.)*, 235(4795):1517–20, March 1987. (Cited on page 3)

Ashkin, A., Dziedzic, J. M., Bjorkholm, J. E., and Chu, S. Observation of a single-beam gradient force optical trap for dielectric particles. *Optics letters*, 11(5):288, May 1986. (Cited on page 3)

Atakhorrami, M., Addas, K. M., and Schmidt, C. F. Twin optical traps for two-particle cross-correlation measurements: eliminating cross-talk. *The Review of scientific instruments*, 79(4):043103, April 2008. (Cited on page 12)

Aubin-Tam, M.-E., Olivares, A. O., Sauer, R. T., Baker, T. a., and Lang, M. J. Single-molecule protein unfolding and translocation by an ATP-fueled proteolytic machine. *Cell*, 145(2):257–67, April 2011. (Cited on pages 2 and 3)

Bakan, A. and Bahar, I. The intrinsic dynamics of enzymes plays a dominant role in determining the structural changes induced upon inhibitor binding. *Proceedings of the National Academy of Sciences of the United States of America*, 106(34):14349–54, August 2009. (Cited on page 59)

Barton, J. P., Alexander, D. R., and Schaub, S. a. Theoretical determination of net radiation force and torque for a spherical particle illuminated by a focused laser beam. *Journal of Applied Physics*, 66(10):4594, 1989. (Cited on page 5)

Beckstein, O., Denning, E. J., Perilla, J. R., and Woolf, T. B. Zipping and unzipping of adenylate kinase: atomistic insights into the ensemble of open<–>closed transitions. *Journal of molecular biology*, 394(1):160–76, November 2009. (Cited on page 33)

Bell, G. I. Models for the specific adhesion of cells to cells. *Science (New York, N.Y.)*, 200(4342):618–27, May 1978. (Cited on page 27)

Berg-Sorensen, K. and Flyvbjerg, H. Power spectrum analysis for optical tweezers. *Review of Scientific Instruments*, 75(3):594, 2004. (Cited on pages 5 and 8)

Berg-Sørensen, K., Peterman, E. J. G., Weber, T., Schmidt, C. F., and Flyvbjerg, H. Power spectrum analysis for optical tweezers. II: Laser wavelength dependence of parasitic filtering, and how to achieve high bandwidth. *Review of Scientific Instruments*, 77(6):063106, 2006. (Cited on pages 8 and 14)

Berry, M. B., Meador, B., Bilderback, T., Liang, P., Glaser, M., and Phillips, G. N. The closed conformation of a highly flexible protein: the structure of E. coli adenylate kinase with bound AMP and AMPPNP. *Proteins*, 19(3):183–98, July 1994. (Cited on pages 1, 32, and 92)

Berry, M. B., Bae, E., Bilderback, T. R., Glaser, M., and Phillips, G. N. Crystal structure of ADP/AMP complex of Escherichia coli adenylate kinase. *Proteins*, 62(2):555–6, February 2006. (Cited on page 32)

Bertz, M. and Rief, M. Mechanical unfoldons as building blocks of maltose-binding protein. *Journal of molecular biology*, 378(2):447–58, April 2008. (Cited on page 38)

Bertz, M., Wilmanns, M., and Rief, M. The titin-telethonin complex is a directed, superstable molecular bond in the muscle Z-disk. *Proceedings of the National Academy of Sciences of the United States of America*, 106(32):13307–133310, August 2009. (Cited on page 38)

Boehr, D. D., Nussinov, R., and Wright, P. E. The role of dynamic conformational ensembles in biomolecular recognition. *Nature chemical biology*, 5(11):789–96, November 2009. (Cited on page 59)

Bosshard, H. R. Molecular recognition by induced fit: how fit is the concept? *News in physiological sciences : an international journal of physiology produced jointly by the International Union of Physiological Sciences and the American Physiological Society*, 16(August):171–3, August 2001. (Cited on page 59)

Brandts, J. F., Halvorson, H. R., and Brennan, M. Consideration of the Possibility that the slow step in protein denaturation reactions is due to cis-trans isomerism of proline residues. *Biochemistry*, 14:4953–4963, 1975. (Cited on page 40)

Brandts, J. F., Brennan, M., and Lung-Nan Lin. Unfolding and refolding occur much faster for a proline-free proteins than for most proline-containing proteins. *Proceedings of the National Academy of Sciences of the United States of America*, 74(10): 4178–81, October 1977. (Cited on page 40)

Bui, J. M. and McCammon, J. A. Protein complex formation by acetylcholinesterase and the neurotoxin fasciculin-2 appears to involve an induced-fit mechanism. *Proceedings of the National Academy of Sciences of the United States of America*, 103 (42):15451–6, October 2006. (Cited on page 59)

Bustamante, C., Marko, J. F., Siggia, E. D., and Smith, S. Entropic elasticity of lambda-phage DNA. *Science (New York, N.Y.)*, 265(5178):1599–600, September 1994. (Cited on page 23)

Carrion-Vazquez, M., Oberhauser, A. F., Fowler, S. B., Marszalek, P. E., Broedel, S. E., Clarke, J., and Fernandez, J. M. Mechanical and chemical unfolding of a single protein: a comparison. *Proceedings of the National Academy of Sciences of the United States of America*, 96(7):3694–9, March 1999. (Cited on page 38)

Carter, A. R., Seol, Y., and Perkins, T. T. Precision surface-coupled optical-trapping assay with one-basepair resolution. *Biophysical journal*, 96(7):2926–34, April 2009. (Cited on page 12)

Cecconi, C., Shank, E. a., Bustamante, C., and Marqusee, S. Direct observation of the three-state folding of a single protein molecule. *Science (New York, N.Y.)*, 309(5743): 2057–60, September 2005. (Cited on page 2)

Cui, Q., Li, G., Ma, J., and Karplus, M. A normal mode analysis of structural plasticity in the biomolecular motor F(1)-ATPase. *Journal of molecular biology*, 340(2):345–72, July 2004. (Cited on page 1)

De Bondt, H. L., Rosenblatt, J., Jancarik, J., Jones, H. D., Morgan, D. O., and Kim, S. H. Crystal structure of cyclin-dependent kinase 2. *Nature*, 363(6430):595–602, June 1993. (Cited on page 1)

Deckert, G., Warren, P. V., Gaasterland, T., Young, W. G., Lenox, A. L., Graham, D. E., Overbeek, R., Snead, M. A., Keller, M., Aujay, M., Huber, R., Feldman, R. A., Short, J. M., Olsen, G. J., and Swanson, R. V. The complete genome of the hyperthermophilic bacterium Aquifex aeolicus. *Nature*, 392(6674):353–8, March 1998. (Cited on page 31)

Deufel, C., Forth, S., Simmons, C. R., Dejgosha, S., and Wang, M. D. Nanofabricated quartz cylinders for angular trapping: DNA supercoiling torque detection. *Nature methods*, 4(3):223–5, March 2007. (Cited on page 3)

Dietz, H. and Rief, M. Protein structure by mechanical triangulation. *Proceedings of the National Academy of Sciences of the United States of America*, 103(5):1244–7, January 2006. (Cited on page 24)

Dietz, H., Douglas, S. M., and Shih, W. M. Folding DNA into twisted and curved nanoscale shapes. *Science (New York, N.Y.)*, 325(5941):725–30, August 2009. (Cited on page 99)

Dill, K. a. and MacCallum, J. L. The protein-folding problem, 50 years on. *Science (New York, N.Y.)*, 338(6110):1042–6, November 2012. (Cited on page 1)

Dreusicke, D., Karplus, P. a., and Schulz, G. E. Refined structure of porcine cytosolic adenylate kinase at 2.1 A resolution. *Journal of molecular biology*, 199(2):359–71, January 1988. (Cited on page 1)

Dudko, O. K., Hummer, G., and Szabo, A. Theory, analysis, and interpretation of single-molecule force spectroscopy experiments. *Proceedings of the National Academy of Sciences of the United States of America*, 105(41):15755–60, October 2008. (Cited on page 21)

Fällman, E. and Axner, O. Design for fully steerable dual-trap optical tweezers. *Applied optics*, 36(10):2107–13, April 1997. (Cited on page 10)

Ferrer, J. M., Lee, H., Chen, J., Pelz, B., Nakamura, F., Kamm, R. D., and Lang, M. J. Measuring molecular rupture forces between single actin filaments and actin-binding proteins. *Proceedings of the National Academy of Sciences of the United States of America*, 105(27):9221–6, July 2008. (Cited on page 18)

Finer, J. T., Simmons, R. M., and Spudich, J. A. Single myosin molecule mechanics: piconewton forces and nanometre steps. *Nature*, 368(6467):113–9, March 1994. (Cited on page 3)

Fischer, G. and Aumüller, T. Regulation of peptide bond cis/trans isomerization by enzyme catalysis and its implication in physiological processes. *Reviews of physiology, biochemistry and pharmacology*, 148:105–50, January 2003. (Cited on page 41)

Frauenfelder, H., Sligar, S. G., and Wolynes, P. G. The energy landscapes and motions of proteins. *Science (New York, N.Y.)*, 254(5038):1598–603, December 1991. (Cited on page 1)

Frauenfelder, H., McMahon, B. H., and Fenimore, P. W. Myoglobin: the hydrogen atom of biology and a paradigm of complexity. *Proceedings of the National Academy of Sciences of the United States of America*, 100(15):8615–7, July 2003. (Cited on page 1)

Fujii, A., Hirota, S., and Matsuo, T. Reversible Switching of Fluorophore Property Based on Intrinsic Conformational Transition of Adenylate Kinase during Its Catalytic Cycle. *Bioconjugate chemistry*, May 2013. (Cited on page 85)

Gebhardt, J. C. M. *Energielandschaften einzelner Proteine gemessen mit der optischen Pinzette*. Phd thesis, TU München, 2009. (Cited on pages 12 and 27)

Gebhardt, J. C. M., Bornschlögl, T., and Rief, M. Full distance-resolved folding energy landscape of one single protein molecule. *Proceedings of the National Academy of Sciences of the United States of America*, 107(5):2013–8, February 2010. (Cited on page 24)

Gilles, a. M., Saint-Girons, I., Monnot, M., Fermandjian, S., Michelson, S., and Bârzu, O. Substitution of a serine residue for proline-87 reduces catalytic activity and increases susceptibility to proteolysis of Escherichia coli adenylate kinase. *Proceedings of the National Academy of Sciences of the United States of America*, 83(16): 5798–802, August 1986. (Cited on page 54)

Green, M. a. Self-consistent optical parameters of intrinsic silicon at 300K including temperature coefficients. *Solar Energy Materials and Solar Cells*, 92(11):1305–1310, November 2008. (Cited on page 14)

Hammes, G. G. Multiple conformational changes in enzyme catalysis. *Biochemistry*, 41(26):8221–8, July 2002. (Cited on page 1)

Hanson, J. a., Duderstadt, K., Watkins, L. P., Bhattacharyya, S., Brokaw, J., Chu, J.-W., and Yang, H. Illuminating the mechanistic roles of enzyme conformational dynamics. *Proceedings of the National Academy of Sciences of the United States of America*, 104 (46):18055–60, November 2007. (Cited on pages 2, 33, and 59)

Henzler-Wildman, K. a., Lei, M., Thai, V., Kerns, S. J., Karplus, M., and Kern, D. A hierarchy of timescales in protein dynamics is linked to enzyme catalysis. *Nature*, 450(7171):913–6, December 2007a. (Cited on pages 31 and 93)

Henzler-Wildman, K. a., Thai, V., Lei, M., Ott, M., Wolf-Watz, M., Fenn, T., Pozharski, E., Wilson, M. a., Petsko, G. a., Karplus, M., Hübner, C. G., and Kern, D. Intrinsic motions along an enzymatic reaction trajectory. *Nature*, 450(7171):838–44, December 2007b. (Cited on pages 1, 2, 33, 46, 59, 70, 75, and 80)

Hessling, M., Richter, K., and Buchner, J. Dissection of the ATP-induced conformational cycle of the molecular chaperone Hsp90. *Nature structural & molecular biology*, 16(3):287–93, March 2009. (Cited on page 1)

Hoffmann, A. and Woodside, M. T. Signal-pair correlation analysis of single-molecule trajectories. *Angewandte Chemie (International ed. in English)*, 50(52):12643–6, December 2011. (Cited on page 21)

Hummer, G. and Szabo, A. Kinetics from nonequilibrium single-molecule pulling experiments. *Biophysical journal*, 85(1):5–15, July 2003. (Cited on page 21)

Jaenicke, R. and Böhm, G. The stability of proteins in extreme environments. *Current opinion in structural biology*, 8(6):738–48, December 1998. (Cited on page 31)

James, L. C., Roversi, P., and Tawfik, D. S. Antibody multispecificity mediated by conformational diversity. *Science (New York, N.Y.)*, 299(5611):1362–7, February 2003. (Cited on page 59)

Junker, J. P. *Ligandenabhängige Gleichgewichtsfluktuationen einzelner Proteine*. PhD thesis, TU München, 2009. (Cited on page 28)

Kalbitzer, H. R., Marquetant, R., Rösch, P., and Schirmer, R. H. The structural isomerisation of human-muscle adenylate kinase as studied by 1H-nuclear magnetic resonance. *European journal of biochemistry / FEBS*, 126(3):531–6, September 1982. (Cited on page 49)

Klepeis, J. L., Lindorff-Larsen, K., Dror, R. O., and Shaw, D. E. Long-timescale molecular dynamics simulations of protein structure and function. *Current opinion in structural biology*, 19(2):120–7, April 2009. (Cited on page 1)

Koshland, D. E. Application of a Theory of Enzyme Specificity to Protein Synthesis. *Proceedings of the National Academy of Sciences of the United States of America*, 44 (2):98–104, February 1958. (Cited on page 59)

Kubitzki, M. B. and de Groot, B. L. The atomistic mechanism of conformational transition in adenylate kinase: a TEE-REX molecular dynamics study. *Structure (London, England : 1993)*, 16(8):1175–82, August 2008. (Cited on page 33)

Kumar, S., Ma, B., Tsai, C. J., Sinha, N., and Nussinov, R. Folding and binding cascades: dynamic landscapes and population shifts. *Protein science : a publication of the Protein Society*, 9(1):10–9, January 2000. (Cited on page 59)

Kupriyanov, V. V., Ferretti, J. A., and Balaban, R. S. Muscle adenylate kinase catalyzes adenosine 5'-tetraphosphate synthesis from ATP and ADP. *Biochimica et biophysica acta*, 869(1):107–11, January 1986. (Cited on page 68)

Landry, M. P., McCall, P. M., Qi, Z., and Chemla, Y. R. Characterization of photoactivated singlet oxygen damage in single-molecule optical trap experiments. *Biophysical journal*, 97(8):2128–36, October 2009. (Cited on page 15)

Lang, M. J., Asbury, C. L., Shaevitz, J. W., and Block, S. M. An automated two-dimensional optical force clamp for single molecule studies. *Biophysical journal*, 83 (1):491–501, July 2002. (Cited on page 21)

Levy, Y., Onuchic, J. N., and Wolynes, P. G. Fly-casting in protein-DNA binding: frustration between protein folding and electrostatics facilitates target recognition. *Journal of the American Chemical Society*, 129(4):738–9, January 2007. (Cited on page 59)

Lienhard, G. E. and Secemski, I. I. P 1 ,P 5 -Di(adenosine-5')pentaphosphate, a potent multisubstrate inhibitor of adenylate kinase. *The Journal of biological chemistry*, 248 (3):1121–3, February 1973. (Cited on page 31)

Lu, K. P., Finn, G., Lee, T. H., and Nicholson, L. K. Prolyl cis-trans isomerization as a molecular timer. *Nature chemical biology*, 3(10):619–29, October 2007. (Cited on page 40)

Mahamdeh, M., Campos, C. P., and Schäffer, E. Under-filling trapping objectives optimizes the use of the available laser power in optical tweezers. *Optics express*, 19(12): 11759–68, June 2011. (Cited on page 9)

Maillard, R. a., Chistol, G., Sen, M., Righini, M., Tan, J., Kaiser, C. M., Hodges, C., Martin, A., and Bustamante, C. ClpX(P) generates mechanical force to unfold and translocate its protein substrates. *Cell*, 145(3):459–69, April 2011. (Cited on pages 2 and 3)

Mangeol, P. and Bockelmann, U. Interference and crosstalk in double optical tweezers using a single laser source. *The Review of scientific instruments*, 79(8):083103, August 2008. (Cited on page 11)

Mapa, K., Sikor, M., Kudryavtsev, V., Waegemann, K., Kalinin, S., Seidel, C. a. M., Neupert, W., Lamb, D. C., and Mokranjac, D. The conformational dynamics of the mitochondrial Hsp70 chaperone. *Molecular cell*, 38(1):89–100, April 2010. (Cited on page 2)

Matsunaga, Y., Fujisaki, H., Terada, T., Furuta, T., Moritsugu, K., and Kidera, A. Minimum free energy path of ligand-induced transition in adenylate kinase. *PLoS computational biology*, 8(6):e1002555, January 2012. (Cited on pages 1, 33, and 59)

McCammon, J. A., Gelin, B. R., and Karplus, M. Dynamics of folded proteins. *Nature*, 267(5612):585–90, June 1977. (Cited on page 1)

Moffitt, J. R., Chemla, Y. R., Izhaky, D., and Bustamante, C. Differential detection of dual traps improves the spatial resolution of optical tweezers. *Proceedings of the National Academy of Sciences of the United States of America*, 103(24):9006–11, June 2006. (Cited on pages 19 and 99)

Müller, C. W. and Schulz, G. E. Structure of the complex between adenylate kinase from Escherichia coli and the inhibitor Ap5A refined at 1.9 A resolution. A model for a catalytic transition state. *Journal of molecular biology*, 224(1):159–77, March 1992. (Cited on pages 1 and 32)

Nugent-Glandorf, L. and Perkins, T. T. Measuring 0.1-nm motion in 1 ms in an optical microscope with differential back-focal-plane detection. *Optics letters*, 29(22):2611–3, November 2004. (Cited on page 18)

Ogawa, A., Takayama, Y., Sakai, H., Chong, K. T., Takeuchi, S., Nakagawa, A., Nada, S., Okada, M., and Tsukihara, T. Structure of the carboxyl-terminal Src kinase, Csk. *The Journal of biological chemistry*, 277(17):14351–4, April 2002. (Cited on page 1)

Okazaki, K.-I. and Takada, S. Dynamic energy landscape view of coupled binding and protein conformational change: induced-fit versus population-shift mechanisms. *Proceedings of the National Academy of Sciences of the United States of America*, 105(32):11182–7, August 2008. (Cited on page 61)

Olsson, U. and Wolf-Watz, M. Overlap between folding and functional energy landscapes for adenylate kinase conformational change. *Nature communications*, 1(8): 111, January 2010. (Cited on page 33)

Onuchic, J. N., Luthey-Schulten, Z., and Wolynes, P. G. Theory of protein folding: the energy landscape perspective. *Annual review of physical chemistry*, 48(1):545–600, January 1997. (Cited on page 1)

Ott, M. *Konformationsänderung und enzymatische Aktivität am einzelnen Molekül*. Phd thesis, University Lübeck, 2008. (Cited on page 92)

Perpina, X., Jorda, X., Vellvehi, M., Millan, J., and Mestres, N. Development of an analog processing circuit for IR-radiation power and noncontact position measurements. *Review of Scientific Instruments*, 76(2):025106, 2005. (Cited on page 13)

Peterman, E. J. G., Gittes, F., and Schmidt, C. F. Laser-induced heating in optical traps. *Biophysical journal*, 84(2 Pt 1):1308–16, February 2003. (Cited on page 6)

Petsko, G. A. Structural basis of thermostability in hyperthermophilic proteins, or "there's more than one way to skin a cat". *Methods in enzymology*, 334(i):469–78, January 2001. (Cited on page 31)

Pfitzner, E., Wachauf, C., Kilchherr, F., Pelz, B., Shih, W. M., Rief, M., and Dietz, H. Rigid DNA Beams for High-Resolution Single-Molecule Mechanics. *Angewandte Chemie*, 125(30):7920–7925, July 2013. (Cited on page 99)

Pirchi, M., Ziv, G., Riven, I., Cohen, S. S., Zohar, N., Barak, Y., and Haran, G. Single-molecule fluorescence spectroscopy maps the folding landscape of a large protein. *Nature communications*, 2:493, January 2011. (Cited on pages 35 and 39)

Potoyan, D. a., Zhuravlev, P. I., and Papoian, G. a. Computing free energy of a large-scale allosteric transition in adenylate kinase using all atom explicit solvent simulations. *The journal of physical chemistry. B*, 116(5):1709–15, February 2012. (Cited on page 33)

Ratner, V., Kahana, E., and Haas, E. The natively helical chain segment 169-188 of Escherichia coli adenylate kinase is formed in the latest phase of the refolding transition. *Journal of molecular biology*, 320(5):1135–45, July 2002. (Cited on page 41)

Ratzke, C., Mickler, M., Hellenkamp, B., Buchner, J., and Hugel, T. Dynamics of heat shock protein 90 C-terminal dimerization is an important part of its conformational cycle. *Proceedings of the National Academy of Sciences of the United States of America*, 107(37):16101–6, September 2010. (Cited on page 2)

Ratzke, C., Berkemeier, F., and Hugel, T. Heat shock protein 90's mechanochemical cycle is dominated by thermal fluctuations. *Proceedings of the National Academy of Sciences of the United States of America*, 109(1):161–6, January 2012. (Cited on page 2)

Reinstein, J., Vetter, I. R., Schlichting, I., Rösch, P., Wittinghofer, a., and Goody, R. S. Fluorescence and NMR investigations on the ligand binding properties of adenylate kinases. *Biochemistry*, 29(32):7440–50, August 1990a. (Cited on pages 32, 35, 50, 51, 52, 63, 72, 73, and 75)

Reinstein, J., Schlichting, I., and Wittinghofer, A. Structurally and catalytically important residues in the phosphate binding loop of adenylate kinase of Escherichia coli. *Biochemistry*, 29(32):7451–7459, August 1990b. (Cited on pages 65 and 98)

Rhoads, D. G. and Lowenstein, J. M. Initial velocity and equilibrium kinetics of myokinase. *The Journal of biological chemistry*, 243(14):3963–72, July 1968. (Cited on page 32)

Rognoni, L. *Molecular Mechanism of the Mechanosensor Filamin*. PhD thesis, TU München, 2014. (Cited on pages 40 and 41)

Rothemund, P. W. K. Folding DNA to create nanoscale shapes and patterns. *Nature*, 440(7082):297–302, March 2006. (Cited on page 99)

Rüdiger, S., Buchberger, A., and Bukau, B. Interaction of Hsp70 chaperones with substrates. *Nature structural biology*, 4(5):342–9, May 1997. (Cited on page 1)

Rundqvist, L., Adén, J., Sparrman, T., Wallgren, M., Olsson, U., and Wolf-Watz, M. Noncooperative folding of subdomains in adenylate kinase. *Biochemistry*, 48(9): 1911–27, March 2009. (Cited on page 45)

Saint Girons, I., Gilles, A. M., Margarita, D., Michelson, S., Monnot, M., Fermandjian, S., Danchin, A., and Bârzu, O. Structural and catalytic characteristics of Escherichia coli adenylate kinase. *The Journal of biological chemistry*, 262(2):622–9, January 1987. (Cited on page 34)

Schlauderer, G. J., Proba, K., and Schulz, G. E. Structure of a mutant adenylate kinase ligated with an ATP-analogue showing domain closure over ATP. *Journal of molecular biology*, 256(2):223–7, February 1996. (Cited on pages 32 and 83)

Schlierf, M., Berkemeier, F., and Rief, M. Direct observation of active protein folding using lock-in force spectroscopy. *Biophysical journal*, 93(11):3989–98, December 2007. (Cited on page 27)

Schnitzer, M. J. and Block, S. M. Kinesin hydrolyses one ATP per 8-nm step. *Nature*, 388(6640):386–90, July 1997. (Cited on page 2)

Schrank, T. P., Bolen, D. W., and Hilser, V. J. Rational modulation of conformational fluctuations in adenylate kinase reveals a local unfolding mechanism for allostery and functional adaptation in proteins. *Proceedings of the National Academy of Sciences of the United States of America*, 106(40):16984–9, October 2009. (Cited on pages 45, 97, and 98)

Schwaiger, I., Kardinal, A., Schleicher, M., Noegel, A. a., and Rief, M. A mechanical unfolding intermediate in an actin-crosslinking protein. *Nature structural & molecular biology*, 11(1):81–5, January 2004. (Cited on page 38)

Seeman, N. C. DNA in a material world. *Nature*, 421(6921):427–31, January 2003. (Cited on page 99)

Shaevitz, J. W., Abbondanzieri, E. a., Landick, R., and Block, S. M. Backtracking by single RNA polymerase molecules observed at near-base-pair resolution. *Nature*, 426 (6967):684–7, December 2003. (Cited on page 2)

Silva, D.-A., Bowman, G. R., Sosa-Peinado, A., and Huang, X. A role for both conformational selection and induced fit in ligand binding by the LAO protein. *PLoS computational biology*, 7(5):e1002054, May 2011. (Cited on page 59)

Sinev, M. a., Sineva, E. V., Ittah, V., and Haas, E. Towards a mechanism of AMP-substrate inhibition in adenylate kinase from Escherichia coli. *FEBS letters*, 397 (2-3):273–6, November 1996. (Cited on page 74)

Snow, C., Qi, G., and Hayward, S. Essential dynamics sampling study of adenylate kinase: comparison to citrate synthase and implication for the hinge and shear mechanisms of domain motions. *Proteins*, 67(2):325–37, May 2007. (Cited on page 33)

Song, H. D. and Zhu, F. Conformational Dynamics of a Ligand-Free Adenylate Kinase. *PLoS ONE*, 8(7):e68023, July 2013. (Cited on pages 33 and 59)

Stanfield, R. L., Takimoto-Kamimura, M., Rini, J. M., Profy, A. T., and Wilson, I. A. Major antigen-induced domain rearrangements in an antibody. *Structure (London, England : 1993)*, 1(2):83–93, October 1993. (Cited on page 1)

Stewart, D. E., Sarkar, a., and Wampler, J. E. Occurrence and role of cis peptide bonds in protein structures. *Journal of molecular biology*, 214(1):253–60, July 1990. (Cited on page 40)

Stigler, J. *Complex ligand-dependent folding of single proteins observed with optical tweezers*. PhD thesis, TU München, 2012. (Cited on pages 28 and 30)

Stigler, J. and Rief, M. Hidden markov analysis of trajectories in single-molecule experiments and the effects of missed events. *Chemphyschem : a European journal of chemical physics and physical chemistry*, 13(4):1079–86, March 2012. (Cited on pages 25 and 46)

Stigler, J., Ziegler, F., Gieseke, A., Gebhardt, J. C. M., and Rief, M. The complex folding network of single calmodulin molecules. *Science (New York, N.Y.)*, 334(6055):512–6, October 2011. (Cited on pages 2 and 3)

Sugase, K., Dyson, H. J., and Wright, P. E. Mechanism of coupled folding and binding of an intrinsically disordered protein. *Nature*, 447(7147):1021–5, June 2007. (Cited on page 59)

Svoboda, K., Schmidt, C. F., Schnapp, B. J., and Block, S. M. Direct observation of kinesin stepping by optical trapping interferometry. *Nature*, 365(6448):721–7, October 1993. (Cited on pages 2 and 3)

Tolić-Nørrelykke, S. F., Schäffer, E., Howard, J., Pavone, F. S., Jülicher, F., and Flyvbjerg, H. Calibration of optical tweezers with positional detection in the back focal plane. *Review of Scientific Instruments*, 77(10):103101, March 2006. (Cited on pages 6 and 8)

Vonrhein, C., Schlauderer, G. J., and Schulz, G. E. Movie of the structural changes during a catalytic cycle of nucleoside monophosphate kinases. *Structure (London, England : 1993)*, 3(5):483–90, May 1995. (Cited on pages 1 and 31)

Walker, J. E., Saraste, M., Runswick, M. J., and Gay, N. J. Distantly related sequences in the alpha- and beta-subunits of ATP synthase, myosin, kinases and other ATP-requiring enzymes and a common nucleotide binding fold. *The EMBO journal*, 1(8): 945–51, January 1982. (Cited on page 31)

Wang, M. D., Yin, H., Landick, R., Gelles, J., and Block, S. M. Stretching DNA with optical tweezers. *Biophysical journal*, 72(3):1335–46, March 1997. (Cited on page 23)

Wedemeyer, W. J., Welker, E., and Scheraga, H. A. Proline cis-trans isomerization and protein folding. *Biochemistry*, 41(50):14637–44, December 2002. (Cited on pages 40 and 54)

Wen, J.-D., Manosas, M., Li, P. T. X., Smith, S. B., Bustamante, C., Ritort, F., and Tinoco, I. Force unfolding kinetics of RNA using optical tweezers. I. Effects of experimental variables on measured results. *Biophysical journal*, 92(9):2996–3009, May 2007. (Cited on page 2)

Wen, J.-D., Lancaster, L., Hodges, C., Zeri, A.-C., Yoshimura, S. H., Noller, H. F., Bustamante, C., and Tinoco, I. Following translation by single ribosomes one codon at a time. *Nature*, 452(7187):598–603, April 2008. (Cited on page 18)

Whitford, P. C., Miyashita, O., Levy, Y., and Onuchic, J. N. Conformational transitions of adenylate kinase: switching by cracking. *Journal of molecular biology*, 366(5): 1661–71, March 2007. (Cited on page 33)

Wlodarski, T. and Zagrovic, B. Conformational selection and induced fit mechanism underlie specificity in noncovalent interactions with ubiquitin. *Proceedings of the National Academy of Sciences of the United States of America*, 106(46):19346–51, November 2009. (Cited on page 59)

Wolf-Watz, M., Thai, V., Henzler-Wildman, K., Hadjipavlou, G., Eisenmesser, E. Z., and Kern, D. Linkage between dynamics and catalysis in a thermophilic-mesophilic enzyme pair. *Nature structural & molecular biology*, 11(10):945–9, October 2004. (Cited on pages 1, 32, 33, 35, 54, and 72)

Woodside, M. T., Anthony, P. C., Behnke-Parks, W. M., Larizadeh, K., Herschlag, D., and Block, S. M. Direct measurement of the full, sequence-dependent folding landscape of a nucleic acid. *Science (New York, N.Y.)*, 314(5801):1001–4, November 2006a. (Cited on pages 2 and 3)

Woodside, M. T., Behnke-Parks, W. M., Larizadeh, K., Travers, K., Herschlag, D., and Block, S. M. Nanomechanical measurements of the sequence-dependent folding landscapes of single nucleic acid hairpins. *Proceedings of the National Academy of Sciences of the United States of America*, 103(16):6190–5, April 2006b. (Cited on page 2)

Yang, Z., Májek, P., and Bahar, I. Allosteric transitions of supramolecular systems explored by network models: application to chaperonin GroEL. *PLoS computational biology*, 5(4):e1000360, April 2009. (Cited on page 1)

Zoldák, G., Stigler, J., Pelz, B., Li, H., and Rief, M. Ultrafast folding kinetics and cooperativity of villin headpiece in single-molecule force spectroscopy. *Proceedings of the National Academy of Sciences of the United States of America*, 110(45):18156–61, November 2013. (Cited on pages 18, 43, 45, and 99)